Recent Progress in Perovskite Solar Cells Modified by Sulfur Compounds

doi: https://doi.org/10.1002/solr.202000713

Recent Progress in Perovskite Solar Cells Modified by Sulfur Compounds

Yi Zhou[2,#], Caiyun Liu[2,#], Fanning Meng[2], Chu Zhang[1], Guoying Wei[1], Liguo Gao[2,*], Yang Li[2,*], and Tingli Ma[1,3,*]

1 Department of Materials Science and Engineering, China Jiliang University, Hangzhou, 310018, P. R. China.

2 State Key Laboratory of Fine Chemicals, Dalian University of Technology, Dalian 116023, China.

3 Graduate School of Life Science and Systems Engineering, Kyushu Institute of Technology, Kitakyushu, Fukuoka 808-0196, Japan.

# These authors contributed equally.

Corresponding Author

*Tingli Ma

E-mail: tinglima@life.kyutech.ac.jp; ORCID: 0000-0002-3310-459X.

*Liguo Gao

E-mail: liguo.gao@dlut.edu.cn; ORCID: 0000-0002-5390-3663.

*Yang Li

E-mail: chyangli@dlut.edu.cn; ORCID: 0000-0002-5719-9044.

Abstract

In the past decade, organic-inorganic hybrid perovskite solar cells (PSCs) have begun to be increasingly studied worldwide because they can achieve a certified power conversion efficiency (PCE) of 25.5% owing to their superior properties. However, some issues have delayed their commercialization, such as their long-term stability, cost reduction, scale-up ability, and efficiency. The introduction of sulfur to PSCs can relieve the above issues because sulfur can passivate interfacial trap states, suppress charge recombination, and inhibit ion migration, thereby enhancing the stability of PSCs. Furthermore, Pb-S bonds provide new channels for carrier extraction. Although sulfur-based PSCs have achieved remarkable success as state-of-the-art technology, no review has focused on the effect of sulfur in PSCs. Herein, we summarize the sulfur-based compounds utilized in PSCs and classify them according to their functions in the different layers of PSCs. The results indicate that these sulfur-based compounds have efficiently promoted the commercialization of PSCs. We hope that this review can help others understand the intrinsic phenomena of sulfur-based PSCs and motivate additional investigations.

Graphic Abstract

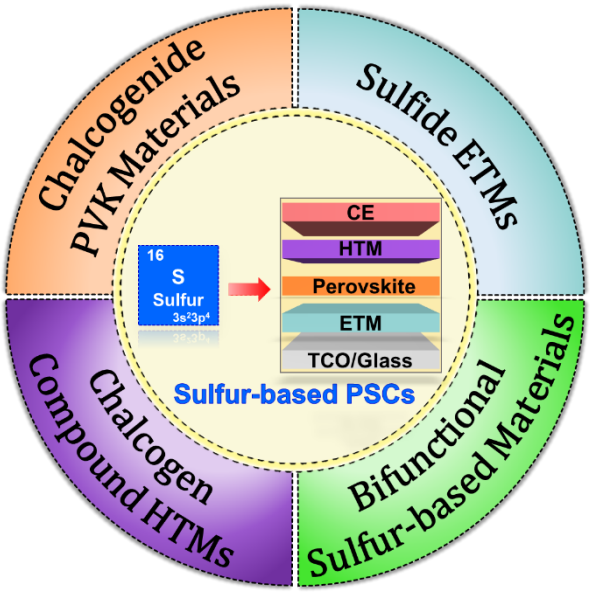

1. Introduction

Since being first reported by Kojima and coworkers in 2009[1], perovskite solar cells (PSCs) have achieved a certified power conversion efficiency (PCE) of up to 25.5% after ten years of rapid development.[2] Such a remarkable achievement results from the outstanding photovoltaic properties of a perovskite material with the ABX_3 crystal structure, as shown in Figure 1, where A = $CH_3NH_3^+(MA^+)$, $NH_2CHNH_2^+(FA^+)$, Ru^+, or Cs^+; B = Pb^{2+} or Sn^{2+}; and X = I^-, Br^-, or Cl^-. These outstanding photovoltaic properties include a wide absorption range, high absorption coefficient, suitable bandgap, and long carrier migration distance.[3] Usually, PSCs are composed of five functional layers, including a transparent conductive oxide (TCO), electron transport material (ETM, n-type semiconductor), perovskite light-absorbing material, hole transport material (HTM, p-type semiconductor), and counter electrodes (CEs). According to the direction of carrier migration, the device can be divided into an n-i-p or a p-i-n architecture, as shown in Figure 1.

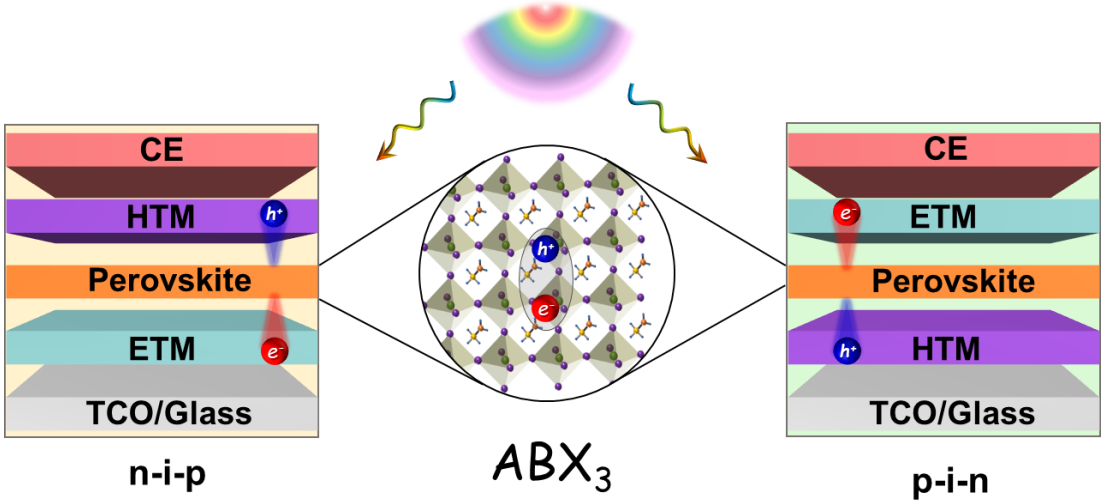

Figure 1. Schematic diagram of PSCs with n-i-p (left) and p-i-n (right) architectures, the middle image is the ABX_3 crystal structure of the perovskite layer.

Although PSCs have demonstrated considerable commercial potential, there are still four issues that need to be solved. First, certified PCEs for small-scale devices are

still far from the highest theoretical PCE (30.5%), which is mainly because of the charge recombination within the perovskite film and at the interfaces.[4] Second, the motivation for cost reduction needs to be improved, including finding alternatives for the expensive noble-metal electrodes and complicated purification processes of carrier transport materials.[5] Third, the applications of PSCs are impeded by several issues related to their stability, such as the sensitivity of the perovskite layer to polar solvents, vulnerability to environmental stress, and occurrence of ion migration.[6] Fourth, the efficiency loss in scaling up PSCs is unavoidable due to the increase in series resistance, uneven films, and inescapable inactive areas.[7]

To solve these issues, some strategies have been developed including the compositional regulation, dimensional engineering, additive of precursor, interface passivators. Compositional regulation has been applied to adjust the optical and electric properties of perovskite materials as well as enhance their stability.[8] Dimensional engineering focuses on improving the stability of PSCs by replacing the 3D perovskite absorber layer with 2D perovskite.[9] Additive of precursor has been proven to affect the crystallization and film formation of perovskite, and optimize the energy band structure and stability of the devices.[10] Interface passivators are widely used for defect passivation and the improvement of film quality, thereby reducing non-radiative recombination and improving device performance.[11]

Sulfur compounds could be used as the compositional regulation, additive of precursor, interface passivators of perovskite, which can significantly improve the PCE, cost reduction, and stability of PSCs, as shown in Figure 2. However, no reviews have focused on the effect of sulfur in PSCs. We summarized the sulfide compounds utilized in PSCs and classified them according to their functions in different layers of PSCs. Due to the different roles of the chalcogen compounds in the perovskite layer, these compounds are divided into perovskite components, additives, and interfacial passivators. For the perovskite component, chalcogenide compounds can improve the stability of the perovskite materials by improving the coulombic

effect and moisture resistance. Sulfur-based additives can improve the film quality and phase stability of the perovskite layer. Utilized as interfacial passivators, chalcogen compounds can passivate defects, reduce charge recombination, suppress ion migration, and establish type-I band alignment. To be dependent on their morphology, sulfide ETMs are classified as zero-dimensional (0D) sulfide ETMs, one-dimensional (1D) sulfide ETMs, two-dimensional (2D) sulfide ETMs, and amorphous sulfide ETMs. By utilizing these sulfide ETMs, the interaction of Pb-S can prevent the ion migration of Pb, thereby inhibiting the decomposition of the perovskite. In addition, the Pb-S bond can offer a new channel for the transmission and extraction of electrons, which can passivate interfacial trap states to suppress charge recombination and facilitate the transfer and extraction of charges. Chalcogen compound HTMs include inorganic chalcogen compound HTMs and organic chalcogen compound HTMs, which have a high charge mobility, low cost, extensive availability, and excellent moisture resistance. According to their unique properties, a portion of sulfur-based compounds can also be utilized for both ETMs and HTMs or for HTMs and co-sensitizers, which are named bifunctional sulfur-based materials.

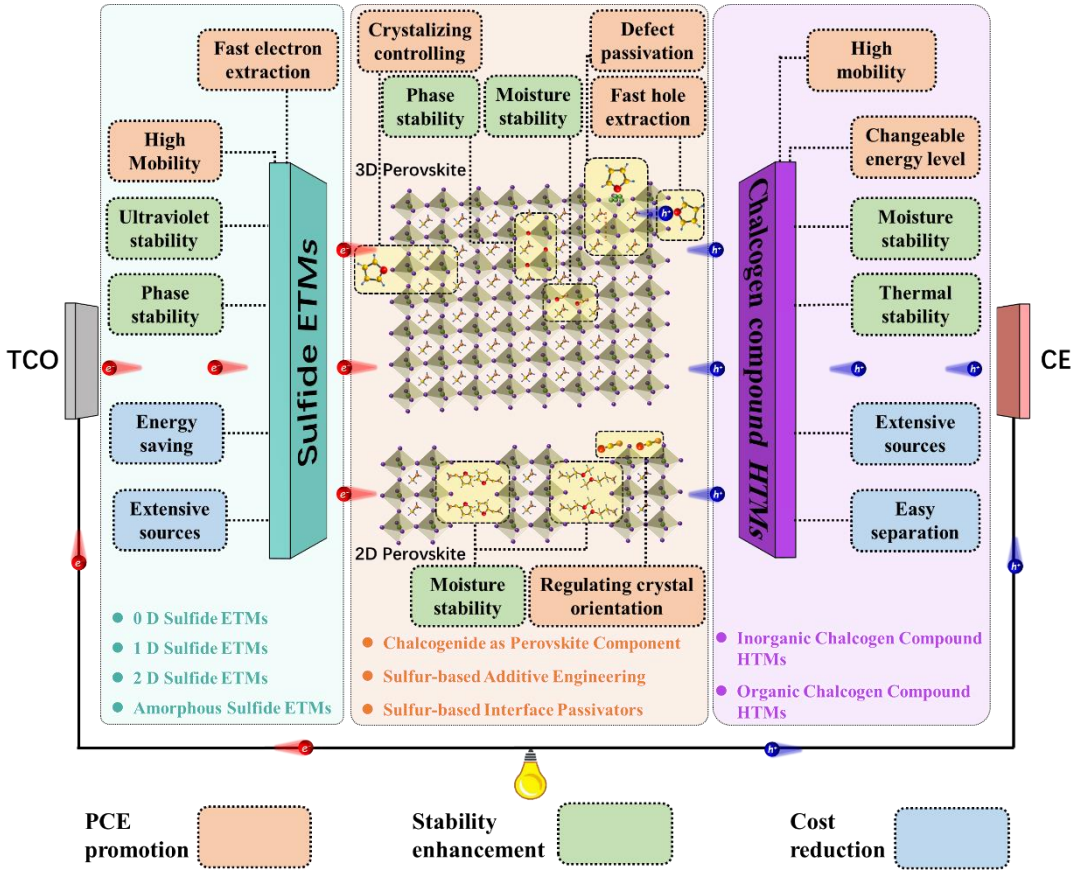

Figure 2. Roles of sulfur compounds in PSCs.

2. Sulfide ETMs

In PSCs, ETMs not only play a role in extracting and transporting photogenerated electrons, but also block holes from the perovskite.[12] Thus, ETMs, including organic compounds and inorganic compounds, need to meet several requirements that include possessing suitable band positions and exhibiting high mobility, along with being capable of low-temperature synthesis. For inorganic ETMs, some binary metal oxides, ternary metal oxides, and sulfides have been synthesized and applied in PSCs. Binary metal oxides ETMs include TiO_2, SnO_2, ZnO, WO_x, CeO_x, Nb_2O_5, In_2O_3, etc. Among them, the commonly used are TiO_2, SnO_2, and ZnO. Despite the excellent PCEs, TiO_2 used as ETMs suffer several disadvantages, such as high energy consumption, low electron mobility, and UV-light instability to

perovskite layer. SnO_2 has a deeper CB than TiO_2, which facilitates the extraction and transfer of electrons. In addition, it has a wide band gap, which can reduce the degradation of device performance caused by ultraviolet light. But the SnO_2 thin film is not fully crystallized and the electron mobility is low.[13] With high charge mobility, ZnO can be synthesized at low temperature and applied in flexible devices. However, due to the lewis alkali property of ZnO, the oxygen-containing functional groups on the surface usually initiate proton transfer reaction at the interface with perovskite, which eventually leads to the perovskite film decomposition and reduces the stability of the devices. Compared with binary metal oxides, ternary oxides have excellent electron mobility, tunable band structure, and high chemical stability even under extreme conditions. However, the synthesis of ternary oxides is a complex challenge, which lead to higher energy consumption.[14]

For sulfide ETMs, the interaction of Pb-S can prevent the ion migration of Pb, thereby inhibiting the decomposition of the perovskite. Furthermore, the Pb-S bond can offer a new channel for the transmission and extraction of electrons, leading to passivate interfacial trap states to suppress charge recombination and facilitate the transfer and extraction of charges. Therefore, devices based on sulfide ETMs can achieve high stability.[15] The summary of sulfide ETMs is shown in Table 1.

2.1. 0D sulfide ETMs

In PSCs, 0D sulfide ETMs mainly include ZnS and CdS. Due to a mismatched ELA with the perovskite layer, PSCs based on a ZnS ETM achieve a low PCE (0.98%).[16] Therefore, ZnS is not suitable for direct utilization as an ETM. However, the wide direct bandgap and outstanding mobility (100-150 $cm^2 \cdot V^{-1} \cdot s^{-1}$) of ZnS render it possible to combine with other ETMs to improve the photovoltaic performance of devices.[17] In 2016, Ke et al. found that the mismatched ELA between a TiO_2 ETM and Sn-based perovskite ($FASnI_3$) led to severe carrier recombination and a low PCE. However, the introduction of ZnS, with a high conduction band (CB),

could promote the quasi-Fermi level of TiO_2, resulting in an improved V_{oc}.[17a] Chavan et al. found that the low mobility and surface defects of TiO_2 could be improved by ZnS.[17b] After depositing a ZnS thin film, the CB of the ETM became higher than that of perovskite. The tunneling effect between the ETM and perovskite layer suppressed carrier recombination at the interfaces, leading to a high PCE (19.10%) with low hysteresis due to the improved charge transfer. Subsequently, Chen et al. expanded such an application of ZnS into a ZnO ETM.[17c] They proved that the Pb-S interaction could create a novel pathway for electron transport and suppress recombination, resulting in a PCE of 20.7% with neglectable hysteresis. Tavakoli et al. deposited CdSe/ZnS quantum dots (QDs) as ETMs by a solid-state ligand exchange method. The devices based on the CdSe/ZnS had a better ELA and charge transfer property than TiO_2, resulting in a champion PCE of 18%. The devices showed a much better UV stability than the device based on TiO_2 ETM. It could retain 90% of its initial PCE after 75 h continuous UV illumination.[18]

As a 0D ETM, CdS has some advantages, such as a low cost, high chemical stability, high mobility, and suitable ELA with a perovskite layer.[19] Since Juarez-Perez et al. first reported CdS as an ETM in PSCs, many researchers have explored their applications.[20] Liu et al. introduced PSCs processed at only low temperatures by using CdS.[16] A uniform and compact CdS film was attained by a low-temperature chemical bath deposition (CBD) method at 65°C. A subsequent investigation by Dunlap-Shohl found that Cd could spread to the perovskite, and excessive Cd doping in the perovskite layer could create an insulating barrier, leading to a lower charge transfer rate.[21] To simplify the assembly process of devices, Dong et al. spin-coated redispersible CdS nanoparticles on fluorine-doped tin oxide (FTO) with an annealing-free process and obtained a PCE of 16.5%.[22] By selecting a suitable toluene solvent, they further found that these redispersible CdS nanoparticles could also be used as an ETM in a p-i-n architecture.[23] Liu et al. manufactured a 0D CdS ETM by a low-temperature thermal evaporation approach for rigid and flexible

carbon-based PSCs, which showed good stability and good ultraviolet stability.[24] Ali et al. found that the combination of TiO_2 with CdS QDs could improve the capability of transport and the injection of electrons.[25]

2.2. 1D sulfide ETMs

Compared with 0D sulfide, 1D sulfide nanorods (NRs) can offer a large area for exciton dissociation and provide a direct speedway for electron transfer. In addition, they can play a role in the perovskite scaffold to improve the FF of devices.[26] However, to date, only a 1D CdS ETM has been reported in previous publications. Gu et al. deposited CdS NRs with a hydrothermal process. The investigation showed that thermal annealing and an ultraviolet ozone (UV-ozone) treatment could passivate the S-vacancy defects in CdS NRs, leading to efficient charge transfer.[27] Subsequently, Song et al. fabricated PSCs with a 3D architecture via physical-chemical vapor deposition (P-CVD). By utilizing P-CVD, they obtained a flat and voidless perovskite film and deposited it on the CdS NR ETM, attaining a PCE of 12.46%.[28]

2.3. 2D sulfide ETMs

2D sulfide nanosheets, including SnS_2, TaS_2, and In_2S_3, can enhance the interfacial contact and create direct channels for electron transmission between an ETM and a perovskite layer, resulting in high charge extraction and transport.[29] Due to a limitation in fabrication, 2D sulfide ETMs can only be used in a device with an n-i-p structure.

SnS_2 is a typical 2D sandwich material with high carrier mobility (50 $cm^2 \cdot V^{-1} \cdot s^{-1}$) and nontoxic properties. In 2018, our group was the first to explore hexagonal SnS_2 nanosheets as an ETM in PSCs. The investigation showed that the SnS_2 nanosheets preferentially grew in situ on the FTO substrate.[30] However, the mismatched ELA of the SnS_2 ETM and perovskite caused a low V_{oc} (0.94) and PCE (13.16%). Therefore,

we utilized SnS to adjust the energy level of SnS_2. Three reasons were demonstrated for the choice of SnS. First, the SnS_2 and SnS nanosheets could be synthesized in one pot, leading to a low cost. Second, the higher CB of SnS could provide a much better ELA with perovskite. Third, the high charge mobility of SnS gave rise to faster electron extraction. After the systematic adjustment of the ELA, the V_{oc} was improved from 0.94 to 1.08 V, as shown in Figure 3a.[31] The results showed that even though the CB of SnS_2/SnS was higher than that of perovskite, electrons could be transferred and extracted. Zhao et al. utilized a self-assembly stacking procedure to deposit few-layer SnS_2 and used it as an ETM in PSCs. It was found that 2D SnS_2 could trigger heterogeneous nucleation on the perovskite precursor film, leading to a high-quality perovskite film, as shown in Figure 3b. In addition, the interaction of Pb-S could passivate the interfacial traps and improve the stability of the devices.[15] Chu et al. employed a RT synthesis of SnS_2 as an ETM on flexible PSCs for the first time.[32] PSCs with negligible hysteresis effects were attained due to good electron extraction and large charge recombination resistance.

With high electron mobility (17.6 $cm^2 \cdot V^{-1} \cdot s^{-1}$) and a suitable bandgap, In_2S_3 has been applied in photovoltaic devices and has shown good performance.[33] In 2017, Hou et al. was the first to synthesize In_2S_3 nanosheets at low temperatures (below 80°C). The PCE of PSCs based on an In_2S_3 ETM was 18.22%, which was much higher than that of PSCs based on a TiO_2 ETM (15.70%).[34] Xu et al. utilized the redispersible In_2S_3 nanosheet method to spin-coat an In_2S_3 ETM and obtained a PCE of 18.83%.[35] In 2019, Yang et al. adopted the CBD method to synthesize In_2S_3 and applied it to all-inorganic semitransparent PSCs.[36] Compared with that of a TiO_2 ETM, the CB of an In_2S_3 ETM was closer to the inorganic perovskite $CsPbIBr_2$, which was beneficial for reducing the electronic transfer barrier and resulted in a relatively high efficiency for $CsPbIBr_2$ (5.59%).

2H (double-layered hexagonal)-TaS_2 nanosheets hold several advantages, including being highly flexible and chemically inert while exhibiting high electron

mobility and few traps.[37] By introducing a dopant, the work function (WF) of TaS_2 could be adjusted from 4.4 to 5.1 eV.[38] Afzali et al. directly synthesized 2H-TaS_2 on FTO by a microwave irradiation method. A high-quality 2H-TaS_2 continuous film with good transparency were attained without any thermal annealing. The devices based on the structure of Glass/FTO/2H-TaS_2/$MAPbI_3$/P3HT/Gold achieved an efficiency of 15.23% and retained 90% of its initial PCE under continuous light illumination for 500 hours.[39]

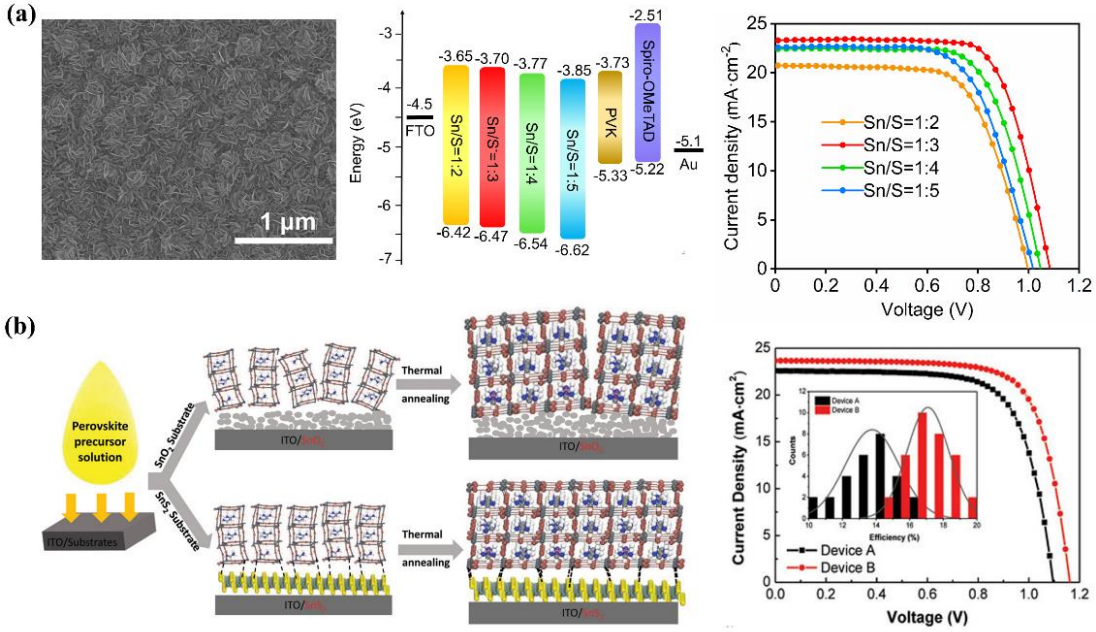

Figure 3. (a) The morphology of SnS_2/SnS nanosheets, the energy levels, and the *J-V* curves of the PSCs based on the different molar ratio of Sn to S.[31] Copyright 2020, American Chemical Society. (b) The interaction diagram of SnS_2 and perovskite; and *J-V* curves (in the reverse scan direction) of devices A based on SnO_2 and devices B based on SnS_2 ETMs, respectively.[15] Copyright 2018 WILEY‐VCH Verlag GmbH & Co. KGaA, Weinheim.

2.4. Amorphous sulfide ETMs

Regarding amorphous materials, the lack of grain boundaries can prevent the penetration of oxygen and moisture, thereby leading to better device stability. At present, the only material used for amorphous sulfide ETMs is Bi_2S_3. In 2016, Li et al.

used a simple thermal evaporation process to prepare amorphous a Bi_2S_3 ETM for PSCs with an inverted architecture (ITO/NiO/$MAPbI_3$/Bi_2S_3/Au). A PCE of 12.3% was obtained due to the advantages of the Bi_2S_3 ETM, such as its high carrier concentration, high carrier mobility (257 $cm^2 \cdot V^{-1} \cdot s^{-1}$), low defect density, and suitable ELA.[40] In addition, a RT thermal evaporation process could minimize the damage of the perovskite layer. Devices based on the Bi_2S_3 ETM retained approximately 80% of their initial PCE and could be stored without encapsulation for 30 days at 25°C and 50−75% humidity.

State-of-the-art, PSCs based on sulfides ETMs have won some achievements. Comparing with others, devices of 2D sulfide ETMs achieve higher PCE. This is because of the excellent properties of 2D materials, such as high carrier mobility and adjustable energy band. Although the PCE of the devices based on 2D sulfide ETMs overed 20%, it is still lower than that of PSCs based on TiO_2 and SnO_2. The reasons could be summarized as follows: First, the 2D sulfide films, fabricated with current methods, are non-uniformity and not compact enough. This inevitably led to some pinholes and serious charge recombination. Second, some sulfide materials have color, which may affect light penetration and light absorption at UV-vis zone, leading to the low J_{sc}.

Despite the enhanced stabilities, the devices based on sulfide ETMs generally show the lower performance than the devices based on commonly used TiO_2 and SnO_2 ETMs. There are two main reasons[41]: one is the unsatisfied ELA of sulfide ETMs and perovskite materials leads to terrible interface energy loss, thus large voltage loss of devices. Second, it is difficult to form a compact sulfide ETMs film, where the surficial defects of sulfide ETMs results in terrible charge recombination. To expand the applications of sulfide ETMs, the element doping and interfacial modification are efficient strategies to regulate the energy level of sulfide ETMs. It is advisable to filtrate out the powerful dopants and modifiers. The micro-level adjustments, including crystal planes, vacancy, and microstructure of the materials,

could be developed to form a pin-hole free sulfide ETMs with lower defects density. Although the PCE of small-area devices based on sulfide ETMs has exceeded 20%, its application and research in the perovskite solar modules (PSMs) are rarely reported. Therefore, it is significant to explore new and suitable sulfide materials and techniques for the PSMs.

Table 1 Summarization of photovoltaic parameters and stability of PSCs based on sulfide ETMs.

Morphology	Formula	CB (eV)	Mobility ($cm^2 \cdot V^{-1} s^{-1}$)	Device Architecture	PCE %	Test conditions	Stability	Ref.
0D	ZnS	-2.5		FTO/ZnS/$MAPbI_3$/Spiro-OMeTAD /Au	0.98	-	-	[16]
	CdS	-	-	FTO/CdS/$MAPbI_3$/Spiro-OMeTAD /Au	1.53	-	-	[20]
		-3.8	4.66	ITO/CdS/$MAPbI_3$/Spiro-OMeTAD/Au	11.17	RH=30-40%, 20-25℃.	24 h,50% of initial PCE	[16]
		-	-	FTO/CdS/$MAPbI_3$/Spiro-OMeTAD/Au	15.24	-	-	[21]
		-3.98	-	ITO/CdS/$MAPbI_3$/Spiro-OMeTAD/Ag	16.1	UV illumination, RH=20-30%, 25℃	10 h,>90% of initial PCE	[42]
		-	-	FTO/CdS/$MAPbI_3$:PbS/Ag	2.98	Ambient conditions	40 d, 50% of initial PCE	[43]
		-3.8	-	FTO/CdS/$MAPbI_3$/Spiro-OMeTAD/Au	2.27	RH=10-20%, RT.	15 d, >68% of initial PCE	[44]
		-	-	FTO/CdS/$Cs_{0.05}(MA_{0.17}FA_{0.83})_{0.95}Pb(I_{0.83}Br_{0.17})_3$/Spiro-OMeTAD/Au	16.5	-	-	[22]
		-3.78	1-10	ITO/CdS/$MAPbI_3$/Spiro-OMeTAD/Au	10.7	-	-	[45]
		-4.2		FTO/CdS/$MAPbI_3$/Spiro-OMeTAD/Ag	14.68	-	-	
		-4.2	-	PET/ITO/CdS/$MAPbI_3$/Spiro-OMeTAD/Ag	9.93	Radius of 8 mm.	100 bending cycles, 49% of initial PCE	[46]
		-3.8		FTO/Cu:NiO_x/$MAPbI_3$/CdS/Au	13.36	RH=45%, 25℃.	144 h, around 85% of initial PCE	[23]
		-4.32	4.66	FTO/CdS/$MAPbI_3$/CuPc/carbon	13.22	RH=30%, RT	500 h, 83.47% of initial PCE	[24]

		-3.9	-	FTO/TiO_2-CdS/$MAPbI_3$/Spiro-OMeTAD/Au	10.52	-	-	[25]
1D	CdS	-	-	ITO/CdS/$MAPbI_3$/Spiro-OMeTAD/MoO_3/Ag	8.36	-	-	[27]
		-4.2	-	FTO/CdS/$MAPbI_{3-x}Cl_x$/Spiro-MeOTAD/Ag	12.46	RH=12%, 18-25℃	4d, 73% of initial PCE	[28]
2D	SnS_2	-4.23	50	FTO/SnS_2/$MAPbI_3$/Spiro-OMeTAD/Au	13.63	-	-	[30]
		-3.70	-	FTO/SnS_2&SnS/ $Cs_{0.05}(FA_{0.83}MA_{0.17})_{0.95}Pb(I_{0.83}Br_{0.17})_3$/Spiro-OMeTAD/Au	18.08	RH=10%, 25℃	500 h, 85% of initial PCE	[31]
		-4.24	7.85×10^{-4}	ITO/SnS_2/$FA_{0.75}MA_{0.15}Cs_{0.1}PbI_{2.65}Br_{0.35}$/Spiro-OMeTAD/Au	20.12	RH=30-40%, RT	600 h, 90% of initial PCE	[15]
		-3.99	-	PEN/ITO/SnS_2/$MAPbI_3$/Spiro/Au	13.20	RH=40-50%, 25℃	30 d, 93% of initial PCE	[32]
	TaS_2	-5.18	-	FTO/2H-TaS_2/$MAPbI_3$/P3HT/Ag	15.23	continuous light illumination	500 h, 90% of initial PCE	[39]
	In_2S_3	-3.98	17.6	FTO/In_2S_3/$MAPbI_3$/Spiro-OMeTAD/Ag	18.22	-	-	[34]
		-3.98	17.6	FTO/In_2S_3/$MAPbI_3$/Spiro-OMeTAD/Au	18.83	UV illumination, ambient conditions	50 h, 81% of initial PCE	[35]
		-3.98	-	FTO/In_2S_3/$CsPbIBr_2$/Spiro-OMeTAD/Ag	5.59	-	-	[36]
Amorphous	Bi_2S_3	3.86	257	ITO/NiOx/$MAPbI_3$/Bi_2S_3/Au	13.1	RH=50-75%, 25℃	30 d, 80% of initial PCE	[40]

3. Chalcogenide Perovskite Materials

Perovskite materials hold a vital position in PSCs and directly influence photovoltaic performance. Due to the introduction of sulfur, the coulomb interaction in chalcogenide perovskite materials is four times stronger than that in their conventional counterparts, leading to improved stability.[47] In addition, the simulation results show that chalcogenide perovskite absorbents are promising candidates for obtaining a high PCE with PSCs.[48] Three strategies have been proposed for obtaining chalcogenide perovskite materials, including perovskite components[49], additives[50], and sulfur-based passivators[51]. The relevant data of PSCs based on chalcogenide perovskite materials are summarized in Table 2.

3.1. Chalcogenide as Perovskite Component

3.1.1. Chalcogenide as Component in 3D Perovskites

The stability of ABX_3 structures can be predicted by a semiempirical geometric parameter, which is referred to as the Goldschmidt tolerance factor (1). Its value is determined by the ionic radii (r_i, i=A, B, X) of each component.

$$t = \frac{r_A + r_X}{\sqrt{2}(r_B + r_X)} \qquad (1)$$

To ensure the ideal photoelectric properties of 3D perovskites, the value of *t* is required to be within the range of $0.81 \leq t \leq 1.0$.[52] Because chalcogenide groups have difficulty meeting suitable radii at the A and B sites, 3D chalcogenide perovskite materials are usually synthesized by replacing atoms at the X site. Depending on whether component B is lead, these materials are divided into lead systems and nonlead systems.

Regarding lead systems, since pseudohalogen thiocyanate ions (SCN^-) hold similar radii and chemical properties compared to I^-, the synthesis of 3D chalcogenide

perovskites of $MAPbI_{3-x}SCN_x$ is possible.[53] Jiang et al. was the first to obtain $MAPbISCN_2$ by replacing two-thirds of the I^- content in typical $MAPbI_3$ with SCN^-. By monitoring perovskite films in the environment with 95% relative humidity (RH) at room temperature (RT), it was found that SCN^- substitution demonstrated significantly improved moisture resistance (Figure 4a).[49] Tai et al. found that even when manufacturing in an ambient environment, the SCN^--based device still obtained a PCE of 15%.[54] To understand how the SCN^- works in regard to its structural and chemical properties, they carried out density functional theory (DFT) calculations. The results showed that there were two types of strong interactions induced by SCN^-: one is coordination between adjacent SCN^- and Pb atoms and hydrogen bonds between MA^+ and SCN^-. Both of these interactions facilitated the stabilization of the $MAPbI_{3-x}SCN_x$ perovskite.

Regarding nonlead systems, sulfur atoms are usually directly substituted for the X site. Nie et al. was the first to report photovoltaic devices based on a lead-free chalcogenide perovskite ($MASbSI_2$), which had a mixture of sulfur and iodine at the X site.[55] The $MASbSI_2$ film was fabricated by a two-step method, as illustrated in Figure 4b. The sulfur-halide-based device manifested outstanding stability, maintaining 90% of its initial PCE after 15 days of storage under environmental conditions with 60% RH without encapsulation. Alternatively, Li et al. applied the low-pressure vapor-assisted solution process (LP-VASP) to precisely control the amount of sulfur in the $MA_3Bi_2I_{9-2x}S_x$ film and successfully regulated the bandgap of a bismuth-based perovskite material.[56] However, due to its ultralow current density (J_{sc}, 0.58 $mA \cdot cm^{-2}$), the PCE was only 0.152%.

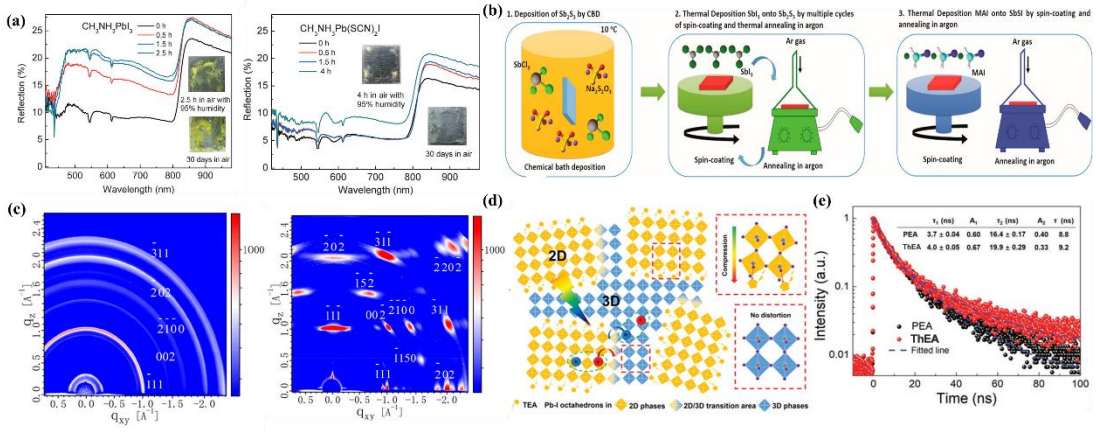

Figure 4. (a) Reflection of the perovskite materials with $MAPbI_3$ (left) and $MAPb(SCN)_2I$ (right) in air with 95% RH;[49] Copyright 2015, WILEY‐VCH Verlag GmbH & Co. KGaA, Weinheim. (b) Detailed process for the preparation of $MASbSI_2$ perovskite film;[55] Copyright 2018, American Chemical Society. (c) Grazing incidence wide-angle X-ray spectrum (GIWAXS) for polycrystalline 2-$ThMA_2MA_{n-1}Pb_nI_{3n+1}$ (n=3) films formed with MACl/MAI weight ratios of 0 (left) and 0.5 (right);[57] Copyright 2018, American Chemical Society. (d) Schematic demonstration of 2D/3D mixed phase in 2-ThEA perovskite material;[58] (e) Time-resolved photoluminescence (TRPL) decays of TEA and PEA based perovskite films and the their lifetime;[58] Creative Commons CC BY license.

3.1.2. Chalcogenide as Component in 2D Perovskites

A pseudohalogenated 2D perovskite ($MA_2PbSCN_2I_2$) has a desirable concentration of holes (1.07×10^{14} cm^{-3}) and good carrier mobility (>1 $cm^2\cdot V^{-1}\cdot s^{-1}$), and these values are comparable to $MAPbI_3$.[59] The calculations from a further investigation reveal that $MA_2PbSCN_2I_2$ will demonstrate a p-type character with a long carrier lifetime with less Pb and more I.[60] Liu et al. found that the solubility and crystallinity of $MA_2PbSCN_2I_2$ could be improved by replacing the commonly used solvent with tetrahydrofuran (THF), a solvent with a low boiling point.[59b] By a convenient solution-deposition process without an annealing treatment, they obtained an $MA_2PbSCN_2I_2$ film with excellent morphology and a high fill factor (FF) of 73%

PSCs. Furthermore, compared with a planar architecture, Guo et al. indicated that a mesoporous scaffold was more beneficial for forming a high-quality 2D perovskite $MA_2PbSCN_2I_2$ film, which led to enhanced light absorption and suppressed charge recombination.[61]

Ruddlesden-Popper (RP) phase 2D perovskite $M_2A_{n-1}B_nX_{3n+1}$ materials are obtained by cutting a 3D perovskite along the (100) crystal plane and inserting a large volume of organic amine ions M^+ as a spacer.[62] The new organic amine groups provide an ideal platform for the design of new chalcogenide materials. Lai et al. was the first to investigate a chalcogenide perovskite ($2\text{-}ThMA_2MA_{n-1}Pb_nI_{3n+1}$) with 2-thiophenemethylammonium (2-ThMA) as the spacer cation.[57] The 2D perovskite $2\text{-}ThMA_2MA_2Pb_3I_{10}$ revealed a nearly single-crystal nanorod morphology and strong perpendicular growth in relation to the substrate by using an MACl additive, as shown in Figure 4c. The PCE of the device dramatically increased from 1.74% to 15.42% with the MACl additive. Alternatively, Yan et al. introduced 2-thienylethylamine (2-ThEA) as a spacer and stabilizer for the perovskite lattice.[58] The spontaneous growth of a 3D perovskite embedded in a 2D perovskite matrix (Figure 4d), where the 2D perovskite materials could form bulk heterojunctions with the 3D perovskite by the Pb-S interaction-induced epitaxial growth. Therefore, compared to the phenethylamine-based perovskite, the 2-ThEA-based counterpart had a long carrier lifetime (Figure 4e), leading to improved photocurrent and efficiency values. Recently, Ren et al. reported the utilization of 2-(methylthio) ethylamine (MTEA) as an organic amine spacer.[63] The S-S interlayer interaction between MTEA molecules resulted in remarkably improved carrier transport and an ultrahigh efficiency of 18.02%. Moreover, the molecular interaction of the additional interlayer also significantly improved the stability of the 2D RP perovskite. After continuous operation at the maximum power point (MPP) for 1000 hours under continuous illumination, the related devices still maintained more than 85% of their initial efficiency.

Generally, the introduction of sulfur can effectively improve the stability of

perovskite materials. The chalcogenide component in the 3D perovskite can provide a stronger force to stabilize the crystal lattice of the perovskite. Besides the above roles, the chalcogenide component in the 2D perovskite can also be used as a spacer layer to block moisture adsorption and ion migration. However, the PCE of PSCs with chalcogenide compounds usually reduced with this stability improvement. State-of-the-art, PSCs based on perovskite materials with chalcogenide compounds show PCE lower than 20%.

3.2. Sulfur-based Additives

From the different roles, additives in perovskite materials are generally divided into ionic liquids, Lewis acids, and Lewis bases.[51] Ionic liquids are often used to control the crystallization process of perovskites to obtain high-quality perovskite films, due to their strong electrostatic force and high solubility for various organic and inorganic compounds.[64] Lewis acids mainly include fullerene derivatives and metal cations, which are employed to passivate the electron-rich defects caused by excessive halide via forming Lewis adducts.[65] Lewis bases usually act as electron donor and coordinate with the uncoordinated Pb^{2+} to form Lewis adducts.[66] Sulfur-based additives, including sulfur atoms with lone electron pairs, are classified as Lewis base additives. Meanwhile, previous researches indicated that sulfur, as a softer donor atoms, performs stronger electron donating capacity than oxygen and nitrogen.[67] Sulfur-based additives have played roles in stabilizing precursors[6c], controlling crystallization kinetics[68], and improving phase stability[69]. Generally, they are divided into inorganic sulfur-based additives and organic sulfur-based additives.

Among the sulfur-based inorganic additives, SCN^- takes effect in both crystallization regulation and stability enhancement. For 3D perovskites, due to the linear structure of the SCN^- group, they can form a strong coordination with Pb^{2+} ions. Therefore, perovskite with the SCN^- additive had a low capture density and good intrinsic stability.[70] Additionally, such an interaction is also confirmed to maintain

the high-activity α-$FAPbI_3$ phase for FA-based perovskites at environmental temperatures (Figure 5a).[71] For 2D perovskite materials, the growth orientation has a considerable influence on the charge transport between layers, where the ideal condition is vertical growth. However, the principle of minimum energy induces the tendency of 2D perovskite to grow parallel to the substrate.[72] This problem can be addressed by proper amounts of SCN^- additives. Since the exposed end of the SCN^- group is negatively charged, it can induce electrostatic interactions with positively charged cations in the perovskite precursor (Figure 5b), resulting in the vertically oriented growth of 2D perovskite in Figure 5c.[73] Moreover, the investigation of Zhang et al. suggested that the energy band structure of 2D perovskite would also shift with the introduction of SCN^-.[73b] This feature will help establish better energy level alignment (ELA) within the device (Figure 5d). However, the introduction of SCN^- also promoted carrier recombination in the perovskite layer.[74] Therefore, a small amount of SCN^- is preferred.

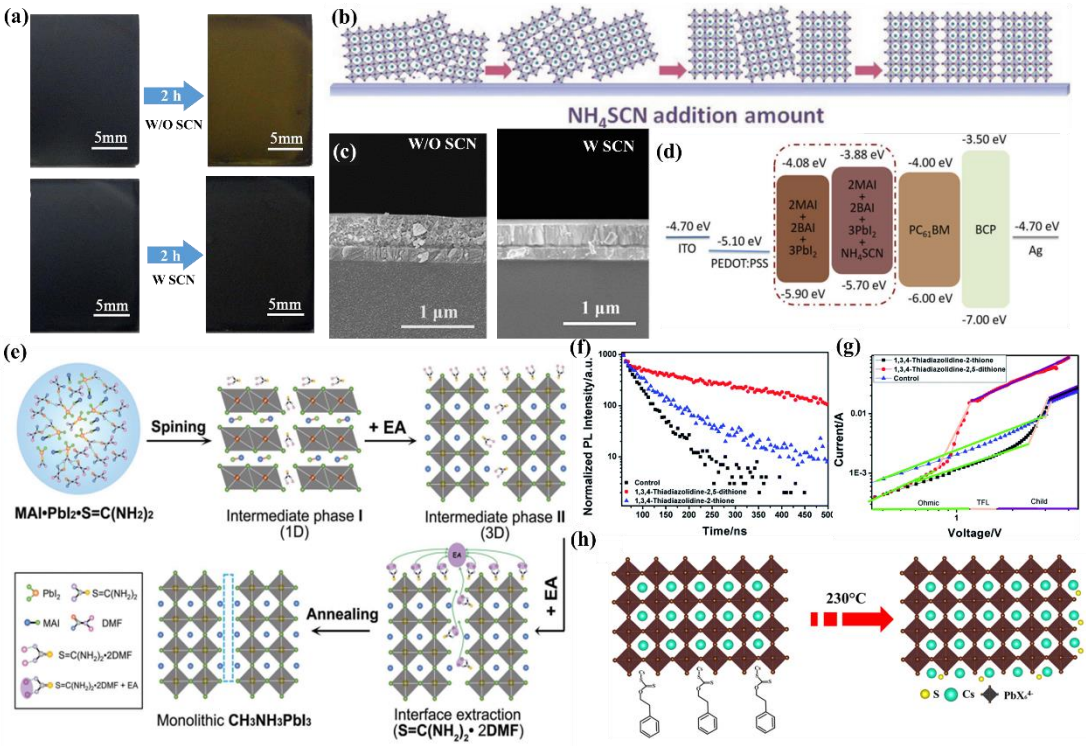

Figure 5. (a) Digital photography of $FAPbI_3$ perovskite films without (above) and with (bottom) SCN additives;[71] Copyright 2016, Royal Society of Chemistry. (b)

Schematic diagram of 2D perovskite growing along the vertical substrate with the increase of SCN^- addition;[73a] Copyright 2019, WILEY‐VCH Verlag GmbH & Co. KGaA, Weinheim. (c) Cross-sectional SEM images and (d) ELA of 2D perovskite layer with and without SCN additive;[73b] Copyright 2017, WILEY‐VCH Verlag GmbH & Co. KGaA, Weinheim. (e) Schematic diagram of the effect of thiourea as an additive on the perovskite crystallization process;[75] Copyright 2016, WILEY‐VCH Verlag GmbH & Co. KGaA, Weinheim. (f) TRPL spectra of perovskite films with and without organic sulfur-based additives and (g) space-charge-limited current (SCLC) of ITO/perovskite/Au constructed device;[76] Copyright 2016, Royal Society of Chemistry. (h) Schematic demonstration of sulfur doping in $CsPbIBr_2$ perovskite and its phase transition. [6d] Copyright 2019, Elsevier.

The typical representatives organic sulfur-based additives are thioacetamide (TAA)[77], thiourea[78], thiophene derivatives[79]. As illustrated in Figure 5e, because of the empty outer orbital provided by S, these additives induce strong coordination with the Pb in the perovskite precursor.[75, 80] Their function is to form a stable intermediate with PbI_2 in the precursor solution and then slowly release as the solvent volatilizes to control the crystallization dynamic.[75] This behavior is beneficial to form better crystallization, , enhance charge lifetime (Figure 5f) and reduce defect density (Figure 5g).[29] The improvement in crystallinity also contributes to eliminating the grain boundaries and inducing a more substantial tolerance to humidity.[76] Moreover, the strong electronegativity of S leads to a low free energy barrier of the phase transition (Figure 5h). This will accelerate the $CsPbIBr_2$ transition into the α-phase and suppress phase separation.[6d]

3.3. Sulfur-based Interface Passivators

Non-radiative recombination has a significant impact on the performance of the devices, which mainly comes from the defects at the perovskite/charge transport layer (CTL) interface.[81] Meanwhile, the defects will also weaken the stability of PSCs,

leading to rapid degradation. Interface passivators are regarded as an effective strategy to suppress the defects and achieve efficient and stable PSCs.

Different passivators have different passivation mechanisms. Sulfur-based passivators work with two different kinds of passivation mechanisms. One is that it can form coordination bonds to passivate the defects of the perovskite surface by accepting the external electron cloud because the outer layer of sulfur atoms has empty orbitals (Figure 6a);[82] the other is that the defects, caused by excessive PbI_2, can be reacted with chalcogenide amine salts, which convert PbI_2 to a 2D chalcogenide perovskite. The 2D chalcogenide perovskite cannot only establish type-I band alignment (Figure 6b) but also act as a barrier to humidity and ion migration, leading to a material with significantly enhanced efficiency and stability.[83]

Thiophene and its derivatives are typical representatives for passivating by coordination bonds.[84] In 2014, Noel et al. was the first to reveal that thiophene could alleviate nonradiative recombination at the interface.[85] After interfacial passivation, the efficiency of the devices increased from 13 to 15.3%. Thiophene and its derivatives are S-donor Lewis bases. Their ability to enhance the photovoltaic performance of PSCs is mainly divided into two factors. On the one hand, owing to the empty orbitals of sulfur atoms, they can effectively coordinate to form adducts with uncoordinated Pb^{2+} or Pb clusters.[51] These adducts will change the position of the electron wave function and keep the electron cloud density away from the surface of perovskite, which is deemed the site of charge recombination.[86] On the other hand, the TRPL decay spectra in Figure 6c shows that the delocalized π-electrons in thiophene rings are considered to be beneficial for fast hole transfer and extraction at the perovskite/HTM interface.[82, 87]

Some functional molecules involving sulfur atoms can also form coordination bonds with perovskites. Yang et al. introduced 3-pyridyl isothiocyanate (Pr-ITC) and phenylene-1,4-diisothiocyanate (Ph-DITC) into an $MAPbI_3$/CuSCN interface.[88] As shown in Figure 6d, Ph-DITC contains two separate -NCS groups, which could

interact with both the Pb in perovskite and the Cu^{+} in CuSCN. Moreover, Pr-ITC could also induce Pb···N interactions with perovskite and Cu···S interactions with CuSCN. The mixture of Pr-ITC and Ph-DITC could not only eliminate defects on the perovskite surface but also connected the perovskite and CuSCN layers, resulting in PSCs with high photovoltaic performance and stability. Alternatively, Hou et al. reported a novel sulfur-oleylamine (S-Oam) precursor for the convenient treatment of perovskite.[89] The precursor produced H_2S and oleylammonium polysulfides (OPs), and then the perovskite film was etched by H_2S and became smooth (Figure 6e). The OPs formed a hydrophobic cover on the surface of the perovskite film by self-assembly. These effects led to devices with excellent efficiency and stability. Yang et al. proposed a strategy of converting the surfaces of lead halide perovskite to water-insoluble oxysalt of Pb^{2+} via reaction with SO_4^{2-}.[90] This $PbSO_4$ layer can stabilize the perovskite materials though forming strong chemical bonds to enhance the hydrophobic property of perovskite. The $PbSO_4$ layers also decreased the defect density on the perovskite surfaces via Pb-S interaction and increased the carrier recombination lifetime of perovskite. Thus, this $PbSO_4$ passivation layer boosted the PCE of PSCs to 21.1%. The passivated devices with encapsulation remained 96.8% of their initial PCE after MPP tracking under AM 1.5 G irradiation for 1200 hours at 65 °C. Mahapatra et al. further proved that $PbSO_4$ passivator processed the capability to annihilate the defects and restrain the unexpected ion migration in the $MAPbBr_3$ single crystals.[91] Results indicated that the interaction between sulfate ions and Pb^{2+} in the $[PbX_6]^{4-}$ octahedral cage occurred, which demonstrated that $PbSO_4$ successfully suppressed the lower-frequency ionic migration in $MAPbBr_3$ under different temperature, resulting in higher average ion migration activation energy as Electrochemical impedance spectroscopy (EIS) in Figure 6f. Additionally, $PbSO_4$ passivation can stabilize the surface of perovskite and improve the hysteresis characteristics induced by high temperature. Recently, Li et al. designed a sulfur-rich bifunctional molecule (SMe-TATPyr) as the passivator. It could not only passivate the

defects in the surface of perovskite, but also promote the hole transfer at the perovskite/HTMs interface, which is similar as the thiophene derivatives. Moreover, this simple interfacial passivation could also improve the stability of PSCs to keep 95% of its initial PCE after stored at ambient environment for 1500 hours, while its control counterpart only maintained only 70%.[92]

The essence of passivation by a 2D chalcogenide amine salt is that it converts PbI_2 to form a chalcogenide 2D perovskite, which mainly has two roles. One is that the wide bandgap of a 2D chalcogenide perovskite can establish a type-I band alignment with a 3D perovskite.[93] The electron barrier formed by the type-I band alignment will effectively suppress the nonradiative carrier recombination between crystal grains or at the perovskite/CTL interfaces.[51] Hu et al. fabricated PSCs with 2D/3D heterostructures by utilizing a 2D chalcogenide amine salt (S-benzyl-1-cysteine (SBLC)) as a passivator.[94] Due to the suppressed recombination in the device (Figure 6g), a high open-current voltage (V_{oc}) of 1.2 V was obtained, which was close to 91% of the Shockley-Queisser limit. On the other hand, the 2D chalcogenide perovskite could also suppress ion migration and act as a moisture barrier for the 3D perovskite on the bottom. The stability, tracked by Hu et al., demonstrated that the device with 2D/3D heterostructures showed an outstanding lifetime compared with the lifetime of a 3D control device. The unencapsulated device retained 80.9% of its initial PCE after 30 days of storage, whereas its 3D counterpart decreased dramatically to 15.6% of its initial value.[94] Recently, Sutanto et al. illustrated the mechanisms of thiophene-based 2D amines as interfacial passivators (Figure 6h).[83] The results showed that the 2D/3D interface constructed by a 2D chalcogenide perovskite was a dynamic phase transition process. Thus, choosing structurally stable 2D amine salts, such as 2-ThEA, could physically prevent ions from moving at the interface and avoid the formation of a quasi-2D perovskite, thereby improving the stability of the device.

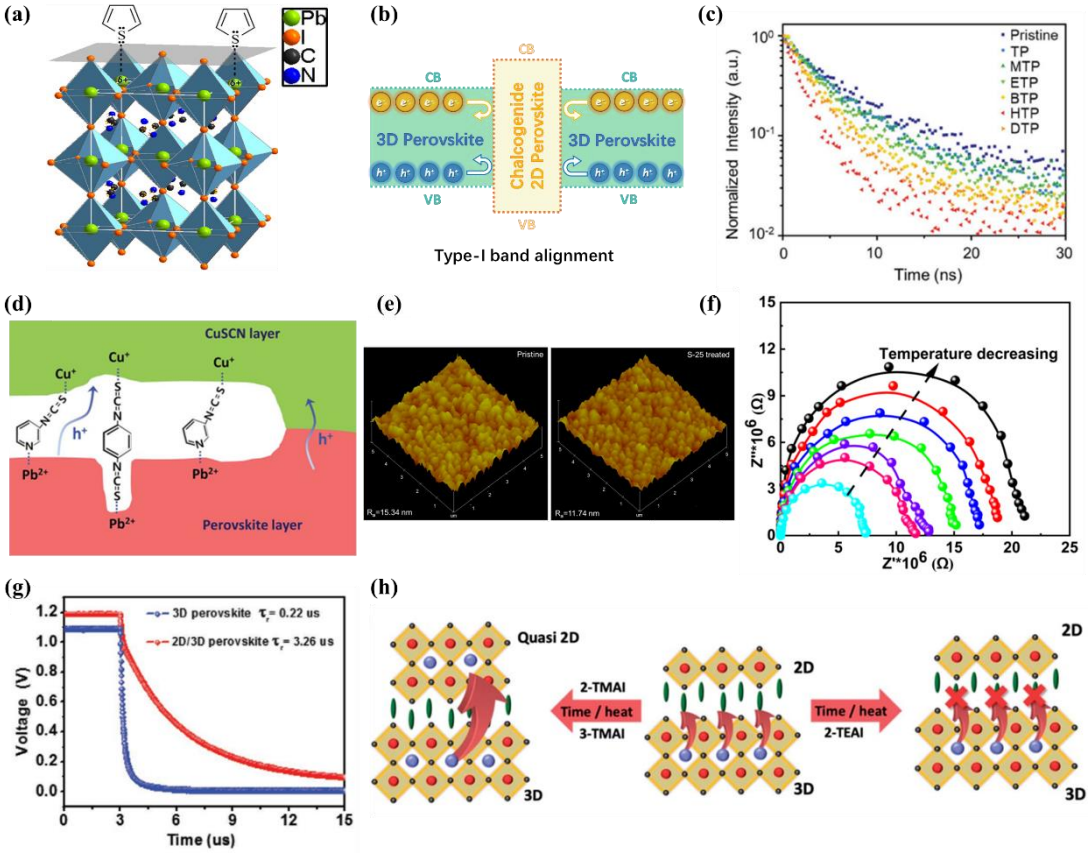

Figure 6. (a) Thiophene molecules coordinate with Pb in perovskite lattice, neutralizing the redundant positive charge;[85] Copyright 2014, American Chemical Society. (b) type-I band alignment at chalcogenide 2D perovskite/3D perovskite interface; (c) TRPL spectra for glass/$MAPbI_3$/2,2',7,7'-Tetrakis[N,N-di(4-methoxyphenyl)amino]-9,9'-Spirobifluoren e (Spiro-OMeTAD) and glass/$MAPbI_3$/thiophene derivatives/Spiro-OMeTAD;[82] Copyright 2018, WILEY‐VCH Verlag GmbH & Co. KGaA, Weinheim. (d) Schematic diagram of the mechanism of employing Pr-ITC and Ph-DITC as the interfacial modification;[88] Copyright 2019, Royal Society of Chemistry. (e) Atomic force microscopy (AFM) roughness images of pristine and S-Oam treated perovskite film;[89] Copyright 2018, Royal Society of Chemistry. (f) Temperature-dependent dark EIS measurements of the $PbSO_4$ passivated $MAPbBr_3$ single crystal;[91] Copyright 2020, AIP Publishing. (g) Transient photovoltage decay of 3D and 2D chalcogenide perovskite treated films;[94] Copyright 2020, WILEY‐VCH Verlag GmbH & Co. KGaA, Weinheim. (h) Schematic diagram of the dynamic process of thiophene based

2D amine passivating the surface of 3D perovskite.[83] Copyright 2019, Royal Society of Chemistry.

Table 2 Summarization of performance parameters of PSCs based on chalcogenide perovskite materials.

Strategy	Device Architecture	PCE %	Test conditions	Stability	Ref.
Chalcogenide as Perovskite Component	ITO/PEDOT:PSS/MAPbISCN$_2$/PCBM/Al	11.07	Continuous a sunlight irradiation, ambient environment	1 h, 92% of the initial PCE	[53]
	FTO/c&m-TiO$_2$/MAPbISCN$_2$/Spiro-OMeTAD/Au	8.3	-	-	[49]
	FTO/c&m-TiO$_2$/MAPbISCN$_2$/Spiro-OMeTAD/Au	15.12	RH=70%, RT	500 h, 86.7% of the initial PCE	[54]
	FTO/c&m-TiO$_2$/MASbSI$_2$/PCPDTBT/Au	3.11	RH=40%, 85 ℃	30 d, 91% of the initial PCE	[55]
	FTO/c&m-TiO$_2$/MA$_3$Bi$_2$I$_{9-2x}$S$_x$/Spiro-OMeTAD/Au	0.15	-	-	[56]
	ITO/PEDOT:PSS/2-ThMA$_2$MA$_2$Pb$_3$I$_{10}$/PCBM/BCP/Ag	15.42	RH=30%, RT	1000 h, 90% of the initial PCE	[57]
	ITO/PEDOT:PSS/2-ThEA$_2$MA$_3$Pb4I$_{13}$/PCBM/BCP/Ag	11.32	RH=60%, 25 ℃	270 h, 80% of the initial PCE	[58]
	ITO/PEDOT:PSS/ThDMA$_2$MA$_4$Pb$_5$I$_{16}$/PCBM/BCP/Au	15.75	Light soaking, N$_2$, RT	162 h, 90% of the initial PCE	[95]
	ITO/PEDOT:PSS/ThFA$_2$MA$_2$Pb$_3$I$_{10}$/PCBM/BCP/Au	16.72	Light soaking, N$_2$, RT	216 h, 90% of the initial PCE	[96]
	ITO/PEDOT:PSS/MTEA$_2$MA$_4$Pb$_5$I$_{16}$/PCBM/BCP/Ag	18.06	Conditions operation at the MMP under 1sun irradiation, N$_2$, RT	1000 h, 87.1% of the initial PCE	[63]
	FTO/c&m-TiO$_2$/MA$_2$PbSCN$_2$I$_2$/Spiro-OMeTAD/Au	0.49	-	-	[61]
	FTO/c&m-TiO$_2$/MA$_2$PbSCN$_2$I$_2$/Spiro-OMeTAD/Au	3.23	-	-	[59b]

Sulfur-based Additives	FTO/c-TiO_2/$MAPbI_3$($MASCN^a$)/Spiro-OMeTAD/Au	18.22	-	-	[70a]
	ITO/PEDOT:PSS/$MAPbI_3$(NH_4SCN^a)/PCBM/LiF/Al	16.47	RH=70%, RT	250 h, 75% of the initial PCE	[70b]
	FTO/c-TiO_2/$FAPbI_3$(NH_4SCN^a)/Spiro-OMeTAD/MoO_3/Ag	11.44	Continuous a sun light irradiation under ambient conditions, RH= 30%, RT	1 h, about 90% of the initial PCE	[71]
	ITO/PEDOT:PSS/$BA_2MA_4Pb_5I_{16}$(NH_4SCN^a)/PCBM/BCP/Ag	8.79	-	-	[73b]
	ITO/PTAA/$BDAMA_4Pb_5I_{16}$(NH_4SCN^a)/PCBM/BCP/Ag	14.53	RH=50%, RT	900 h, 90% of the initial PCE	[73a]
	ITO/SnO_2/$MAPbI_3$(TAA^a)/Spiro-OMeTAD/Au	18.9	RH=25~35%, RT	816 h, 88.9% of the initial PCE	[77]
	FTO/c-TiO_2/$MA_{0.9}FA_{0.1}PbI_3$(thiourea^a)/Spiro-OMeTAD/Au	19.57	Conditions operation at (MMP) at the atmosphere condition, RH=15%, 20 ℃	60 d, 98% of the initial PCE	[78]
	FTO/c&m-TiO_2/$MAPbI_3$(2-pyridylthiourea^a)/Spiro-OMeTAD/Au	18.2	RH=30%, 65 ℃	30 d, 95% of the initial PCE	[79]
	FTO/PEDOT:PSS/$(FAPbI_3)_{0.95}(MAPbBr_3)_{0.05}$($S8^a$)/PTAA/BCP/Ag	20.91	-	-	[6c]
	ITO/SnO_2/$MA_{0.15}FA_{0.85}PbI_3$(2-$ThMA^a$)/Spiro-OMeTAD/Au	21.49	Continuous light soaking (100 mW cm^{-2}) in N_2	1680 h, over 99% of the initial PCE	[68]
	ITO/SnO_2/ $CsPbIBr_2$($CsXth^a$)/P3HT/Au	9.78	RH=65%, RT	10 h, without any degradation	[6d]
Sulfur-based Interface Passivators	FTO/c-TiO_2/$MAPbI_3$/thiophene^b/Spiro-OMeTAD/Au	15.3	-	-	[85]
	FTO/c-TiO_2/$MAPbI_3$/OPs^b/Spiro-OMeTAD/Ag	15.71	RH=40 ±10%, RT	14 d, 70% of the initial PCE	[89]
	FTO/c&m-TiO_2/$MAPbI_3$/Pr-ITC+Ph-$DITC^b$/CuSCN/Au	18.57	RH=30±5%. 25 ℃	200 d, 86% of the initial PCE	[88]
	FTO/c&m-TiO_2/$Cs_{0.08}MA_{0.12}FA_{0.8}PbI_{2.4}Br_{0.6}$/2-$ThEAI^b$/Spiro-OMeTAD/Au	20.59	Continuous 1 sun illumination in an Ar	1000 h, 90% of the	[83]

			atmosphere	initial PCE	
	ITO/PTAA//CsFAMA-perobskite/$PbSO_4$[b]/C_{60}/BCP/Cu	21.1	Conditions operation at (MMP) at the 65 ℃	1200 h, 96.8% of the initial PCE	[90]
	FTO/TiO_2-SnO_2/$MAPbI_3$/PbS_x[b]/Spiro-OMeTAD/Ag	19.45	Dark desiccator	30 d, 95% of the initial PCE	[97]
	ITO/SnO_2/$FA_{1-x}MA_xPbI_3$/SMe-TATPyr[b]/Spiro-OMeTAD/Au	22.34	Ambient conditions	1500 h, 95% of the initial PCE	[92]
	ITO/PTAA/$MAPbI_3$/SBLCI[b]/PCBM/BCP/Au	20.14	RH=50% ±10%, RT	30 d, 80.9% of the initial PCE	[94]
	ITO/SnO_2/$CsPbIBr_2$/ATI[b]/P3HT/Au	13.91	RH=65%, 80 ℃	200 h, 85% of initial PCE.	[87]
	FTO/TiO_2/Sb_2S_3[b]/$CsPbIBr_2$/P3HT/Au	9.31	RH=65%, 80 ℃	30 h, 90% of the initial PCE	[98]
	ITO/PTAA/WS_2[b]/$Cs_{0.05}MA_{0.05}FA_{0.9}PbI_{2.7}Br_{0.3}$/PCBM/BCP/Ag	21.1	-	-	[99]

“a” is referred to as additive materials.

“b” is referred to as passivation materials.

PCBM is [6,6]-phenyl-C61-butyric acid methyl ester.

BCP is 2,9-Dimethyl-4,7-diphenyl-1,10-phenanthroline.

4. Chalcogen Compound HTMs

HTMs have the following three functions: (1) improving hole extraction and transport efficiency; (2) avoiding damage to devices caused by the direct contact of the metal counter electrode and perovskite; and (3) separating the top electrode from the bottom electrode to suppress charge recombination. Spiro-OMeTAD is a commonly used HTM in high-efficiency devices. Nevertheless, due to dopant molecules, devices based on Spiro-OMeTAD show poor stability.[100] To cope with the commercial demand of PSCs, multiple alternatives to Spiro-OMeTAD have been reported. Among them, chalcogen compound HTMs usually demonstrate high mobility as well as superior stability and are considered potential competitors. In this section, chalcogen compound HTMs are divided into inorganic and organic categories.

4.1. Inorganic Chalcogen Compound HTMs

Compared with organic chalcogen compound HTMs, p-type inorganic chalcogen compound HTMs possess excellent intrinsic hole mobility and electrical conductivity. Therefore, they can achieve high efficiency without dopants. Moreover, they usually exhibit outstanding hydrophobic properties, thereby helping resist degradation due to humidity. Detailed photovoltaic performances based on inorganic chalcogen compound HTMs are summarized in Table 3.

CuSCN, with high hole mobility and a suitable ELA with perovskite, is a typical representative of inorganic chalcogen compound HTMs (Figure 7a). To obtain high-efficiency devices based on CuSCN, three matters need to be considered. First, device architecture has a critical effect. For a p-i-n architecture, the roughness of the CuSCN surface will affect the crystallization process of the perovskite layer. Therefore, CuSCN is more suitable for use in an n-i-p architecture (Figure 7b).

Second, the solvent selection is important because the solvent needs to be able to highly dissolve CuSCN while avoiding perovskite damage. Third, preparation techniques are vital because they not only maintain the flatness of the CuSCN film but also prevent perovskite layer destruction.

Ye et al. was the first to report CuSCN as an HTM in PSCs with a p-i-n architecture and compared perovskite fabrication methods for a CuSCN HTM.[101] Wijeyasinghe et al. synthesized a CuSCN HTM by changing conventional diethyl sulfide (DES) solvents to aqueous ammonia (NH_3 aq).[102] The results showed that the complexation between CuSCN and NH_3 (Figure 7c) led to the CuSCN HTM having high compositional purity, enhanced hole mobility (0.1 $cm^2 \cdot V^{-1} \cdot s^{-1}$), and superior planarization. Furthermore, they achieved a PCE of 17.5%. However, other investigations suggested that the uneven CuSCN surface was not favorable for the crystallization of perovskite.[103] Thus, since Ito et al. first developed CuSCN in n-i-p PSCs and obtained a PCE of 4.86%[104], multiple investigations have focused on applying CuSCN to this architecture.[105] Qin et al. deposited a CuSCN film by a low-temperature solution deposition method onto an optimized perovskite film and increased the PCE to 12.4%.[106] In 2018, Arora et al. reported a high-performance PSC with an n-i-p architecture that exceeded 20% PCE and was fabricated with a CuSCN HTM.[107] They revealed the mechanism of potential-induced degradation of the CuSCN/Au contact. Therefore, a reduced graphene oxide (rGO) spacer was applied to separate the CuSCN and Au. The corresponding device exhibited superstability, with an initial efficiency of over 95% after tracking its MPP at 60°C in a nitrogen atmosphere for 1000 hours. Liu et al. further replaced rGO with dithiophene-benzene (DTB), which not only prevented the potential-induced degradation of the CuSCN/Au contacts but also modified the ELA and promoted carrier extraction and transportation (Figure 7d).[108] The relevant device achieved an ultrahigh PCE of 22.0%, which is the recorded value for CuSCN-based PSCs.

To highly dissolve CuSCN and avoid perovskite damage in PSCs with an n-i-p

architecture, the commonly used solvent for CuSCN HTMs is mercaptan. Qin et al. revealed that even if weakly polar dipropyl sulfide (DS) was used as the solvent, the perovskite layer would dissolve and lead to an increase in contact between the TiO_2 and CuSCN layers. This increased contact led to an accumulation of charge that could effectively pass through the contact and recombine.[106] To solve this problem, Murugadoss et al. reported the effect of a compound solvent.[109] They tried several types of mixed solvents, including a mixture of DS+chlorobenzene (1:1), isopropanol (IPA)+methylammonium iodide (MAI, 10 mg/mL), and DS+IPA (1:2)+MAI (10 mg/mL) to dissolve CuSCN. The results suggested that the perovskite layer was most stable if CuSCN was coated with the solvent (a mixture of DS+IPA (1:2)+MAI (10 mg/mL)).

Several commonly used, state-of-the-art approaches (Figure 7e) have been applied to fabricate CuSCN HTMs, including doctor-blading[110], drop-casting[111], spray-coating[112], and spin-coating[113]. Ito et al. was the first to prepare a CuSCN film by doctor-blading and obtained a PCE of 4.85%.[104] However, the doctor-blading approach exhibited difficulty for controlling the thickness of the CuSCN film. A CuSCN film that is too thick will lead to a high series resistance, which is harmful to charge transport.[114] Chavhan et al. proposed a drop-casting method to control the thickness of CuSCN HTMs and increased the PCE to 6.4%.[115] Liu et al. reported a spray-coating technique to deposit a CuSCN layer on a perovskite substrate.[112] By controlling the spray-coating speed, they obtained a uniform CuSCN HTM film, and the relevant devices showed 13.3% PCE and considerable reproducibility. The spin-coating approach was first adopted to fabricate CuSCN films in PSCs with a p-i-n architecture by Zhao et al.[116] Jung et al. extended this spin-coating approach into PSCs with an n-i-p architecture and obtained a high PCE of 18.0%.[117] Compared with other techniques, the spin-coating approach can achieve a uniform morphology and prevent the perovskite from being damaged by the solvent.[118]

CuSCN can also be utilized as a dopant to other HTMs for enhancing their

conductivity, hole extraction ability, and hydrophobic stability. Li et al. utilized a CuSCN dopant into Spiro-OMeTAD, which could suppress the crystallization and aggregation of Spiro-OMeTAD and resulted in an efficient hole extraction ability.[119] The PCE of relevant devices improved from 14.82 to 18.02%. Additionally, the introduction of CuSCN enhanced the humidity resistance of the device. The unencapsulated devices based on CuSCN-doped Spiro-OMeTAD retained 60% of their initial PCE after 180 hours of storage in an atmosphere with 25% RH, while the devices based on pristine Spiro-OMeTAD only maintained 35% PCE under the same conditions. Liu et al. further investigated the effect of a CuSCN-doped poly(triarylamine) (PTAA) layer in PSCs.[120] The CuSCN dopant could promote the crystallization and hole transport of the PTAA HTM, leading to PSCs with an enhanced PCE and stability, while exhibiting negligible hysteresis. Xiong et al. applied CuSCN as a dopant into PEDOT:PSS.[121] The results showed that CuSCN significantly modified the ELA of PEDOT:PSS to diminish the energy loss at the perovskite/HTM interface (Figure 7f), resulting in efficient carrier transport (Figure 7g). Moreover, Xu et al. suggested that the CuSCN dopant in PEDOT:PSS could contribute to the smooth surface of the HTM (Figure 7h), resulting in the improved crystallinity of $MAPbI_3$.[122]

Alternatively, CuSCN can maintain both high transparency (Figure 7i) and excellent hole transport ability (Figure 7j); thus, CuSCN can be used in semitransparent PSCs. Jung et al. was the first to adopt a CuSCN HTM into p-i-n semitransparent PSCs.[123] The relevant device obtained a PCE exceeding 10% and an average visible-light transmittance of 25%. Fan et al. further developed CuSCN-based bifacial semitransparent PSCs with an n-i-p planar architecture (Figure 7k).[124] The front and rear incidence of the devices obtained PCEs of 12.47 and 8.74%, respectively. Subsequently, Wang et al. fabricated bifacial colorful semitransparent PSCs with a CuSCN HTM, which were suitable for settings with substantial shading requirements, such as shading sheds.[125]

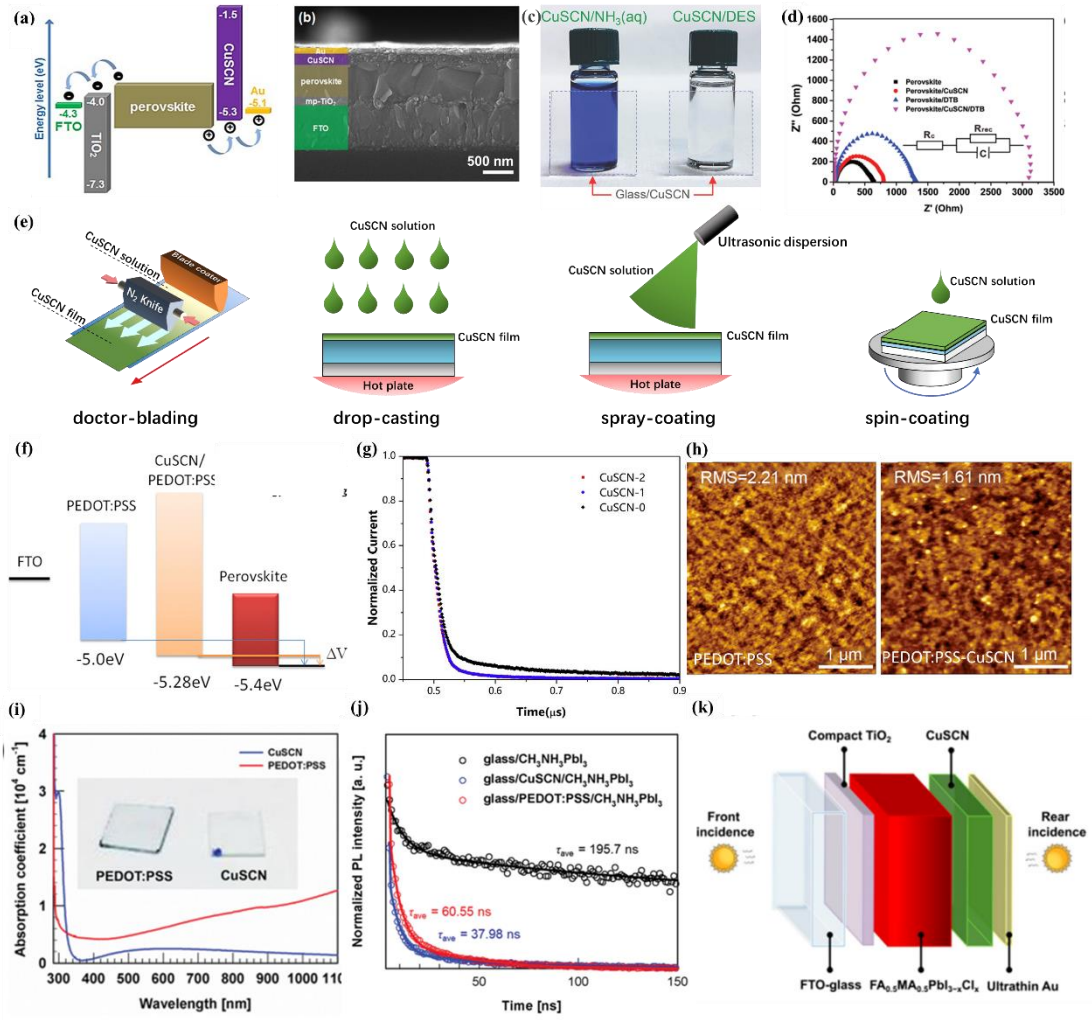

Figure 7. (a) ELA in CuSCN based device and (b) the cross-sectional SEM image of the CuSCN based n-i-p device;[117] Copyright 2016, WILEY‐VCH Verlag GmbH & Co. KGaA, Weinheim. (c) Digital photography of the sample bottles containing the CuSCN solutions in NH_3 (aq) or DES solvent, placed behind a 2×2 cm^2 transparent glass coated with CuSCN thin film;[102] Copyright 2017, WILEY‐VCH Verlag GmbH & Co. KGaA, Weinheim. (d) EIS of CuSCN, DTB, and CuSCN/DTB-based PSCs, insert image shows Equivalent fitting circuit;[108] Copyright 2020, WILEY‐VCH Verlag GmbH & Co. KGaA, Weinheim. (e) Several CuSCN deposition techniques; (f) The energy level scheme of perovskite and CuSCN modified HTMs;[121] Copyright 2018, Elsevier. (g) Transient photo-current (TPC) decay of CuSCN modified PEDOT:PSS;[121] Copyright 2018, Elsevier. (h) AFM images of (PEDOT:PSS and PEDOT:PSS-CuSCN on ITO substrates;[122] Copyright 2020,

Elsevier. (i) Absorption spectra of PEDOT:PSS and CuSCN films, insert image is digital photograph of each films coated on ITO substrates;[123] Copyright 2015, WILEY‐VCH Verlag GmbH & Co. KGaA, Weinheim. (j) TRPL spectra of $MAPbI_3$ films on glass, CuSCN, and PEDOT:PSS substrates;[123] Copyright 2015, WILEY‐VCH Verlag GmbH & Co. KGaA, Weinheim. (k) Schematic illustration of the bifacial semitransparent n-i-p PSCs.[124] Copyright 2018, American Chemical Society.

Copper sulfide (CuS) has high charge mobility, conductivity, and chemical stability, while also having a compatible ELA with perovskite.[126] Rao et al. was the first to apply CuS nanoparticles as an HTM in inverted PSCs (Figure 8a).[127] The deposition of CuS nanoparticles could not only retain the surface roughness and transmittance of ITO substrates but also decrease the interfacial carrier injection barrier and facilitate hole extraction (Figure 8b), resulting in a PCE that was over 16.2% with low hysteresis and excellent stability. Tirado et al. reported an inorganic CuS HTM produced solely in solution and applied it in PSCs based on two different perovskite materials, $MAPbI_3$ and $(FAPbI_3)_{0.78}(MAPbBr_3)_{0.14}(CsPbI_3)_{0.08}$. The results showed that CuS had a better ELA with $MAPbI_3$ (Figure 8c). The cost accounting of the device showed that the use of CuS was 23 times cheaper than the use of Spiro-OMeTAD.[128] To overcome the severe degradation problem of Spiro-OMeTAD, Lei et al. fabricated a Spiro-OMeTAD/CuS double-layer HTM (Figure 8d). The high intrinsic mobility of CuS could enhance hole transport and reduce charge recombination, yielding a high PCE of 18.58%. In addition, the hydrophobic properties of CuS could protect the Spiro-OMeTAD HTM, resulting in long-term stability. The device maintained 90% of its original PCE after 1000 hours of storage without encapsulation in an environmental atmosphere with 40% RH, as shown in Figure 8e.[129]

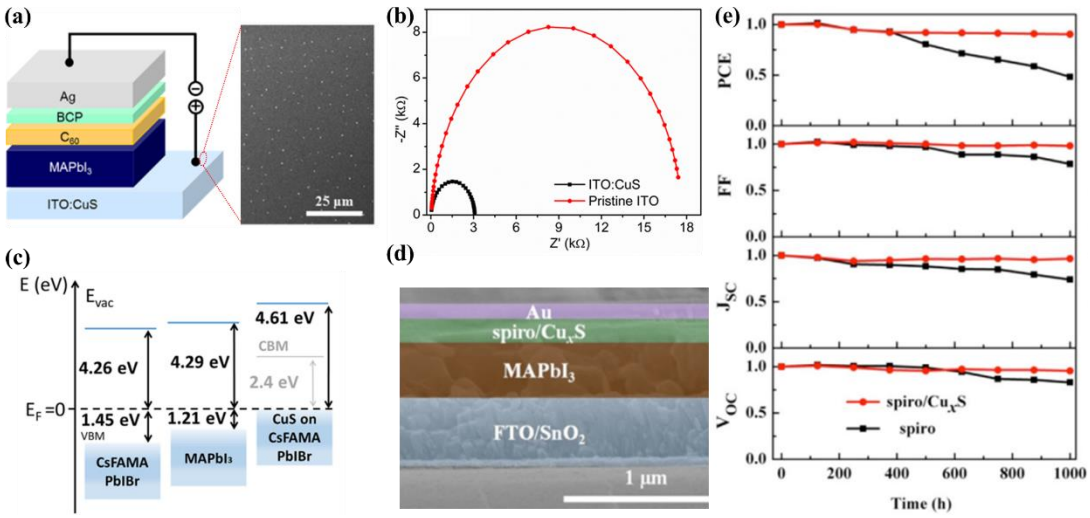

Figure 8. (a) Devices architecture and the SEM image of the CuS modified ITO and (b) EIS of device fabricated with pristine and modified ITO;[127] Copyright 2018, American Chemical Society. (c) Energy level position and WF of CsFAMAPbIBr, $MAPbI_3$ and CuS;[128] Copyright 2018, Elsevier. (d) Cross-sectional SEM image of device with double-layer HTM structure;[129] Copyright 2017, WILEY‐VCH Verlag GmbH & Co. KGaA, Weinheim. (e) Photovoltaic parameters monitoring of devices stored at environment atmosphere with 40% RH for 1000 hours.[129] Copyright 2017, WILEY‐VCH Verlag GmbH & Co. KGaA, Weinheim.

Compared with a metastable sphalerite structure (β-MnS) and fiber zincite structure (γ-MnS), a rock salt structure (α-MnS) is more stable and has a better ELA with perovskite (Figure 9a).[130] Li et al. fabricated PSCs with a dense MnS thin film as an HTM by vacuum vapor deposition technology.[6e] Due to its high hole mobility and conductivity, devices based on the MnS HTM had a better PCE (19.86%) than that of PSCs based on Spiro-OMeTAD (18.44%), as shown in Figure 9b. Unencapsulated devices based on MnS retained more than 90% of their original PCE after 1000 hours of storage (Figure 9c) in 80% RH, while devices based on Spiro-OMeTAD lost their performance entirely after 200 hours. Furthermore, they used this MnS HTM in an all-inorganic perovskite device (FTO/c&m-TiO_2/$CsPbBr_3$/MnS/C). Compared with the control group without MnS, devices based on structure above achieved a better ELA with a decreased charge

recombination and obtained up to 1.52 V V_{oc} and 10.82% efficiency.[131]

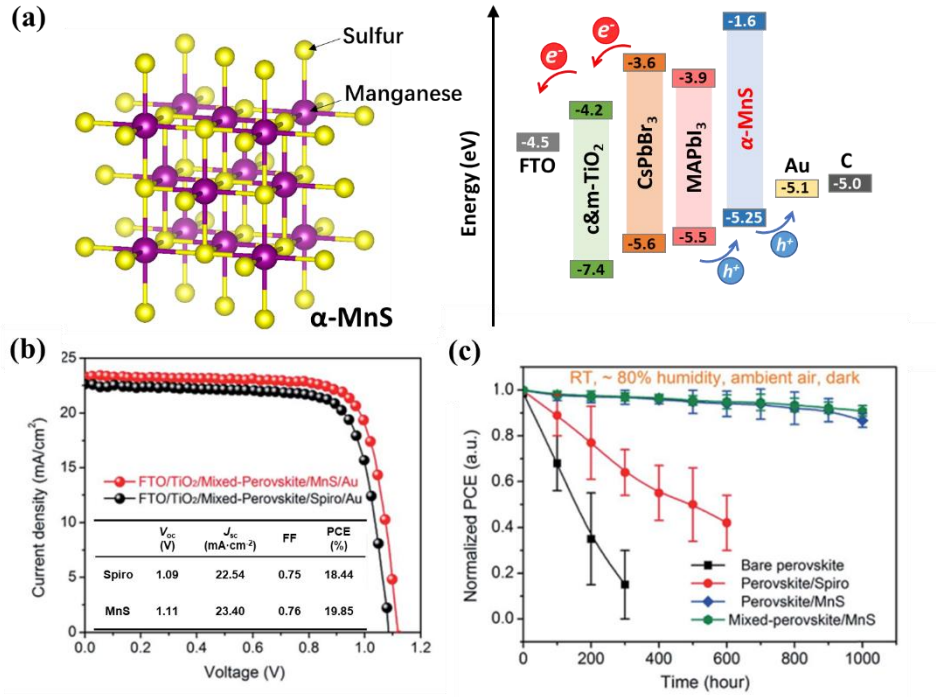

Figure 9. (a) Lattice structure diagram of α-MnS (left) and ELA diagram (right) of MnS based PSCs. (b) *J-V* curves of devices based on Spiro and MnS; (c) Normalized PCE evolution of different devices storage in dark condition.[6e] Copyright 2019, Royal Society of Chemistry.

With an abundance of resources and a low cost, FeS_2, as a nontoxic semiconductor, has a valence band (VB) of 5.30 eV (Figure 10a); thus, FeS_2 can act as an HTM and extract holes from perovskite. Huckaba et al. fabricated PSCs (Figure 10b) by using mineral iron pyrite FeS_2 as the HTM and obtained a PCE of 11.2%. They analyzed the cost of mineral iron pyrite FeS_2, and it was more than 300 times cheaper than Spiro-OMeTAD.[132] To improve the moisture-proof properties of FeS_2, Koo et al. reported octadecylamine-capped pyrite nanoparticles (ODA-FeS_2 NPs) as an HTM in PSCs. These modified HTMs exhibited excellent humidity resistance compared with Spiro-OMeTAD (Figure 10c). The relevant device achieved an efficiency of 12.56%. Additionally, after aging in a 50% RH environment for 1000 hours, the cell retained nearly 90% of its initial PCE.[133]

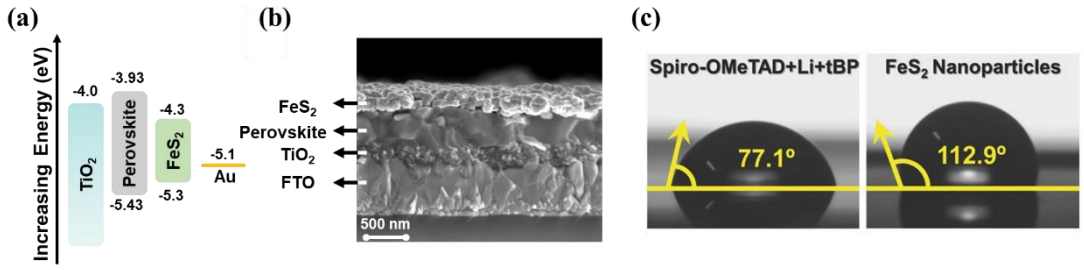

Figure 10. (a) ELA in FeS_2 based device; (b) Cross-sectional SEM images of FeS_2 based device (the scale bar is 500 nm);[132] Copyright 2016, WILEY - VCH Verlag GmbH & Co. KGaA, Weinheim. (c) Water contact angles on the surface of Spiro-OMeTAD and ODA-FeS_2 film.[133] Copyright 2016, WILEY - VCH Verlag GmbH & Co. KGaA, Weinheim.

Table 3 Summarization of performance parameters of PSCs based on inorganic chalcogen compound HTMs.

Formula	Deposition method	Device Architecture	PCE %	Test condition	Stability	Ref.
CuSCN	Doctor Blading	FTO/c&m-TiO_2/$(FAPbI_3)_{0.85}(MAPbBr_3)_{0.15}$/CuSCN/Au	16.6	-	-	[110]
	Doctor Blading	FTO/c&m-TiO_2/$MAPbI_3$/CuSCN/Au	12.4	-	-	[106]
	Doctor Blading	FTO/c-TiO_2/$MAPbI_3$/CuSCN/Au	9.6	-	-	[134]
	Doctor Blading	FTO/m-TiO_2/$MAPbI_3$/CuSCN/Au	4.85	-	-	[104]
	Electrodeposited	FTO/CuSCN/$MAPbI_{3-x}Cl_x$/PCBM/Ag	3.8	-	-	[115]
	Electrodeposited	ITO/CuSCN/$MAPbI_3$/C_{60}/BCP/Ag	16.6	Ambient air	38 h, 82% of the initial PCE	[101]
	Spray-Coating	FTO/c&m-TiO_2/$MAPbI_3$/CuSCN/Au	13.3	Ambient air, 85 ℃	45 d, 80% of the initial PCE	[112]
	Spray-Coating	FTO/c&m-TiO_2/$MAPbI_3$/CuSCN/Au	17.1	RH=30%, RT	100 d, 94.2% of the initial PCE	[135]
	Spray-Coating	FTO/c&m-TiO_2/$(FAPbI_3)_{0.85}(MAPbBr_3)_{0.15}$/CuSCN/rGO/Au	18.78	RH=30%, 65 ℃	1000 h, 95 of the initial PCE	[136]
	Spin-Coating	ITO/PEDOT:PSS/CuSCN/$MAPbI_3$/PTBT-Th/$PC_{70}BM$/BCP/Al	17.5	One-sun illumination	10 min, 99.5% of the initial PCE	[102]
	Spin-Coating	ITO/CuSCN/$MAPbI_3$/PCBM/BCP/Ag	10.8	-	-	[116]
	Spin-Coating	ITO/CuSCN/$MAPbI_3$/PCBM/BCP/Ag	14.9	Dark, vacuum	50 d, 90% of the initial PCE	[103]
	Spin-Coating	ITO/rGO/CuSCN/$MAPbI_3$/PCBM/BCP/Ag	14.3	Continuous light soaking	100 h, 95% of the initial PCE	[137]
	Spin-Coating	FTO/c&m-TiO_2/$CsFAMAPbI_{3-x}Br_x$/CuSCN/rGO/Au	20.4	Continuous illumination at 60 ℃ in	1000 h, >85% of the	[107]

			a N_2 atmosphere	initial PCE	
Spin-Coating	ITO/SnO_2/$(FAPbI_3)_{0.92}(MAPbBr_3)_{0.08}$/CuSCN/DTB/Au	22.0	Continuous illumination in a N_2 atmosphere	1000 h, >95% of the initial PCE	[108]
Spin-Coating	FTO/c&m-TiO_2/$MAPbI_3$/CuSCN/Au	11.02	-	-	[113]
Spin-Coating	FTO/c&m-TiO_2/$(FAPbI_3)_{0.85}(MAPbBr_3)_{0.15}$/CuSCN/Au	18.0	RH=40%, 125 ℃	2 h, 65% of the initial PCE	[117]
Spin-Coating	ITO/CuSCN/$MAPbI_3$/C_{60}/BCP/Ag	14.9	-	-	[123]
Spin-Coating	FTO/c&m-TiO_2/$(FAPbI_3)_{0.88}(CsPbBr_3)_{0.12}$/$(5\text{-}AVA)_2PbI_4$/CuSCN/Au	16.8	RH=10%, RT	63 d, 98% of the initial PCE	[105a]
Spin-Coating	FTO/c&m-TiO_2/$CsFAMAPbI_{3-x}Br_x$/CuSCN/C	17.58	RH=85%, RT	100 h, 95% of the initial PCE	[105b]
Spin-Coating	FTO/c-TiO_2/SnO_2/$(FAPbI_3)_{0.85}(MAPbBr_3)_{0.15}$/CuSCN/C	18.1	Continuous UV illumination, encapsulated	1000 h, 95% of the initial PCE	[105c]
Spin-Coating	FTO/c&m-TiO_2/$(FAPbI_3)_{0.85}(MAPbBr_3)_{0.15}$/Cs:$NiO_x$/CuSCN/Au	19.24	85 ℃, Air environment	1000 h, 85% of the initial PCE	[105d]
Spin-Coating	ITO/SnO_2/$MAPbI_3$/polydimethylsiloxane(PDMS)/CuSCN/Au	19.04	RH=55%, 25 ℃	1000 h, 90% of the initial PCE	[105e]
Drop-casting	FTO/c-TiO_2/$MAPbI_{3-x}Cl_x$/CuSCN/Au	6.4	-	-	[115]
Drop-casting	FTO/c&m-TiO_2/$CsFAMAPbI_{3-x}Br_x$/CuSCN/graphene/Au	15.8	/$MAPbI_3$	30 d, 94% of the initial PCE	[111]
Drop-casting	FTO/SnO_2/$Cs_{0.05}FA_{0.81}MA_{0.14}PbI_{2.55}Br_{0.45}$/CuSCN/C	13.6	RH=30%, 23 ℃	90 d, negligible performance drop	[138]
Doping	ITO/c-TiO_2/$MAPbI_3$/Spiro-OMeTAD(CuSCN doped)/Ag	18.02	RH=25%, RT	180 h, 60% of the initial PCE	[119]
Doping	FTO/PTAA(CuSCN doped)/$Cs_{0.05}FA_{0.81}MA_{0.14}PbI_{2.55}Br_{0.45}$/PCBM/Ag	18.16	RH=30%, RT	200 h, 75% of the initial	[120]

	Doping	FTO/PEDOT:PSS(CuSCN doped)/$MAPbI_3$/PCBM/BCP/Ag	10.9	-	PCE -	[121]
	Doping	ITO/PEDOT:PSS(CuSCN doped)/$MAPbI_3$/PCBM/C_{60}/LiF/Al	15.3	N_2, one sun illumination	175 h, 71% of the initial PCE	[122]
Formula	**CB eV**	**Device Architecture**	**PCE %**	**Test condition**	**Stability**	**Ref.**
MnS	5.25	FTO/c&m-TiO_2/$MAPbI_3$/MnS/Au	19.85	RH=85%, 80 ℃	400 h, 80% of the initial PCE	[6e]
	5.25	FTO/c&m-TiO_2/$CsPbBr_3$/MnS/C	8.16	RH=85%, 80 ℃	100 d, 80% of the initial PCE	[131]
FeS_2	-5.3	FTO/c&m-TiO_2/$FA_{0.98}MA_{0.02}PbI_{0.98}Br_{0.02}$/$FeS_2$/Au	11.22	-	-	[132]
	-4.95	FTO/c&m-TiO_2/$MAPbI_3$/ODA-FeS_2/Au	12.56	RH=50%, RT	1000 h, 92% of the initial PCE	[133]
NiS	-	FTO/c&m-TiO_2/$MAPbI_3$/NiS+C	5.2	ambient condition	10 d, 78% of the initial PCE	[139]
CuS	-5.1	ITO/CuS/$MAPbI_3$/C_{60}/BCP/Ag	16.2	-	-	[127]
	-4.61	FTO/c&m-TiO_2/$Cs_{0.08}(FA_{0.83}MA_{0.17})_{0.92}Pb(I_{0.83}Br_{0.17})_3$/CuS/Au	13.47	RH=40%, 20 ℃	504 h, 80% of the initial PCE	[128]
	-5.2	FTO/c&m-TiO_2//$MAPbI_3$/Spiro-OMeTAD/CuS/Au	18.58	RH=40%, 25 ℃	1000 h, 90% of the initial PCE	[129]

4.2. Organic Chalcogen Compound HTMs

Organic HTMs exhibit an outstanding ability to be processed, a high glass transition temperature and an adjustable energy band structure. Generally, organic HTMs are divided into small-molecule HTMs and polymer HTMs. Small-molecule HTMs mainly include Spirobifluorenes[100a], thiophene[140], pyrrole[141], triazine[142], porphyrin[143], carbazole[144] and other types[145]. Polymer HTMs can be divided into neutral conjugated polymer HTMs and ionic conjugated polymer HTMs.[146] Among them, Spiro-OMeTAD is commonly used.[147] However, Spiro-OMeTAD has intrinsically low conductivity and mobility. Usually, this problem is solved by molecular dopants, such as lithium bis(trifluoromethane sulfonyl)imide (Li-TFSI) and 4-tert-butyl pyridine (*t*BP).[148] However, these dopant molecules undermine the hydrophobic property of the HTMs, thus inducing a decrease in the stability of PSCs.[149] Moreover, the complicated purification process increases the cost of Spiro-OMeTAD. Therefore, multiple efforts have been devoted to finding alternatives.

Organic chalcogen compound HTMs are regarded as promising candidates in PSCs. Usually, organic chalcogen compound HTMs have intrinsically high carrier mobility and conductivity. Therefore, dopants are no longer necessary, resulting in a significant increase in stability. In addition, organic chalcogen HTMs have a significant cost advantage over Spiro-OMeTAD, which facilitates their commercialization in PSCs. We divided the organic chalcogen compound HTMs into chalcogen molecule HTMs and chalcogen polymer HTMs, and the detailed performance parameters of devices based on organic chalcogen compound HTMs are summarized in Table 4 and 5.

4.2.1. Chalcogen Molecule HTMs

Sulfur atoms are introduced at two sites in chalcogen molecule HTMs, the core and the linker. The chalcogenide core mainly includes thiophene derivatives,

phenothiazine (PTZ) derivatives, and tetrathiofulvalene (TTF) derivatives. Among them, thiophene derivatives are the most reported chalcogen molecule HTMs, including thiophene, ethylenedioxythiophene (EDOT), bithiophene (BT), benzodithiophene (BDT), benzotrithiophene (BTT), and p-conjugated dithieno[3,2-b:20,30-d]pyrrole (DTP).

Wu et al. reported HTMs (BTPA-1) based on a thiophene core with two *p*-methoxytriphenylamine (OMeTPA) arms. BTPA-1 had the highest occupied molecular orbital (HOMO) level (-5.25 eV). Additionally, the device based on the BTPA-1 HTM obtained a PCE of 12.76%.[150] Li et al. demonstrated an H111 HTM with a lower HOMO level (-5.31 eV) than BTPA-1 by synthesizing four OMeTPA arms.[151] The relevant device obtained a PCE of 15.4%.

EDOT derivative HTMs (H101) were first reported by Li et al. in 2014.[152] The device based on an H101 HTM with and without a dopant demonstrated PCEs of 10.9% and 13.8% (Figure 11a), respectively; these values were comparable to their Spiro-OMeTAD counterpart. Then, Petrus et al. synthesized EDOT-OMeTPA via a Schiff base condensation with a high atom economy and without the use of a noble-metal catalyst.[153] EDOT-OMeTPA exhibited a lower HOMO level (-5.28 eV) than Spiro-OMeTAD and H101, as shown in Figure 11b. The cost accounting showed that EDOT-OMeTPA was approximately an order of magnitude cheaper than Spiro-OMeTAD. In 2015, Ganesan developed a Spiro-OMeTAD-like HTM (PST1) based on an EDOT core.[154] PST1 showed a HOMO level of -5.15 eV. The PCEs of dopant and dopant-free devices based on PST1 were 13.44 and 12.74%, respectively. Chen et al. compared the different linkers, TPA and OMeTPA, of an EDOT-based core (PheDOT).[155] The results showed that the OMeTPA linker induced more hydrogen bonds, resulting in a short molecular distance and significantly enhanced hole mobility. Recently, Zhang et al. synthesized a novel thiophene-cored HTM (D1) with approximately 1/30 the cost of Spiro-OMeTAD and a favourable hole extraction ability (Figure 11c), thus the PCE of the relative device obtained a PCE exceeding

16%.[156]

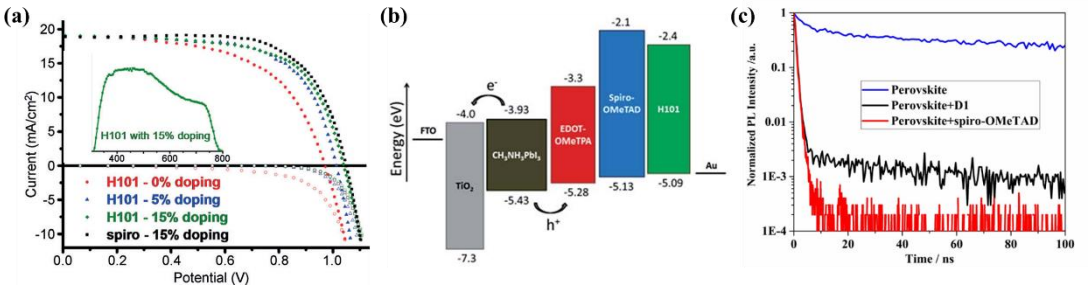

Figure 11. (a) *J-V* curves of PSCs based doped Spiro-OMeTAD and H101 HTMs;[152] Copyright 2013, WILEY‐VCH Verlag GmbH & Co. KGaA, Weinheim. (b) The energy level scheme of PSCs with EDOT-OMeTPA, Spiro-OMeTAD and H101 HTMs;[153] Creative Commons Attribution 3.0 Unported Licence. (c) TRPL spectra of perovskite, Spiro-OMeTAD and D1 coated on the perovskite films.[156] Copyright 2019, Elsevier.

In 2014, BT derivatives (KTM3) were first utilized as an HTM in PSCs by Krishnamoorthy et al. in which the core of Spiro-OMeTAD was replaced with swivel-cruciform 3,30-bithiophene.[157] Due to the better ELA of KTM3 with perovskite, devices based on KTM3 obtained a higher V_{oc} and FF than devices based on Spiro-OMeTAD (Figure 12a). Later, similar to H111, an H112 HTM based on a bithiophene core with a HOMO level of -5.29 eV were reported by Li et al.[151] The device based on H112 HTMs showed a PCE of 15.2%. In 2015, Abate et al. employed silolothiophene as the core of HTMs (PEH-2) in PSCs.[158] A stability analysis showed that the PSCs based on PEH-2 and Spiro-OMeTAD showed a double-exponential-decay trend in the first 200 hours, and the half-life period of PSCs based on PEH-2 was six times greater than that of Spiro-OMeTAD (Figure 12b), indicating that the former was more stable. In 2016, Saliba et al. performed an N,N-di-p-methoxyphenylamine (OMeDPA) group substitution on a fluoren-dithiophene (FDT) core and obtained a highly efficient chalcogen molecule HTM. Devices based on such an HTM achieved an efficiency of 20.3%.[159] They proved that the strong molecular polarity of the FDT core led to easy separation; thus, the synthesis cost of FDT-based HTMs was only 1/5 that of Spiro-OMeTAD. In 2017,

Liu et al. revealed that HTMs based on thienothiophene (TT) cores demonstrated higher mobility (Figure 12c) than their thiophene core counterparts.[160] In 2018, Le et al. investigated the effect of the OMeTPA linker position on the thienothiophene core and applied them as an HTM in PSCs (Figure 12d).[161] The results showed that the 2,5-site substitution (TT-2,5-TPA) compared to the 3,6-site substituted isomer (TT-3,6-TPA) exhibited better π-conjugation.

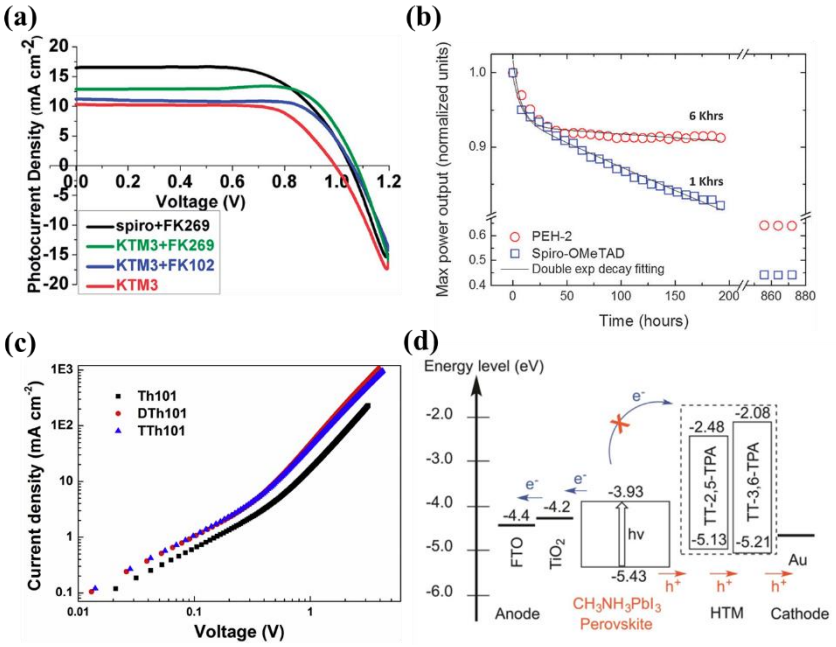

Figure 12. *J-V* curves of PSCs based doped Spiro-OMeTAD and KTM3 HTMs;[157] Copyright 2014, Royal Society of Chemistry. (b) MPP tracking of PSCs prepared in a same batch, employing Spiro-OMeTAD and PEH-2 as HTMs;[158] Copyright 2015, Royal Society of Chemistry. (c) SCLC curves of hole-only devices based on several TT core HTMs;[160] Copyright 2016, Elsevier. (d) ELA in devices based on TT-2,5-TPA and TT-3,6-TPA HTMs;[161] Copyright 2018, Wiley‐VCH Verlag GmbH & Co. KGaA, Weinheim.

BDT derivatives inherit the easy separation feature of thiophene, demonstrating an advantage in cost.[162] However, they usually have lower HOMO levels than perovskite materials, which is not suitable for their direct utilization as HTMs in PSCs.[163] Therefore, applying these materials in PSCs without any energy level regulation will induce exponentially increased recombination and terrible Voc loss at

the perovskite/HTM interface.[164] In this case, adjusting linkers is a feasible solution for regulating the HOMO level of BDT-based chalcogen molecule HTMs. The results showed that OMeTAP as linkers can effectively increase the HOMO value to achieve a good ELA with perovskite.[165] However, the application of additives introduces unstable factors in PSCs. To fabricate an efficient and stable device, dopant-free BDT-based HTMs have been developed.[166] Chen et al. employed BDT as the core, thiophene, and benzo-[c][1,2,5]-thiadiazole (BTZ) derivatives as π-conjugation components and obtained a novel dopant-free HTM BDT-C1.[167] BDT-C1 demonstrated a favorable HOMO level at -5.26 eV, as well as remarkable hole mobility and conductivity even without a dopant. The device based on BDT-C1 obtained a PCE of 13.9%. Additionally, the dopant-free BDT-C1 film demonstrated a contact angle of 107.4°, which was higher than that of doped Spiro-OMeTAD. The BDT-C1-based PSC maintained more than 80% of its initial PCE after 7 days of storage at 25°C and 30% RH. Recently, Chen et al. further improved the performance of BDT-based HTMs by replacing the linker with phenothiazine (PTZ) and phenoxazine (POZ)-based groups. The relevant devices obtained excellent PCEs of 18.26 and 19.16%, respectively. The difference in PCE was attributed to the faster hole extraction and transport of BDT-POZ, resulting in an ultrahigh FF of 0.82. To date, 19.16% is the highest PCE achieved by a BDT-based HTM in a conventional lead halide perovskite.[168]

Benzotrithiophene (BTT) has also been adopted as a core for chalcogen molecule HTMs (Figure 13a).[169] Molina-Ontoria et al. was the first to report devices fabricated with a BTT-based HTM.[170] The device based on BTT-3 obtained a PCE of 18.2% (Figure 13b), which was higher than that of BTT-1 (16.0%) and BTT-2 (17.0%). This improved PCE was ascribed to the HOMO level and planar construction of the BTT-3 HTM, which was revealed by a DFT calculation.[171] Although the electron-rich linker groups did not change the length of the π-conjugated BTT core, different linkers would determine their planar construction, which was deemed favorable for hole

extraction. Subsequently, this group demonstrated that the thiophene rings in the BTT core arrangement also affected hole mobility, inducing a PCE improvement (19.0%) and surpassing PSCs based on BTT-3 (Figure 13c).[172] Furthermore, Peng et al. synthesized BTT-based HTMs by directly catalyzing C-H arylation with Pd. The product YKP03-incorporated EDOT π-spacer showed a promising PCE without a dopant (16.15%), and this value was higher than PSCs based on BTT-3.[173] Furthermore, these dopant-free YKP03-based PSCs exhibited better long-term stability than their doped counterparts.

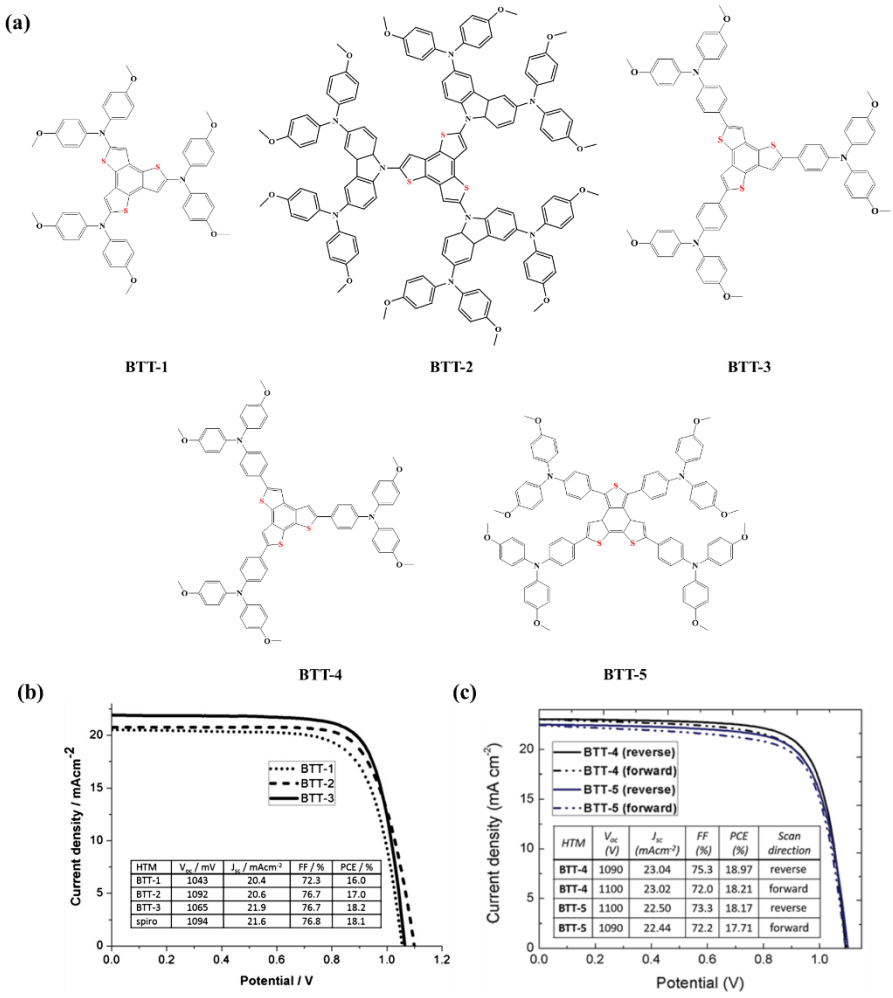

Figure 13. (a) Several structural formula of BTT based HTMs; (b) *J-V* curves of PSCs based on BTT-1, BTT-2, and BTT-3 HTMs;[170] Copyright 2015, Wiley‐VCH Verlag GmbH & Co. KGaA, Weinheim. (c) *J-V* curves of PSCs based on BTT-4 and BTT-5 HTMs;[172] Copyright 2017, Royal Society of Chemistry.

A DTP-based chalcogen molecule HTM was first designed for use in PSCs by

Mabrouk et al.[174] The strongly electronegative sulfur atom in the DTP core increases the conjugation effect (Figure 14a), inducing fast charge transport and high conductivity. PSCs based on H16 and H18 manifested PCEs of 18.16 and 15.29%, respectively. This result was opposite to that of Liu et al. for a benzene-arylamine-based HTM, where H-Tri with three 4-methoxy-N-(4-methoxyphenyl)-N-phenylaniline arms showed better performance than an H-Di HTM with two arms.[175] Moreover, the unencapsulated devices based on both H16 and H18 could retain 90% of their initial PCE after aging for 60 days at 20% RH under ambient air conditions. Zheng et al. studied the performance of HTMs with n-propyl (n-P) and 4-methoxyphenyl (4-OMeP) as side substituents in the DPZ core.[176] Compared to the AZ1 HTM with n-P substituents, the AZ2 HTM with 4-OMeP substituents had closer intermolecular packing, resulting in higher mobility and lower HOMO levels (Figure 14b). The device based on AZ2 had a PCE of 19.4%, which was superior to the Spiro-OMeTAD reference (19.1%). Additionally, the weak O-Pb interaction induced by 4-OMeP and Pb at the perovskite boundaries could enhance hole extraction kinetics and suppress traps on the perovskite surface, leading to negligible hysteresis. Zhou et al. precisely regulated the DTP core with π-conjugation elongation and N-alkylation strategies to obtain a high-quantity HTM, which had a low HOMO level and excellent hole mobility and film-forming properties (Figure 14c).[177] Devices with an optimized HTM demonstrated a PCE of 20.38%. Yin et al. reported dopant-free DTP-cored molecules (DTP-C6Th), which had a high hole mobility and fast hole extraction (Figure 14d).[178] With polymethyl methacrylate (PMMA) as the passivator and optimizing the composition of the perovskite, a PCE of 21.04% was achieved. The device, without encapsulation, exhibited no degradation after storage in a glove box for 60 days. Even in a 35% RH environment, the devices still retained more than 85% of their initial PCE after 60 days of storage.

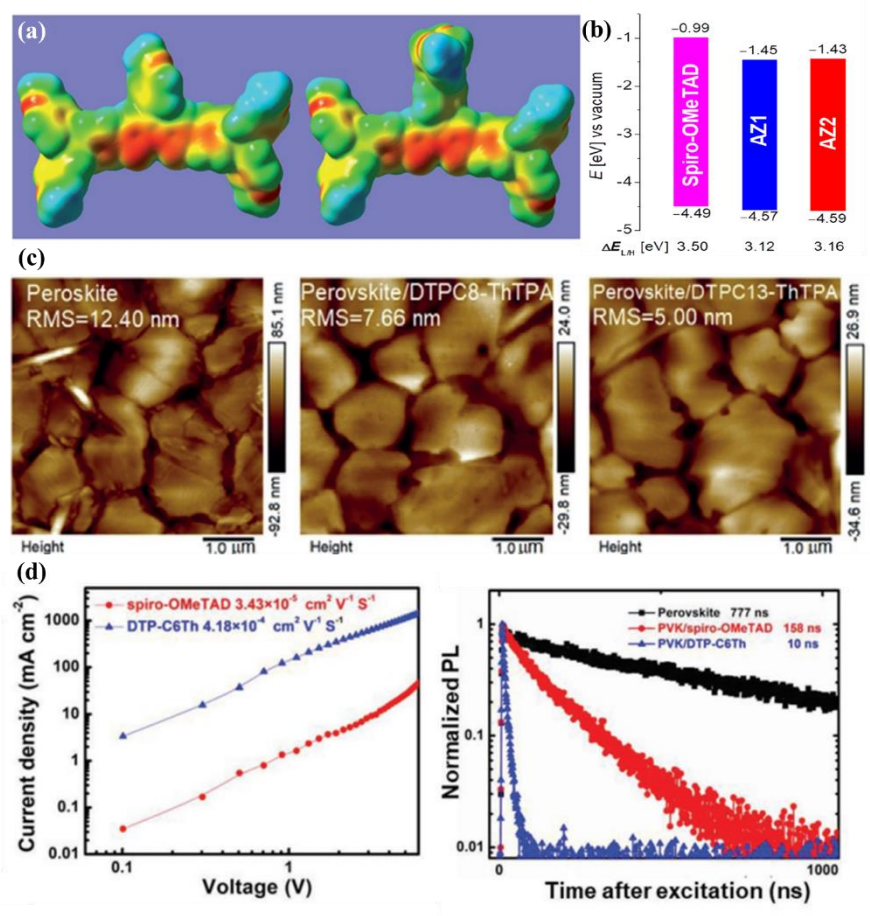

Figure 14. (a) Electrostatic surface potential (ESP) of H16 and H18 HTMs, where the red and blue are respective for the electro-negative and electro-positive parts;[174] Copyright 2018, Royal Society of Chemistry. (b) The energy band structure between perovskite and AZ1, AZ2 HTMs;[176] Copyright 2018, American Chemical Society (c) AFM images of perovskite layer and HTMs layers deposited onto the perovskite;[177] Copyright 2019, Wiley‐VCH Verlag GmbH & Co. KGaA, Weinheim. (d) SCLC properties of hole-only devices based on Spiro-OMeTAD and DTP-C6Th HTMs (left) and TRPL decay obtained from perovskite layer, perovskite/DTP-C6Th, and perovskite/Spiro-OMeTAD (right);[178] Copyright 2019, Wiley‐VCH Verlag GmbH & Co. KGaA, Weinheim.

PTZ is an electron-rich aromatic compound consisting of two benzene rings connected to sulfur and nitrogen atoms; thus, PTZ is considered a promising core for cost-efficient chalcogen molecule HTMs (6 $\$\cdot kg^{-1}$).[179] In 2017, Grisorio et al. was the first to report an HTM based on a PTZ core in PSCs and obtained a PCE of 17.6%,

which was comparable to devices based on the Spiro-OMeTAD counterpart (17.7%).[180] Further research by Salunke et al. suggested that the symmetrical double-substituted structure in AZO-II induced one order of magnitude higher mobility than AZO-I.[181] This could be attributed to the two electron-donating OMeTPA groups, inducing the electron-rich PTZ core and enhancing hole injection.[180, 182] The stability test showed that the relevant device based on AZO-II maintained 91% of its original PCE after 60 days of storage under environmental conditions with 30% RH. The cost accounting showed that the total cost of AZO-II was only 12 $\$\cdot g^{-1}$ in the laboratory-scale synthesis.[181] Ding et al. oxidized the PTZ core to phenothiazine 5,5-dioxide (PDO) with an electron-withdrawing sulfone group. Such a strategy revealed a positive effect on the HOMO level and carrier mobility of an HTM based on the PDO core, leading to a PCE exceeding 20%.[183] In a RT environment with 30~45% RH, an unencapsulated device maintained 84.7% of its initial PCE after 500 hours of storage.

TTF derivatives exhibit high intermolecular π-conjugation, promoting the latent possibility for high-performance HTMs. Liu et al. was the first to report a TTF-based HTM in PSCs. Because of the excellent charge mobility and conductivity of TTF derivatives, the corresponding dopant-free devices showed superior performance than devices based on Spiro-OMeTAD.[184] Additionally, devices based on dopant-free TTF derivatives showed significantly increased durability compared with Spiro-OMeTAD. Subsequently, carboxyl groups were introduced into the TTF core to design a novel HTM (TTA) by Chen et al. TTA demonstrated a favorable HOMO level (-5.26 eV) and excellent hole mobility properties. Additionally, the perovskite layer deposited on the TTA substrate showed better morphology, inducing an increased Jsc and FF. The device based on a dopant-free TTA HTM achieved a 16.7% efficiency in an inverted PSC.[185] Alternatively, Kaneko et al. reported a TTF derivative, including two amide units (Bis-amide-TTF), which could form supramolecular assemblies and stack with each other.[186] Bis-amide-TTF had a low HOMO level (-5.26 eV) and excellent

electrical conductivity (1.28×10^{-5} $S\cdot cm^{-1}$), resulting in fast charge transport.

The introduction of sulfur in the linker groups is another feasible strategy. Overall, thioether bonds[187], thiophene[188], dithiafulvenyl[189], and PTZ[190] are feasible choices for introducing sulfur into the linker. Chen et al. compared the different linkers OMeTAD and p-methylsulfanyl triphenylamine (SMeTAD).[191] The results indicated that SMeTAD induced a low HOMO level and increased Pb-S interaction with perovskite, thereby inducing fast hole extraction. Cao et al. developed a thiolated graphene material as an HTM in PSCs.[187] Due to the hydrophobicity of this HTM, the unencapsulated device can maintain more than 85% of its original efficiency after 10 days of storage at 45% RH.

Table 4 Summarization of photovoltaic parameters and stability of PSCs based on chalcogenide molecule HTMs.

Materials	**HOMO eV**	**Mobility $cm^2 V^{-1} s^{-1}$**	**Device Architecture**	**PCE %**	**Dopant[a]**	**Test condition**	**Stability**	**Ref.**
Th101	-5.25	3.88×10^{-6}	FTO/c&m-TiO_2/$MAPbI_3$/HTM/Au	3.19	W	-	-	[160]
BTPA-1	-5.25	2.7×10^{-6}	FTO/c-TiO_2/$FA_{0.85}MA_{0.15}PbI_3$/HTM/Au	12.76	-	RH=40%	192 h, 66% of the initial PCE	[150]
H111	-5.29	-	FTO/c&m-TiO_2/$MAPbI_3$/HTM/Au	15.40	W	70 ℃	14 d, 84% of the initial PCE	[151]
H01	-5.16	-	FTO/c&m-TiO_2/$MAPbI_3$/HTM/Au	13.8	W	70 ℃	7 d, 85% of the initial PCE	[152]
EDOT-OMeTPA	-5.28	-	FTO/c&m-TiO_2/$MAPbI_3$/HTM/Au	11.0	W	RH=30%, RT	1000 h, 90% of the initial PCE	[153]
PST1	-5.15	-	FTO/c&m-TiO_2/$MAPbI_3$/HTM/Au	13.44 12.7	W W/O	- -	- -	[154]
H-PheDOT	-5.45	2.9×10^{-5}	FTO/c&m-TiO_2/$MAPbI_3$/HTM/Au	6.69	W/O	-	-	[155]
Me-PheDOT	-5.32	1.3×10^{-4}		10.64		-	-	
D1	-5.12	6.15×10^{-5}	FTO/c&m-TiO_2/$MAPbI_3$/HTM/Au	16.50	W/O	RH=40%, RT	1000 h, 72.3% of the initial PCE	[156]
Z25	-5.18	7.66×10^{-5}	FTO/c&m-TiO_2/$Cs_{0.05}MA_{0.15}FA_{0.80}PbI_{2.5}Br_{0.5}$/HTM/Au	16.9	W	RH=30%, RT	800 h, 88.5% of the initial PCE	[192]
Z26	-5.16	1.34×10^{-4}		20.1		RH=30%, RT	800 h, 66.8% of the initial PCE	
KTM-3	-5.29	-	FTO/c&m-TiO_2/$MAPbI_3$/HTM/Au	11.00	W	-	-	[157]

H112	-5.16	-	FTO/c&m-TiO_2/$MAPbI_3$/HTM/Au	15.20	W	70 ℃	14 d, 84% of the initial PCE	[151]
P1H-2	-5.17	-	FTO/c&m-TiO_2/$MAPbI_3$/HTM/Au	11.7	W	MPP tracking	200 h, 92% of the initial PCE	[158]
FDT derivate	-5.16	-	FTO/c&m-TiO_2/$FA_{0.85}MA_{0.15}PbI_{2.55}Br_{0.45}$/HTM/Au	20.20	W	-	-	[159]
TT-2,5-TPA	-5.13	-	FTO/c&m-TiO_2/$MAPbI_3$/HTM/Au	13.40	W	-	-	[161]
TT-3,6-TPA	-5.21	-	FTO/c&m-TiO_2/$MAPbI_3$/HTM/Au	0.70	W	-	-	[161]
DOR3T-TBDT	-5.1	0.26	ITO/c-TiO_2/$MAPbI_{3-x}Cl_x$/HTM/Ag	14.9	W/O	-	-	[162]
DR3TBDTT	-5.39	10^{-4}	FTO/c-TiO_2/$MAPbI_3$/HTM/Au	8.80	W/O	RH=20%, RT	14 d, 92.3% of the initial PCE	[163]
OMeTPA-DPP	-5.13	-	FTO/c&m-TiO_2/$MAPbI_3$/HTM/Au	8.63	W	Continuous 1 sun illumination	10 d, 86% of the initial PCE	[165]
OMeTPA-BDT	-5.19	-		10.89		Continuous 1 sun illumination	10 d, 87% of the initial PCE	
BDT-4MeOTPA	-5.13	7.4×10^{-5}	FTO/c&m-TiO_2/$Cs_{0.05}MA_{0.15}FA_{0.80}PbI_{2.5}Br_{0.5}$/HTM/Au	8.78	W/O	80 ℃	1200 h, 89% of the initial PCE	[166]
BDT-C1	-5.26	3.2×10^{-4}	FTO/c&m-TiO_2/$MAPbI_3$/HTM/Au	17.00	W/O	RH=30%, 25 ℃	10 d, 80% of the initial PCE	[167]
BDT-2D	-5.18	1.1×10^{-3}	FTO/c&m-TiO_2/$FASnI_3$/HTM/Au	5.04	W	-	-	[193]
BDT-4D	-5.13	1.8×10^{-3}		7.32		-	-	
BDT-PTZ	-5.04	9.8×10^{-5}	ITO/HTM/$MAPbI_3$/C_{60}/BCP/Ag	18.26	W/O	RH=60%, RT	400 h, 80% of the initial PCE	[168]
BDT-POZ	-4.83	2.1×10^{-4}		19.16		RH=60%, RT	400 h, 80% of the initial PCE	
M1	-5.29	2.7×10^{-4}	ITO/ZnO/$PC_{70}BM$/$MAPbI_3$/HTM/Ag	13.20	W/O	-	-	[194]

BTT-1	-5.20	-		16.00	W	-	-	
BTT-2	-5.20	-	FTO/c&m-TiO_2/$MAPbI_3$/HTM/Au	17.00		-	-	[170]
BTT-3	-5.40	-		18.20		-	-	
BTT-3	-5.37	-	FTO/c&m-TiO_2/$(FAPbI_3)_{1-x}(MAPbBr_3)_x$/HTM/Au	18.20	W	-	-	[169]
BTT-4	-5.33	-	FTO/c&m-TiO_2/$FA_{0.85}MA_{0.15}PbI_{2.55}Br_{0.45}$/HTM/Au	18.97	W	-	-	[172]
BTT-5	-5.18	-		18.17		-	-	
YKP-06	-5.37	4.5×10^{-4}		13.92	W	-	-	
YKP-03	-5.16	5.8×10^{-4}	FTO/c&m-TiO_2/$MAPbI_3$/HTM/Au	14.63	W	RH=5%, 25 ℃	800 h, 10% of the initial PCE	[173]
YKP-03	-5.16	5.7×10^{-4}		16.15	W/O	RH=5%, 25 ℃	800 h, over 80% of the initial PCE	
BTT(DPP)3-C8	-5.15	1.4×10^{-4}		8.63		-	-	
BTT(DPP)3-EH	-5.16	9.9×10^{-5}	FTO/c-TiO_2/$MAPbI_3$/HTM/Au	8.39	W/O	-	-	[188]
BTT(DPP-Th)3-EH	-5.12	5.3×10^{-4}		12.87		-	-	
BTT(DPP-Th)3-EH	-5.12	1.3×10^{-3}		14.13	W	-	-	
H16	-4.97	5.6×10^{-4}	FTO/c&m-TiO_2/$FA_{0.85}MA_{0.15}PbI_{2.55}Br_{0.45}$/HTM/Au	18.16	W	RH=20%, RT	60 d, 90% of the initial PCE	[174]
H18	-4.96	2.2×10^{-4}	FTO/c&m-TiO_2/$FA_{0.85}MA_{0.15}PbI_{2.55}Br_{0.45}$/HTM/Au	15.39	W	RH=20%, RT	60 d, 90% of the initial PCE	
AZ1	-4.57	1.0×10^{-4}	FTO/c&m-TiO_2/$Cs_{0.05}MA_{0.15}FA_{0.80}PbI_{2.5}Br_{0.5}$/HTM/Au	17.4	W	-	-	[176]
AZ2	-4.59	1.2×10^{-4}		19.4	W	-	-	
DTP-C6Th	-4.94	4.2×10^{-4}	FTO/SnO_2/C_{60}/$MA_{0.7}FA_{0.3}PbI_{2.775}Br_{0.225}$/PMMA/HTM/Au	21.04	W/O	RH=35%, RT	60 d, 85% of the initial PCE	[178]
DTPC8-ThTPA	-4.94	3.5×10^{-5}	FTO/SnO_2/C_{60}/$MA_{0.7}FA_{0.3}PbI_{2.85}Br_{0.15}$/PMMA/HTM/Au	18.37	W/O	RH=25%, RT	60 d, 90% of the initial PCE	[177]

DTPC13-ThTPA	-5.04	2.2×10^{-4}	FTO/SnO_2/C_{60}/$MA_{0.7}FA_{0.3}PbI_{2.85}Br_{0.15}$/PMMA/HTM/Au	20.38		RH=25%, RT	60 d, 78% of the initial PCE	
PTZ-1	-4.77	-	FTO/c&m-TiO_2/$Cs_{0.05}MA_{0.15}FA_{0.80}PbI_{2.5}Br_{0.5}$/HTM/Au	2.10	W	-	-	[180]
PTZ-2	-5.15	-		17.50		-	-	
AZO-I	-4.97	2×10^{-6}	ITO/SnO_2/$Cs_{0.05}MA_{0.95-y}FA_yPbI_{3-x}Cl_x$/HTM/Au	14.30	W/O	RH=30%, RT	60 d, 68% of the initial PCE	[181]
AZO-II	-4.94	2×10^{-5}		15.60		RH=30%, RT	60 d, 91% of the initial PCE	
PDO1	-5.25	1.8×10^{-4}	FTO/c-TiO_2/SnO_2/$(FAPbI_3)_{0.85}(MAPbBr_3)_{0.15}$/HTM/Au	16.70	W	RH=30~45%, RT	450 h, 84.6% of the initial PCE	[183]
PDO2	-5.24	5.9×10^{-4}		20.20		RH=30~45%, RT	450 h, 84.7% of the initial PCE	
PTZ-TPA	-5.21	6.8×10^{-4}	FTO/SnO_2/PCBM/$MAPbI_3$/HTM/Au	14.30	W/O	RH=30%, RT	180 h, 92% of the initial PCE	[179]
Z28	-5.39	6.2×10^{-5}	FTO/c&m-TiO_2/$Cs_{0.05}MA_{0.15}FA_{0.80}PbI_{2.5}Br_{0.5}$/HTM/Au	17.77	W	RH=40%, RT	1008 h, 67.1% of the initial PCE	[182]
Z29	-5.44	6.8×10^{-6}		14.65		RH=40%, RT	1008 h, 50.1% of the initial PCE	
Z30	-5.27	6.7×10^{-5}		19.17		RH=40%, RT	1008 h, 85.1% of the initial PCE	
TTF-1	-5.05	0.1	FTO/c&m-TiO_2/$MAPbI_3$/HTM/Ag	11.13	W/O	RH=40%, RT, illumination	360 h, 80% of the initial PCE	[184]
TTA	-5.26	-	ITO/HTM/$MAPbI_3$/PCBM/BCP/Ag	16.70	W/O	RH=40%, RT, illumination	9 d, 80% of the initial PCE	[185]
Bis-amide-TTF	-5.25	2.2×10^{-4}	FTO/c&m-TiO_2/$Cs_{0.05}MA_{0.15}FA_{0.80}PbI_{2.5}Br_{0.5}$/HTM/Au	14.30	W/O	-	-	[186]

TPP-SMeTAD	-5.18	10^{-4}~10^{-5}	ITO/HTM/$MAPbI_3$/PCBM/ZnO/Al	16.60	W/O	-	-	[191]
DBTMT	-5.02	-	ITO/HTM/$MAPbI_3$/C_{60}/BCP/Ag	21.12	W/O	N_2 atmosphere, RT	600 h, 96% of the initial PCE	[195]
TSHBC	-5.40	-	FTO/c&m-TiO_2/$MAPbI_3$/HTM/Au	12.81	W	RH=45%, RT, illumination	10 d, 90% of the initial PCE	[187]
SFX-DTF1	-5.16	1.5×10^{-4}	FTO/c-TiO_2/$MAPbI_3$/HTM/Au	10.67	W/O	RH=30%, RT	24 d, 74.8% of the initial PCE	[189]
SFX-DTF2	-5.19	3.1×10^{-5}		8.78		RH=30%, RT	24 d, 71.5% of the initial PCE	
TPB(2-TPTZ)	-5.34	2.1×10^{-4}	FTO/ZnO-MgO-EA/m-TiO_2/$MAPbI_3$/HTM/Au	4.32	W	RH=30%, RT	300 h, 85% of the initial PCE	[190]
SCPDT-BiT	-5.07	4.5×10^{-6}	ITO/PEDOT:PSS/SCPDT-BiT/ $MAPbI_3$/MoO_3/Au	10.39	W/O	-	-	[196]

a where with and without are referred to as W and W/O.

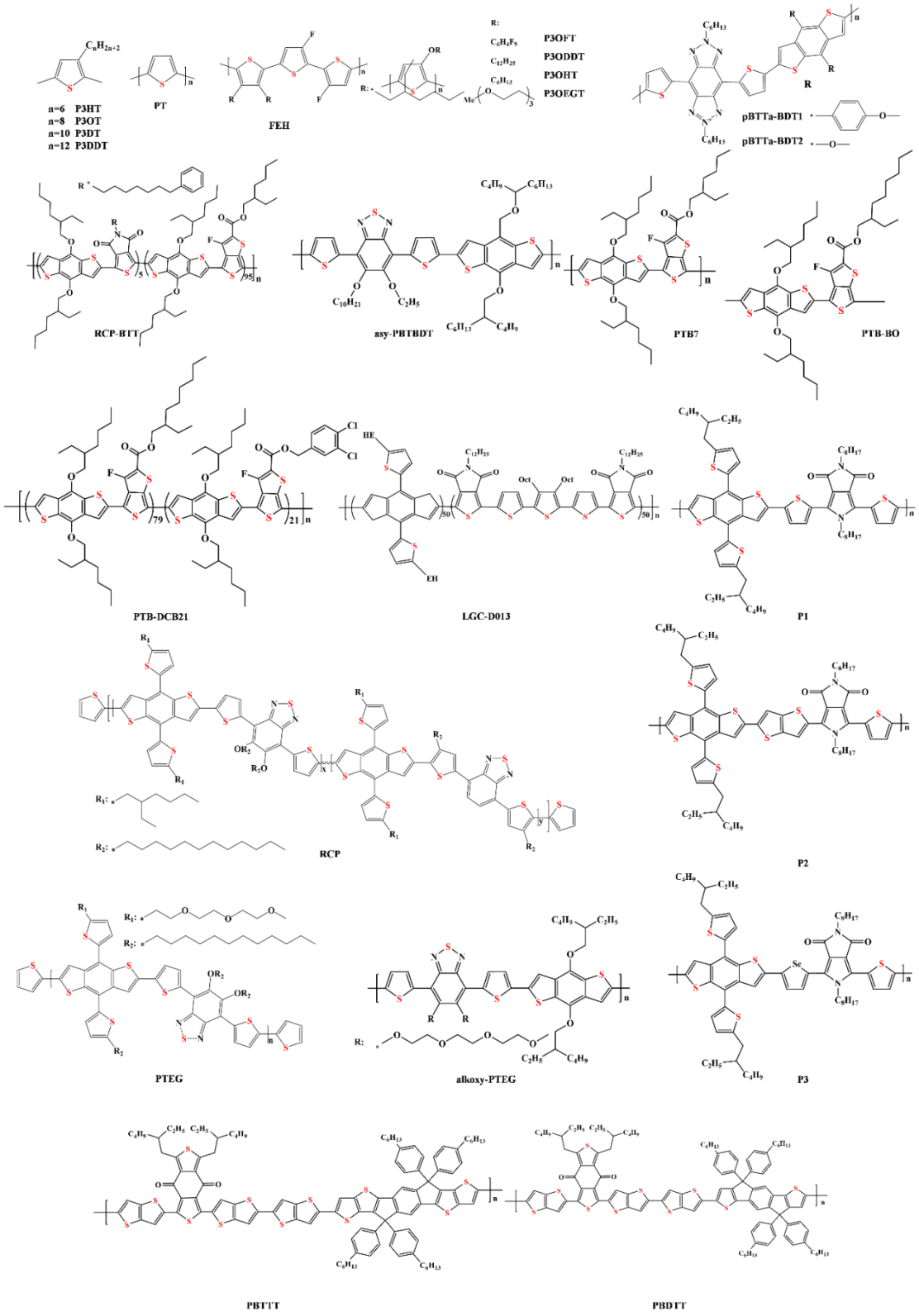

Figure 15. Structural formulas of neutral conjugated polymer HTMs.

4.2.2. Chalcogen Polymer HTMs

The properties of chalcogen conjugated polymers depend primarily on the properties of monomers. The chalcogen donor units of monomers promise them to transport the holes effectively, leading to being used as HTMs in PSCs. The chalcogen conjugated polymers can be divided into neutral chalcogen conjugated polymers (NCCPs) and ionic chalcogen conjugated polymers (ICCPs) according to interchain ions.

NCCPs, with no interchain ions, contain all-donor units or donor-acceptor (D-A) units, as shown in Figure 15. Polythiophene (PT) is a representative all-donor NCCP that has been widely investigated as an HTM.[197] However, the short alkyl side chain of PT causes it to have an edge-on interfacial orientation on the perovskite layer, which limits its mobility and hole transportation. Xiao et al. reported that PT derivatives with a long alkyl side chain would cause different orientations of the PT backbone.[198] A perpendicular interfacial contact with the perovskite layer would be better for hole extraction and would result in an improved J_{sc} (Figure 16a), despite the ELA, mobility, and bulk structure within the derivatives remaining similar. A further investigation indicated that side chains containing fluorine were beneficial for lowering the HOMO level and enhancing the hydrophobicity of the film, resulting in PSCs with an improved PCE and stability.[199]

Poly(3-hexylthiophen -2,5-diyl) (P3HT) is a typical PT derivative with a suitable alkyl side chain and has transitioned into commercial application.[200] However, the relatively low mobility (3×10^{-4} $cm^2\cdot V^{-1}\cdot s^{-1}$) of P3HT results in terrible charge recombination at the perovskite/P3HT interfaces.[200b] To solve this problem, dopants have been introduced into P3HT.[201] Heo et al. revealed the mechanism of a Li-TFSI/t-BP dopant for P3TH.[202] These doped molecules could transport holes to the CEs, thereby acting as redox shuttles in the liquid or gel electrolytes and improving hole mobility. Cai et al. reported bamboo-structured carbon nanotubes (BSCNs) as dopants in P3HT.[203] The results showed that BSCNs could form a

continuous carrier transport nanonetwork in the P3HT film, and the π-π stacking interaction of BSCN dopants could improve the crystallinity of P3HT, resulting in efficient hole transport.[204] Although multiple investigations have proven that dopant molecules increase efficiency, dopants also introduce unstable elements in PSCs.[205] Therefore, Jung et al. reported a strategy to avoid dopants for P3HT.[206] They developed a novel architecture with a self-assembled wide-bandgap halide between perovskite and P3HT (Figure 16b). The intermediate halide layer could improve hole mobility and prevent charge recombination. Therefore, the relative device achieved a certified PCE of 22.7%, which is the current record for PSCs based on P3HT. In addition, the device exhibited outstanding stability. After leaving the unencapsulated device in an 85% RH atmosphere for 1008 hours, 80% of the initial PCE was retained. After tracking the MMP under continuous one sun illumination at RT for 1370 hours, the encapsulated device retained 95% of its initial PCE.

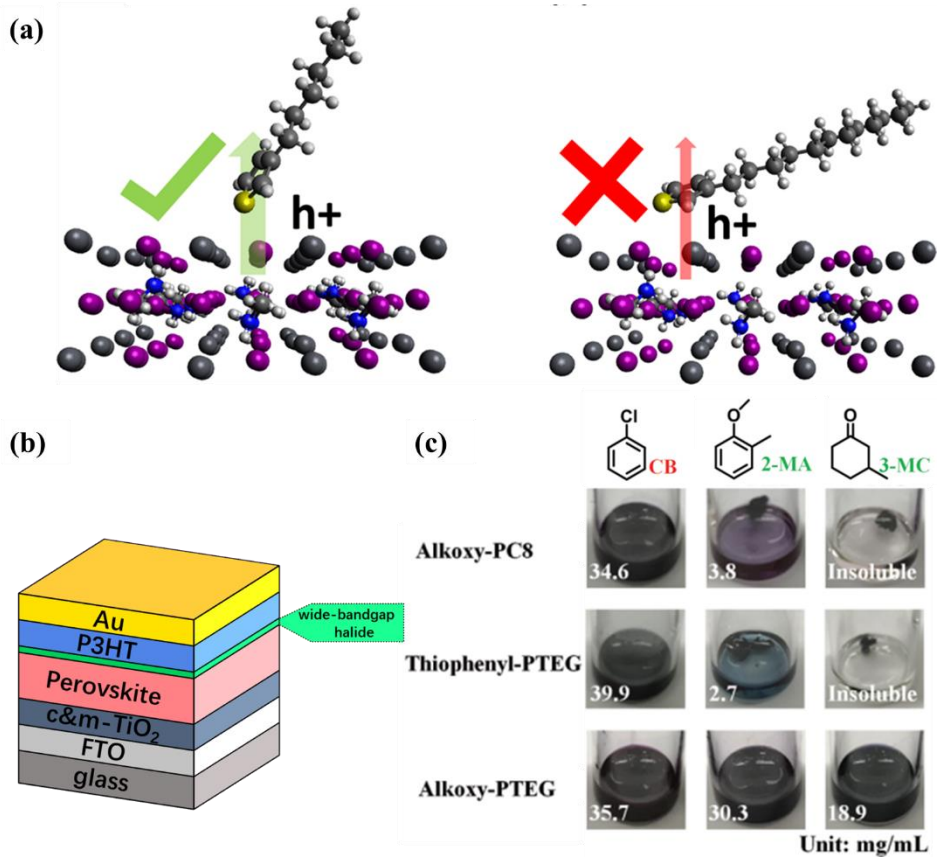

Figure 16. (a) Diagram of the effect of PTs alkyl chain length on hole extraction ability;[198] Copyright 2017, American Chemical Society. (b) Inserting a

wide-bandgap halide buffer layer between P3TH and perovskite; (c) The structural formula of products obtained by substituting BT with tetraethylene glycol (TEG) and their solubility in different solvents;[207] Copyright 2020, WILEY‐VCH Verlag GmbH & Co. KGaA, Weinheim.

Usually, PT derivatives have a unique HOMO level, and it is difficult to achieve the desired ELA with perovskite materials because PT derivatives possess different energy levels due to their various components. Therefore, D-A-type NCCPs are proposed to address the poor energy-level flexibility of all-donor NCCPs.[208] The character of D-A type polymers is that the donor unit guarantees considerable hole mobility, while the acceptor unit provides diversity in the HOMO level.[209] D-A type NCCPs utilize BDT derivatives as donor units.[210] Kim et al. was the first to report D-A NCCPs based on BDT donor units and benzothiadiazole acceptor units, and these D-A NCCPs showed a HOMO level (-5.41 eV) that was close with the valence band (VB) of perovskite.[211] The relative device achieved a PCE of 17.3% and maintained good stability for 1400 hours in a 75% RH environment. Additionally, the D-A architecture regulated the side chains of both the donor and acceptor units[212], which could improve the mobility and solubility of NCCPs.[213] Lee et al. designed a series of D-A type NCCPs with different side chains in an acceptor and utilized them as an HTM in PSCs (Figure 16c). By substituting the benzothiadiazole acceptor units with tetraethylene glycol (TEG), these NCCPs could be dissolved in green solvents, namely, 2-methylanisole (2-MA) and 3-methylcyclohexanone (3-MC). The high-quality HTM films resulted in efficiencies of 21.2%.[207] More importantly, the TEG group could induce chelation with the Pb ions, which prevented the possibility of lead leakage. In addition to regulating the donor and acceptor units, the introduction of a π-bridge (such as thiophene and thienothiophene) between the donor and acceptor has proven to be a favorable strategy for improving hole transport. Gunasekaran et al. demonstrated that the inserted thiophene π-bridge could induce the exposure of strong Pb-S interactions at the perovskite/HTM interface, resulting in

efficient hole transport.[214]

The typical representative ICCP is poly(3,4-ethylenedioxythiophene) (PEDOT), which exhibits outstanding resistance to oxygen and water degradation due to the substituted 3 and 4 positions of thiophene. However, pristine PEDOT has poor solubility in many solvents, so a poly(styrene sulfonate) (PSS) complex (Figure 17) was developed.[215] PSS plays two main roles: 1) acting as a counter ion to stabilize PEDOT and 2) increasing the solubility of PEDOT. This PEDOT:PSS composite has excellent conductivity, high light transmittance, and a good ELA with perovskite. However, it is usually dissolved in aqueous solution and applied in PSC with a p-i-n architecture. In 2013, Jeng et al. was the first to report PSCs based on PEDOT:PSS as an HTM.[216] The device achieved 3.9% PCE. After the development of a series of strategies, such as dopant engineering[217], solvent engineering[218], post-treatment engineering[219], and composite or bilayer engineering[220], the PCE of PSCs based on a PEDOT:PSS HTM rapidly increased to 20.1%[221]. Unfortunately, the further exploration of PEDOT:PSS-based devices is limited by the following factors. First, PSS exhibits high acidity, which is harmful to the TCO substrate and perovskite layer. Second, PEDOT:PSS is clearly hydrophilic, which will trap water molecules from the air and degrade the perovskite layer.[221] Third, the MAI in perovskite will react with PEDOT:PSS, resulting in a WF of PEDOT:PSS that is lower than -5.1 eV, leading to an ELA mismatch.[220a] Finally, our experiments found that the ITO/PEDOT:PSS substrate did not match well with the mixed-cation perovskite.[222]

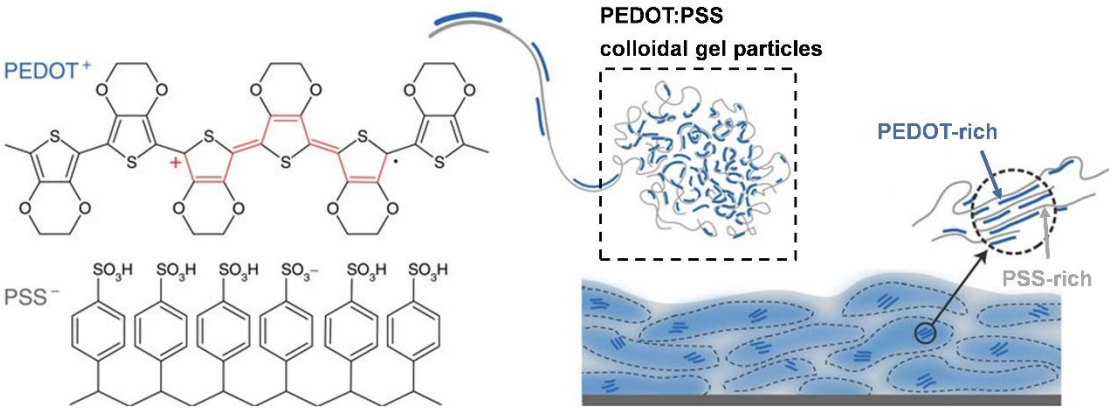

Figure 17. Illustration of the structure and morphology of PEDOT:PSS.[223] Copyright

2016, Creative Commons CC BY license.

Some ICCP alternatives of PEDOT:PSS have also been developed. Choi et al. developed poly[2,6-(4,4-bis-potassium butanylsulfonate-4H-cyclopenta-[2,1-b; 3,4-b ']-dithiophene)-alt-4,7-(2,1,3-benzothiadiazole)] (CPE-K) as an HTM for PSCs.[220b] Devices based on CPE-K reveal full coverage and excellent hole extraction, resulting in a PCE of 12.51%. Li et al. synthesized two ICCP HTMs for inverted p-i-n PSCs, P3CT-Na, and P3CT-CH_3NH_2.[224] Compared to P3CT-Na, P3CT-CH3NH2 solved the aggregation phenomenon through counterion tailoring and solvent optimization, leading to good crystallinity and a large grain size in the perovskite films. Devices based on the P3CT-CH_3NH_2 HTM obtained a PCE of 19.6 and 18.2% on a flexible substrate. Jo et al. synthesized 1,4-bis(4-sulfonatobutoxy) benzene and thiophene moieties (PhNa-1T) and used them as an HTM for inverted PSCs.[225] Compared with PEDOT:PSS, PhNa-1T exhibited hydrophobic properties and a low WF (-5.2 eV), which showed good stability and suppressed recombination at the perovskite/HTM interface. Therefore, the air stability of the relative device was effectively improved.

Table 5 Summarization of photovoltaic parameters and stability of PSCs based on chalcogen polymer HTMs.

Materials	HOMO/WF eV	Mobility $cm^2 V^{-1} s^{-1}$	Device Architecture	Dopant	PCE %	Test condition	Stability	Ref.
P3HT	-5.10[a]	<0.1	FTO/c&m-TiO_2/$MAPbBr_3$/HTM/Au	W/O	0.52	-	-	[200a]
	-	0.1	FTO/c&m-TiO_2/$MAPbI_3$/HTM/Au	W/O	4.5	-	-	[200b]
	-	-	FTO/c&m-TiO_2/$MAPbI_3$/HTM/Au	W	14.2	-	-	[202]
	-4.90[a]	1	FTO/c&m-TiO_2/$MAPbI_3$/HTM/Au	W	14.58			[226]
	-	-	FTO/c&m-TiO_2/$FA_{0.95}MA_{0.05}PbI_{2.85}Br_{0.15}$/WBH/HTM/Au	W/O	22.7	RH=85%, RT	1008h, 80% of initial PCE	[206]
					9.64	MMP tracking	1370 h, 95% of initial PCE	
P3OT	-5.00[a]	-	ITO/c-TiO_2/$MAPbI_3$/HTM/Ag	W/O	6.86	-	-	[198]
P3DT					6.64	-	-	
P3DDT					3.91	-	-	
P3HT	-4.60[a]	7.8×10^{-3}	FTO/c&m-TiO_2/$MAPbI_3$/HTM/Au	W	10.8	RH=50-60%, RT	500 h, >80% of initial PCE	[199a]
FEH	-5.10[a]	2.1×10^{-3}		W	18	RH=50-60%, RT	500 h, >75% of initial PCE	
P3OFHT	-	-	ITO/ZnO/$MAPbI_3$/HTM/Ag	W	3.3	-	-	[199b]
P3ODDT	-	-		W	6.7	-	-	
P3OHT	-	-		W	4.7	-	-	
P3OEGT	-	-		W	0.5	-	-	
PT	-5.20[a]	-	ITO/HTM/$MAPbI_3$/C_{60}/BCP/Ag	W/O	11.1	-	-	[227]
PT	-5.18	-	ITO/HTM/$MAPbI_3$/C_{60}/BCP/Ag	W/O	15.4	-	-	[228]
alkoxy-PTEG	-5.31[a]	4.1×10^{-4}	FTO/SnO_2/$Cs_{0.06}FA_{0.78}MA_{0.16}PbI_{2.4}Br_{0.6}$/HTM/Au	W/O	21.2	RH=40-50%, RT	30 d, 88% of initial PCE	[207]

pBBTa-BDT1	-5.11[a]	4.6×10^{-5}	FTO/c-TiO_2/$MAPbCl_{3-x}I_x$/HTM/Au	W/O	7	RH=65, 85℃	90% of initial PCE	[208]
pBBTa-BDT2	-5.21[a]	2.0×10^{-3}		W/O	14.5	-	-	
RCP-BTT	-5.28[a]	5.7×10^{-5}		W/O	8.45	RH=85%, 85℃	150 h, 35% of initial PCE	
RCP-BTT	-5.28[a]	2.4×10^{-3}	FTO/c&m-TiO_2/$Cs_{0.05}MA_{0.15}FA_{0.80}PbI_{2.5}Br_{0.5}$/HTM/Au	W	14.57	-	-	[209]
PTB7	-5.15[a]	-		W/O	6.91	RH=85%, 85℃	150 h, 40% of initial PCE	
PTB7	-5.15[a]	5.2×10^{-4}		W	12.02	-	-	
RCP	-5.41[a]	3.1×10^{-3}	FTO/SnO_2/$MAPbI_3$/HTM/Au	W/O	17.3	RH=75%, RT	1400 h, 100% of initial PCE	[211]
LGC-D013	-5.56[a]	2.0×10^{-4}	ITO/ZnO/$MAPbI_3$/HTM/Ag	W/O	12.22	-	-	[212]
asy-PBTBDT	-5.36[a]	4.8×10^{-3}	FTO/c&m-TiO_2/$FA_{0.95}MA_{0.05}PbI_{2.55}Br_{0.45}$/HTM/Au	W	17.1	RH=50-70%, RT	30 d, 91% of initial PCE	[213a]
	-5.36[a]	1.3×10^{-3}		W/O	20.0	-	-	
PTEG	-5.40[a]	1.6×10^{-3}	FTO/SnO_2/$Cs_{0.05}MA_{0.15}FA_{0.80}PbI_{2.5}Br_{0.5}$/HTM/Au	W/O	19.8	-	-	[213b]
P1	-5.40[a]	1.0×10^{-3}		W/O	12.13	RH=50%, RT	20000 m, around 90% of initial PCE	
P2	-5.37[a]	1.7×10^{-3}	FTO/c&m-TiO_2/$MAPbI_3$/HTM/Au	W/O	7.69	RH=50%, RT	20000 m, > 90% of initial PCE	[214]
P3	-5.42[a]	1.2×10^{-3}		W/O	13.99	RH=50%, RT	20000 m, > 90% of initial PCE	
PBDTT	-5.31[a]	7.1×10^{-4}	FTO/c&m-TiO_2/$Cs_{0.07}MA_{0.14}FA_{0.79}PbI_{2.5}Br_{0.5}$/HTM/Au	W/O	20.28	RH=30%, RT	720 h, >80% of initial PCE	[229]
PBTTT	-5.24[a]	7.0×10^{-4}		W/O	19.48	RH=30%, RT	720 h, >80% of initial PCE	
HSL-1	-5.16[b]	8.1×10^{-4}	ITO/PEDOT:PSS/HTM/$MAPb(I_{0.3}Br_{0.7})_xCl_{3-x}$/PCBM/Ag	-	15.40			[220a]
HSL-2	-5.39[b]	3.2×10^{-4}		-	16.60			
PEDOT:PSS	-5.00[b]	-	ITO/HTM/$MAPbI_3$/PCBM/Ca/Al	-	20.10	Glove box	30 d, >90% of initial PCE	[221]
CPE-K	-4.90[b]	-	ITO/PEDOT:PSS/HTM/$MAPbI_{3-x}Cl_x$/PCBM/Al	-	12.51	air exposure	12 h, 55% of initial PCE	[220b]

P3CT-Na	-5.26[b]	0.8×10^{-5}	ITO/HTM/$MAPbI_3$/PCBM/C_{60}/Ag	W/O	16.60	-	-	[224a]
P3CT-CH_3NH_2	-5.25[b]	1.1×10^{-5}	ITO/HTM/$MAPbI_3$/PCBM/BCP/Ag	W/O	19.60	-	-	[224b]
PhNa-1T	-5.20[b]	-	ITO-PEN/HTM/$MAPbI_3$/PCBM/Ag	-	14.70	RH=40%, 25℃	300 h, 66% of initial PCE	[225]

Where ‘a’ and ‘b’ refer to HOMO and WF, respectively.

5. Bifunctional Sulfur-based Materials

5.1. Sulfides as ETMs and HTMs

Transition metal disulfides (TMDs) are conventional semiconductor materials with a general formula of MS_2, where M is the transition metal atom.[230] The electronic and optical characteristics of TMDs vary significantly depending on the number of layers.[29] Their sizable bandgap can be changed from indirect (multilayer) to direct (single layer).[231]Moreover, the properties of a TMD semiconductor can be adjusted from an n-type to a *p*-type, according to the synthesis procedure. Therefore, TMDs can be utilized both as an ETM or HTM in PSCs. These materials include MoS_2, TiS_2, and WS_2. The detailed photovoltaic performance of relevant devices is summarized in Table .

5.1.1. Molybdenum Disulfide (MoS_2)

MoS_2 is inherently an n-type semiconductor. MoS_2 as a CTL has several advantages, such as a favorable WF, high transparency, fast carrier transport in the vertical direction, and few traps.[232] In addition, the semiconductor properties of MoS_2 can be tuned by elemental doping, surface functionalization, etc.[233] Singh et al. synthesized MoS_2 by the microwave-assisted low-temperature method and first utilized it as an ETM in PSCs, obtaining a PCE of 13.1%.[234] Recently, Mahmood et al. used MoS_2 nanosheets as an ETM for PSCs by the electrospray deposition method.[235] Compared with the hydrothermal synthesis method, the MoS_2 nanosheets fabricated by the electrospray deposition method had more uniform surface coverage and a larger surface contact area with the perovskite, resulting in rapid carrier extraction in the vertical direction and a PCE of 16.17%.

After surface functionalization, the semiconductor property of MoS_2 can be

changed from an n-type to a p-type. After a plasma treatment, Peng et al. found that the lattice of MoS_2 was distorted, which was equivalent to p-type doping and led to the single-layer MoS_2 with p-type properties.[236] This p-type MoS_2 inclines to reach type-I alignment with perovskite, which would limit the transportation of holes. However, Shi et al. predicted the cooperative effect between iodine vacancies in $MAPbI_3$ and sulfur vacancies in MoS_2 could reverse the band offset and accelerate hole transfer at the $MAPbI_3/MoS_2$ interface. This interplay not only improved the charge-transfer efficiency but also decreased the time-scale of charge transfer.[237] Additionally, research predicted that single layers 2D MoS_2 would form an appropriate ELA with $MAPbI_3$ to extract holes and block electrons.[236] Dasgupta et al. obtained 2D MoS_2 by a liquid-based exfoliation method and ozone treatment, and utilized this material as an HTM in PSCs. Uniform and homogeneous thin films of single- or few-layered 2H-phase MoS_2 was achieved. They found that the 2D MoS_2 HTM could form a better type-II alignment with $MAPbI_3$, which was conducive to the hole extraction.[238] Shin et al. found that the WF of MoS_2 could be increased to 4.94 eV and had an excellent ELA with perovskite because of the co-doping effect on the graphene surface. Flexible p-i-n-type perovskite photodiode (PD)/solar cell bifunctional (PPSB) devices exhibited good current (10^6 times by illumination even at 0 V) and excellent mechanical properties. Devices based on the MoS_2 HTM only showed 38% degradation after 30 days (25°C, 30% humidity).

5.1.2. Titanium Disulfide (TiS_2)

TiS_2, with a high carrier concentration and mobility, is widely used in PSCs. The Hall effect indicates that TiS_2 is an n-type semiconductor.[239] Yin et al. was the first to prepare 2D TiS_2 nanosheets as an ETM in PSCs by a simple solution exfoliation method and achieved a PCE of 17.37%.[240] The TiS_2 film had a better ELA with $MAPbI_3$ than TiO_2. Moreover, PSCs based on the TiS_2 ETM could maintain 90% of their initial PCE for 50 hours of light soaking, whereas 44% of the original PCE is

retained in PSCs based on TiO_2. Huang et al. found that UV-ozone could partially oxidize TiS_2, passivate S vacancies, and adjust the energy level of TiS_2 (from -4.79 to 4.64 eV).[241] The above observations resulted in an increase in PCE (18.79%) and excellent stability. Furthermore, they introduced TiS_2 to SnO_2 to form a SnO_2/2D TiS_2 double structure ETM. Due to the matched ELA and low electron trap state densities of the SnO_2/2D TiS_2 double structure ETM, it obtained a high PCE (21.37%) with a small hysteresis.[242]

Theoretical and experimental reports certify that the morphology can tune the bandgap of TiS_2.[243] Huckaba et al. synthesized amorphous TiS_2 and applied it as an HTM for PSCs.[244] The VB of TiS_2 was 0.15 eV higher than that of the mixed perovskite, which facilitated hole extraction and obtained a PCE of 13.54%. In addition, the cost of TiS_2 synthesis is only 3.33% that of Spiro-OMeTAD.

5.1.3. Tungsten Disulfide (WS_2)

Due to its high carrier mobility (116 $cm^2 \cdot V^{-1} \cdot s^{-1}$) and good conductivity, WS_2 is an HTM candidate for PSCs. In 2016, Kim et al. was the first to synthesize atomically thin polycrystalline WS_2 as an HTM in PSCs by a chemical deposition method, where the WF of WS_2 was 5.0 eV and had a good ELA with perovskite. The devices based on WS_2 achieved a PCE of 8.02%, which could be comparable to PEDOT:PSS.[245] To improve carrier extraction and decrease untrapped charges in the perovskite layer, Liu et al. introduced an ultrathin 2D WS_2 interlayer. After WS_2 interlayer deposition, a high-quality perovskite film with superior crystallinity and a large grain size was obtained by van der Waal quasi-epitaxial growth. The 2D WS_2 interlayer could inhibit the native defects and make the deep defect levels within perovskite shallower. Devices based on ITO/PTAA/WS_2/RbCsFAMA/PMMA:PCBM/C_{60}/ZnSe/Cu(Ag) achieved a PCE of 20.92%, which could be stabilized for 20 days and retaining 90% of its initial PCE (in the dark and in an air atmosphere with 30% RH).[246] Theoretical calculations also predicted that WS_2 could be utilized as an ETM in PSCs. Sobayel et

al. simulated ideal planar PSCs by using WS_2 as an ETM. They investigated the amphoteric defects at the interfaces of the CTL/perovskite layer and in the perovskite layer. The results showed that the amphoteric defects in the perovskite layer influenced the device performance more severely. Calculations for devices based on the structure of FTO/WS_2/$MAPbI_{3-x}Cl_x$/Spiro-OMeTAD/Ni could achieve a high PCE of 25.70%.[247]

Table 6 Summarization of photovoltaic parameters and stability of PSCs employed TMDs as charge transport materials.

Materials	Types	CB eV	VB eV	Device Architecture	PCE %	Test condition	Stability	Ref.
MoS_2	ETM		-	FTO/MoS_2/$MAPbI_3$/Spiro-OMeTAD/Au	13.14	-	-	[234]
	HTM		-	ITO/MoS_2/$MAPbI_3$/$PC_{60}BM$/Ag	6.01	-	-	[238]
TiS_2	ETM	-	-	FTO/TiS_2/$FA_{0.85}MA_{0.15}PbI_3$/Spiro-OMeTAD/Au	17.37	UV illumination	50 h, 90% of initial PCE	[240]
				ITO/TiS_2/$FA_xMA_{1-x}PbI_yBr_{3-y}$ /Spiro-OMeTAD/Ag	18.79	RH=10%, RT	816 h, 95.8% of initial PCE	[241]
		-	-4.63	ITO/TiS_2/ $FA_xMA_{1-x}PbI_yBr_{3-y}$ /Spiro-OMeTAD/Ag	21.73	RH=10%, RT	800 h, 92% of initial PCE	[242]
	HTM	-	-	FTO/c&m-TiO_2/$(FAPbI_3)_{0.85}(MAPbBr_3)_{0.15}$/$TiS_2$/Au	13.54	-	-	[244]
WS_2	ETM	-4.2	-	Cathode/WS_2/$MAPbX_3$/Spiro-OMeTAD/Ni	25.7 (simulation)	-	-	[247]
	HTM	-	-	ITO/WS_2/$MAPbI_{3-x}Cl_x$/PCBM/Al	8.02	-	-	[245]
		-	-5.21	ITO/PTAA/WS_2/RbCsFAMA/PMMA:PCBM/C_{60}/ZnSe/Cu(Ag)	20.92	30% RH, dark in air	20 d, 90% of initial PCE	[246]

Table 7 Summarization of photovoltaic parameters and stability of PSCs employed sulfur-based compounds as HTMs and co-sensitizer.

Materials	**CB/LUMO** **eV**	**VB/HOMO** **eV**	**Device Architecture**	**PCE** **%**	**Test condition**	**Stability**	**Ref.**
PbS	-3.7	-5.1	FTO/c&m-TiO_2/PbS/$MAPbI_3$/Au	3.6	-	-	[248]
	-	-	FTO/c&m-TiO_2/PbS/$MAPbI_3$/Au	3.2	argon atmosphere	45 d, >90% of initial PCE	[249]
	-3.7	-5.1	ITO/PbS/$MAPbI_3$/PCBM/Al	7.5	-	-	[250]
	-3.8	-5.2	FTO/c&m-TiO_2/$MAPbI_3$/PbS/Au	7.88	dry air, 25℃	4 d, 89% of initial PCE	[251]
S,N-heteropentacene Derivate	-3.77	-5.26	FTO/c&m-TiO_2/$MAPbI_3$/EES-1/Au	10.5	-	-	[252]
	-3.74	-5.1	FTO/c&m-TiO_2/$MAPbI_3$/EES-2/Au	9.5	-	-	
	-3.8	-5.2	FTO/c&m-TiO_2/$MAPbI_3$/JMCA-1/Au	11.4	-	-	[253]
	-3.77	-5.28	FTO/c&m-TiO_2/$MAPbI_3$/JMCA-2/Au	10.3	-	-	

5.2. Sulfur-based Compounds as HTMs and Co-sensitizer

The light absorption of perovskite is limited to its bandgap. One of the strategies to improve the spectral response of perovskite materials is using co-sensitizers with infrared (IR) absorbing nanoparticles, such as IR QDs and organic co-sensitizers. Usually, these co-sensitizers can act as bifunctional materials, enlarging the spectral response, and enhancing hole extraction. Detailed photovoltaic performances of the relevant devices are summarized in Table 7.

5.2.1. Lead Sulfide (PbS)

PbS QDs with a low bandgap have been intensively researched due to their high absorption coefficient and tunable bandgap.[254] In 2014, Etgar et al. applied PbS QDs into PSCs as an HTM and co-sensitizer to attain solar cells with perovskite and PbS QD heterojunctions.[248] The devices based on PbS QDs showed an improvement in J_{sc} of 24.63 $mA \cdot cm^{-2}$ due to the panchromatic response from the visible to near-IR regions of perovskite. Hu et al. used colloidal PbS QDs as an HTM and co-sensitizer for PSCs.[250] Owing to the quantum confinement effect, the bandgap of PbS QDs could be adjusted, allowing a better ELA with perovskite. In addition, PbS QDs could extend the absorption spectrum of PSCs into the infrared region. Li et al. applied PbS QDs as an HTM and co-sensitizer for PSCs.[251] The PCE of PSCs could be enhanced by 43% after PbS QD deposition.

5.2.2. *S,N*-heteropentacene Derivate

A low-bandgap *S,N*-heteropentacene derivative, with excellent stability and high charge carrier mobilities, has good hole transport performance and strong absorbance in the visible and near-IR regions. Qin et al. was the first to report A–D–A-type *S,N*-heteroacene-based oligothiophenes as hole-transporting and light-absorbing materials in PSCs.[252] Solution-processed $MAPbI_3$-based devices with these

bifunctional materials achieved a 38% PCE increase compared with devices without an HTM. Subsequently, they synthesized two new low-bandgap HTMs by retaining the *S,N*-heteropentacene core and replacing the branch chain with a 3,4-ethylenedioxythiophene/thiophene spacer. They found that the improved absorption in the visible and near-infrared regions could contribute to charge transport and enhance the photocurrent of the device.[253]

6. Prospect and Outlook

Due to rapid development, PSCs are expected to become candidates for low-cost power generation. To promote competitiveness, factors such as efficiency, long-term stability, and cost-effectiveness still need to be improved. A variety of strategies have been developed to overcome these problems in the past few years. The introduction of sulfur into different species of PSCs can make the resultant PSCs much better. The sulfur compounds can passivate the interfacial trap states and reduce charge recombination. In addition, the interaction of Pb-S can prevent the ion migration of Pb, thereby inhibiting the decomposition of perovskite. Moreover, the Pb-S bond can offer a new channel for the transmission and extraction of charges. Although sulfur-based PSCs have achieved remarkable success at present, different challenges persist.

The first matter is how to regulate the sulfur-based perovskite layer at the molecular level. Uniform and high-quality perovskite films are vital to guarantee highly efficient and stable PSCs. Regulating the crystallization and growth process of sulfur-based perovskite materials at the molecular level is a significant strategy. Sulfur can not only participate in the formation of the perovskite lattice but also improve the mobility of perovskite. Regarding synthetic chemistry, accelerating the formation of the crystal nucleus and slowing down the crystallization growth of perovskite can form a high-quality perovskite film. Therefore, a deeper understanding of the

nucleation mechanisms, crystal growth dynamics, and roles of sulfur components and additives is still needed. In particular, more powerful tools should be applied to provide critical, insightful information at the molecular level.

The second matter is passivation at the interfacial contact, including at the interfaces of the CTL/perovskite layer and CTL/electrode. Further PSC improvements include better control of the vacancies and defects at the interfacial surfaces. Sulfur compounds such as CTLs and interfacial passivators can interact with lead in the perovskite layer, leading to the passivation of defects on the perovskite surface, creating a barrier against humidity and ion migration, and stabilizing the perovskite-based materials and devices. However, trap states that act as carrier accumulators and recombination centers are inevitable. The design of new sulfur-based interfacial engineering materials to mitigate nonradiative losses, prevent structural phase transitions and decrease photoinduced ion migration in perovskite films is of importance.

The third matter is for the design of CTLs with a low cost and high efficiency. Sulfide ETMs and chalcogen compound HTMs usually exhibit high mobility as well as superior stability and are considered potential competitors to develop flexible device fabrication at low temperature. In addition, inorganic sulfur compound CTLs have the characteristics of low price and wide availability of sources. Nevertheless, their solubility and processing technology limit their application. Therefore, the synthesis of new sulfur-based CTLs with high conductivity, solubility, and excellent carrier extraction needs to be further developed.

Although sulfur-based materials have achieved some efforts to promote the efficiency and long-term stability of PSCs, additional research is required to realize commercialization goals. We hope that this review is a significant guide for understanding the intrinsic phenomena of sulfur-based materials and encourage additional investigations to address the remaining issues with sulfur-based PSCs.

Acknowledgments

This work was supported by the National Natural Science Foundation of China (Grant No. 51772039, 21703027, 21903010 and 51972293), and the Grant-in-Aid for Scientific Research (KAKENHI) program, Japan (B, Grant Number 19H02818).

Reference

[1] A. Kojima, K. Teshima, Y. Shirai, T. Miyasaka, *J. Am. Chem. Soc.* **2009**, *131*, 6050.

[2] *National Renewable Energy Laboratory* https://www.nrel.gov/pv/cell-efficiency.html (accessed Dec. 05. 2020).

[3] a) H. J. Snaith, *J. Phys. Chem. Lett.* **2013**, *4*, 3623-3630; b) G. C. Xing, N. Mathews, S. Y. Sun, S. S. Lim, Y. M. Lam, M. Grätzel, S. Mhaisalkar, T. C. Sum, *Science* **2013**, *342*, 344-347; c) Y. Zhao, K. Zhu, *J. Phys. Chem. Lett.* **2013**, *4*, 2880-2884; d) V. D'Innocenzo, G. Grancini, M. J. P. Alcocer, A. R. S. Kandada, S. D. Stranks, M. M. Lee, G. Lanzani, H. J. Snaith, A. Petrozza, *Nat. Commun.* **2014**, *5*.

[4] J. Chen, N.-G. Park, *Adv. Mater.* **2019**, *31*, 1803019.

[5] Y. G. Rong, Y. Hu, A. Y. Mei, H. R. Tan, M. I. Saidaminov, S. I. Seok, M. D. McGehee, E. H. Sargent, H. W. Han, *Science* **2018**, *361*, 7.

[6] a) R. Wang, M. Mujahid, Y. Duan, Z.-K. Wang, J. Xue, Y. Yang, *Adv. Funct. Mater.* **2019**, *29*, 1808843; b) C. C. Boyd, R. Cheacharoen, T. Leijtens, M. D. McGehee, *Chem. Rev.* **2019**, *119*, 3418-3451; c) H. Min, G. Kim, M. J. Paik, S. Lee, W. S. Yang, M. Jung, S. I. Seok, *Adv. Energy Mater.* **2019**, *9*, 1803476; d) Z. Wang, A. K. Baranwal, M. A. kamarudin, c. h. Ng, M. Pandey, T. Ma, S. Hayase, *Nano Energy* **2019**, *59*, 258-267; e) X. Li, J. Yang, Q. Jiang, H. Lai, S. Li, Y. Tan, Y. Chen, S. Li, *J. Mater. Chem. A* **2019**, *7*, 7065-7073.

[7] Z. Li, T. R. Klein, D. H. Kim, M. Yang, J. J. Berry, M. F. A. M. van Hest, K. Zhu, *Nat. Rev. Mater.* **2018**, *3*, 18017.

[8] a) M. Saliba, T. Matsui, J.-Y. Seo, K. Domanski, J.-P. Correa-Baena, M. K. Nazeeruddin, S. M. Zakeeruddin, W. Tress, A. Abate, A. Hagfeldt, M. Grätzel, *Energy Environ. Sci.* **2016**, *9*, 1989-1997; b) H. Lu, A. Krishna, S. M. Zakeeruddin, M. Gratzel, A. Hagfeldt, *Science* **2020**, *23*, 101359.

[9] a) G. Grancini, M. K. Nazeeruddin, *Nat. Rev. Mater.* **2019**, *4*, 4-22; b) Y. Zhou, J. Hu, F. Meng, C. Liu, L. Gao, T. Ma, *Prog. Chem.* **2020**, *32*, 966-977; c) C. Ortiz-Cervantes, P. Carmona-Monroy, D. Solis-Ibarra, *ChemSusChem* **2019**, *12*, 1560-1575.

[10] a) T. Li, Y. Pan, Z. Wang, Y. Xia, Y. Chen, W. Huang, *J. Mater. Chem. A* **2017**, *5*, 12602-12652; b) A. Mahapatra, D. Prochowicz, M. M. Tavakoli, S. Trivedi, P. Kumar, P. Yadav, *J. Mater. Chem. A* **2020**, *8*, 27-54; c) M. Azam, K. Liu, Y. Sun, Z. Wang, G. Liang, S. Qu, P. Fan, Z. Wang, *J. Phys. D: Appl. Phys.* **2020**, *53*, 183002.

[11] a) F. Meng, C. Liu, L. Gao, T. Ma, *Prog. Chem.* **2020**, *32*, 817-835; b) F. Meng, A. Liu, L. Gao, J. Cao, Y. Yan, N. Wang, M. Fan, G. Wei, T. Ma, *J. Mater. Chem. A* **2019**, *7*, 8690-8699; c) M. Ye, C. He, J. Iocozzia, X. Liu, X. Cui, X. Meng, M. Rager, X. Hong, X. Liu, Z. Lin, *Journal Of Physics D-Applied Physics* **2017**, *50*, 373002.

[12] K. Mahmood, S. Sarwar, M. T. Mehran, *RSC Adv.* **2017**, *7*, 17044-17062.

[13]W. Ke, D. Zhao, A. J. Cimaroli, C. R. Grice, P. Qin, Q. Liu, L. Xiong, Y. Yan, G. Fang, *J. Mater. Chem. A* **2015**, *3*, 24163-24168.

[14] a) L. Zhu, Z. Shao, J. Ye, X. Zhang, X. Pan, S. Dai, *Chem Commun (Camb)* **2016**, *52*, 970-973; b) S. S. Shin, E. J. Yeom, W. S. Yang, S. Hur, M. G. Kim, J. Im, J. Seo, J. H. Noh, S. I. Seok, *Science* **2017**, *356*, 167-171.

[15] X. Zhao, S. Liu, H. Zhang, S.-Y. Chang, W. Huang, B. Zhu, Y. Shen, C. Shen, D. Wang, Y. Yang, M. Wang, *Adv. Funct. Mater.* **2019**, *29*.

[16]J. Liu, C. Gao, L. Luo, Q. Ye, X. He, L. Ouyang, X. Guo, D. Zhuang, C. Liao, J. Mei, W. Lau, *J. Mater. Chem. A* **2015**, *3*, 11750-11755.

[17]a) W. Ke, C. C. Stoumpos, J. L. Logsdon, M. R. Wasielewski, Y. Yan, G. Fang, M. G. Kanatzidis, *J. Am. Chem. Soc.* **2016**, *138*, 14998-15003; b) R. D. Chavan, P. Yadav, M. M. Tavakoli, D. Prochowicz, A. Nimbalkar, S. P. Bhoite, P. N. Bhosale, C. K. Hong, *Sustainable Energy Fuels* **2020**, *4*, 843-851; c) R. Chen, J. Cao, Y. Duan, Y. Hui, T. T. Chuong, D. Ou, F. Han, F. Cheng, X. Huang, B. Wu, N. Zheng, *J. Am. Chem. Soc.* **2019**, *141*, 541-547.

[18] M. M. Tavakoli, D. Prochowicz, P. Yadav, R. Tavakoli, *Phys. Status Solidi RRL.* **2020**, *14*.

[19] B. L. Williams, J. D. Major, L. Bowen, L. Phillips, G. Zoppi, I. Forbes, K. Durose, *Sol. Energy Mater. Sol. Cells* **2014**, *124*, 31-38.

[20] E. J. Juarez-Perez, M. Wussler, F. Fabregat-Santiago, K. Lakus-Wollny, E. Mankel, T. Mayer, W. Jaegermann, I. Mora-Sero, *J. Phys. Chem. Lett.* **2014**, *5*, 680-685.

[21] W. A. Dunlap-Shohl, R. Younts, B. Gautam, K. Gundogdu, D. B. Mitzi, *J. Phys. Chem. C* **2016**, *120*, 16437-16445.

[22] J. Dong, J. Wu, J. Jia, L. Fan, Y. Lin, J. Lin, M. Huang, *J. Mater. Chem. C* **2017**, *5*, 10023-10028.

[23] J. Jia, J. Wu, J. Dong, L. Fan, M. Huang, J. Lin, Z. Lan, *Chem. Commun.* **2018**, *54*, 3170-3173.

[24] Z. Liu, X. Liu, B. Sun, X. Tan, H. Ye, Y. Tu, T. Shi, Z. Tang, G. Liao, *Org. Electron.* **2019**, *74*, 152-160.

[25]S. M. Ali, S. M. Ramay, M. H. Aziz, N. Ur-Rehman, M. S. AlGarawi, S. S. AlGhamd, A. Mahmood, T. S. Alkhuraiji, S. Atiq, *Org. Electron.* **2018**, *62*, 21-25.

[26] S. Wu, C. Chen, J. Wang, J. Xiao, T. Peng, *ACS Appl. Energy Mater.* **2018**, *1*, 1649-1657.

[27] Z. Gu, F. Chen, X. Zhang, Y. Liu, C. Fan, G. Wu, H. Li, H. Chen, *Sol. Energy Mater. Sol. Cells* **2015**, *140*, 396-404.

[28] Z. Song, G. Tong, H. Li, G. Li, S. Ma, S. Yu, Q. Liu, Y. Jiang, *Nanotechnology* **2018**, *29*, 025401.

[29] B. Wang, J. Iocozzia, M. Zhang, M. Ye, S. Yan, H. Jin, S. Wang, Z. Zou, Z. Lin, *Chem. Soc. Rev.* **2019**, *48*, 4854-4891.

[30] E. Zhao, L. Gao, S. Yang, L. Wang, J. Cao, T. Ma, *Nano Res.* **2018**, *11*, 5913-5923.

[31] L. Gao, C. Liu, F. Meng, A. Liu, Y. Li, Y. Li, C. Zhang, M. Fan, G. Wei, T. Ma, *ACS Sustainable Chem. Eng.* **2020**, *8*, 9250-9256.

[32] W. Chu, X. Li, S. Li, J. Hou, Q. Jiang, J. Yang, *ACS Appl. Energy Mater.* **2019**, *2*, 382-388.

[33]M. Wang, F. Cao, L. Meng, W. Tian, L. Li, *Adv. Mater. Inter.* **2019**, *6*, 1801526.

[34] Y. Hou, X. Chen, S. Yang, Y. L. Zhong, C. Li, H. Zhao, H. G. Yang, *Nano Energy* **2017**, *36*, 102-109.

[35]Z. Xu, J. Wu, Y. Yang, Z. Lan, J. Lin, *ACS Appl. Energy Mater.* **2018**, *1*, 4050-4056.

[36] B. Yang, M. Wang, X. Hu, T. Zhou, Z. Zang, *Nano Energy* **2019**, *57*, 718-727.

[37] a) J. Peng, Z. Yu, J. Wu, Y. Zhou, Y. Guo, Z. Li, J. Zhao, C. Wu, Y. Xie, *ACS Nano* **2018**, *12*, 9461-9466; b) E. Navarro-Moratalla, J. O. Island, S. Manas-Valero, E. Pinilla-Cienfuegos, A. Castellanos-Gomez, J. Quereda, G. Rubio-Bollinger, L. Chirolli, J. Angel Silva-Guillen, N. Agrait, G. A. Steele, F. Guinea, H. S. J. van der Zant, E. Coronado, *Nat. Commun.* **2016**, *7*,*11043*.

[38] L. Quyet Van, N. Thang Phan, K. S. Choi, Y.-H. Cho, Y. J. Hong, S. Y. Kim, *Phys. Chem. Chem. Phys.* **2014**, *16*, 25468-25472.

[39] M. Afzali, A. Mostafavi, T. Shamspur, *J. Alloys Compd.* **2020**, *817*, 152742.

[40] D.-B. Li, L. Hu, Y. Xie, G. Niu, T. Liu, Y. Zhou, L. Gao, B. Yang, J. Tang, *ACS Photonics* **2016**, *3*, 2122-2128.

[41] Z. Cao, C. Li, X. Deng, S. Wang, Y. Yuan, Y. Chen, Z. Wang, Y. Liu, L. Ding, F. Hao, *J. Mater. Chem. A* **2020**, *8*, 19768-19787.

[42]H. Peng, W. Sun, Y. Li, W. Yan, P. Yu, H. Zhou, Z. Bian, C. Huang, *J. Photonics Energy* **2016**, *6*, 022002.

[43] D. A. A. Leal, S. Shaji, D. A. Avellaneda, J. A. A. Martínez, B. Krishnan, *Appl. Surf. Sci.* **2020**, *508*.

[44] J. Wang, L. Liu, S. Liu, L. Yang, B. Zhang, S. Feng, J. Yang, X. Meng, W. Fu, H. Yang, *Sustainable Energy Fuels* **2017**, *1*, 504-509.

[45] M. Abulikemu, J. Barbe, A. El Labban, J. Eid, S. Del Gobbo, *Thin Solid Films* **2017**, *636*, 512-518.

[46] G. Tong, Z. Song, C. Li, Y. Zhao, L. Yu, J. Xu, Y. Jiang, Y. Sheng, Y. Shi, K. Chen, *RSC Adv.* **2017**, *7*, 19457-19463.

[47] Q. Sun, H. Chen, W.-J. Yin, *Chem. Mater.* **2018**, *31*, 244-250.

[48] a) W. Meng, B. Saparov, F. Hong, J. Wang, D. B. Mitzi, Y. Yan, *Chem. Mater.* **2016**, *28*, 821-829; b) Y. Y. Sun, M. L. Agiorgousis, P. Zhang, S. Zhang, *Nano Lett.* **2015**, *15*, 581-585; c) S. Niu, H. Huyan, Y. Liu, M. Yeung, K. Ye, L. Blankemeier, T. Orvis, D. Sarkar, D. J. Singh, R. Kapadia, J. Ravichandran, *Adv. Mater.* **2017**, *29*, 1604733; d) M.-G. Ju, J. Dai, L. Ma, X. C. Zeng, *Adv. Energy Mater.* **2017**, *7*, 1700216.

[49] Q. Jiang, D. Rebollar, J. Gong, E. L. Piacentino, C. Zheng, T. Xu, *Angew. Chem. Int. Ed.* **2015**, *54*, 7617-7620.

[50] S. Liu, Y. Guan, Y. Sheng, Y. Hu, Y. Rong, A. Mei, H. Han, *Adv. Energy Mater.* **2020**, *10*, 1902492.

[51] B. Chen, P. N. Rudd, S. Yang, Y. Yuan, J. Huang, *Chem. Soc. Rev.* **2019**, *48*, 3842-3867.

[52] J. S. Manser, J. A. Christians, P. V. Kamat, *Chem. Rev.* **2016**, *116*, 12956-13008.

[53] Y. Chen, B. Li, W. Huang, D. Gao, Z. Liang, *Chem. Commun.* **2015**, *51*, 11997-11999.

[54] Q. Tai, P. You, H. Sang, Z. Liu, C. Hu, H. L. W. Chan, F. Yan, *Nat. Commun.* **2016**, *7*,11105.

[55] R. Nie, A. Mehta, B. W. Park, H. W. Kwon, J. Im, S. I. Seok, *J. Am. Chem. Soc.* **2018**, *140*, 872-875.

[56] J. Li, X. Liu, J. Xu, J. Chen, C. Zhao, M. Salma Maneno, B. Zhang, J. Yao, *Sol. RRL* **2019**, *3*, 1900218.

[57]H. Lai, B. Kan, T. Liu, N. Zheng, Z. Xie, T. Zhou, X. Wan, X. Zhang, Y. Liu, Y. Chen, *J. Am. Chem. Soc.* **2018**, *140*, 11639-11646.

[58] Y. Yan, S. Yu, A. Honarfar, T. Pullerits, K. Zheng, Z. Liang, *Adv. Sci.* **2019**, *6*, 1900548.

[59] a) J. G. Labram, N. R. Venkatesan, C. J. Takacs, H. A. Evans, E. E. Perry, F. Wudl, M. L. Chabinyc, *J. Mater. Chem. C* **2017**, *5*, 5930-5938; b) J. Liu, J. Shi, D. Li, F. Zhang, X. Li, Y. Xiao, S. Wang, *Synth. Met.* **2016**, *215*, 56-63.

[60] Z. Xiao, W. Meng, J. Wang, Y. Yan, *Phys. Chem. Chem. Phys.* **2016**, *18*, 25786-25790.

[61] L. Guo, O. Wang, D. Zhao, X. Gan, H. Liu, *Polyhedron* **2018**, *145*, 16-21.

[62] L. Gao, F. Zhang, X. Chen, C. Xiao, B. W. Larson, S. P. Dunfield, J.

J. Berry, K. Zhu, *Angew. Chem. Int. Ed.* **2019**, *58*, 11737-11741.

[63]H. Ren, S. Yu, L. Chao, Y. Xia, Y. Sun, S. Zuo, F. Li, T. Niu, Y. Yang, H. Ju, B. Li, H. Du, X. Gao, J. Zhang, J. Wang, L. Zhang, Y. Chen, W. Huang, *Nat. Photonics* **2020**, *14*, 154–163.

[64] a) S. Bai, P. Da, C. Li, Z. Wang, Z. Yuan, F. Fu, M. Kawecki, X. Liu, N. Sakai, J. T.-W. Wang, S. Huettner, S. Buecheler, M. Fahlman, F. Gao, H. J. Snaith, *Nature* **2019**, *571*, 245-250; b) X. Deng, L. Xie, S. Wang, C. Li, A. Wang, Y. Yuan, Z. Cao, T. Li, L. Ding, F. Hao, *Chem. Eng. J.* **2020**, *398*, 125594.

[65] a) L. Wang, H. Zhou, J. Hu, B. Huang, M. Sun, B. Dong, G. Zheng, Y. Huang, Y. Chen, L. Li, Z. Xu, N. Li, Z. Liu, Q. Chen, L.-D. Sun, C.-H. Yan, *Science* **2019**, *363*, 265-270; b) N. Li, S. Tao, Y. Chen, X. Niu, C. K. Onwudinanti, C. Hu, Z. Qiu, Z. Xu, G. Zheng, L. Wang, Y. Zhang, L. Li, H. Liu, Y. Lun, J. Hong, X. Wang, Y. Liu, H. Xie, Y. Gao, Y. Bai, S. Yang, G. Brocks, Q. Chen, H. Zhou, *Nat. Energy* **2019**, *4*, 408-415.

[66] T. Wu, Y. Wang, X. Li, Y. Wu, X. Meng, D. Cui, X. Yang, L. Han, *Adv. Energy Mater.* **2019**, *9*, 1803766.

[67] a) I. Wharf, T. Gramstad, R. Makhija, M. Onyszchuk, *Can. J. Chem.* **1976**, *54*, 3430-3438; b) J. C. Hamill, O. Romiluyi, S. A. Thomas, J. Cetola, J. Schwartz, M. F. Toney, P. Clancy, Y. L. Loo, *J. Phys. Chem. C* **2020**, *124*, 14496-14502.

[68] T. Zhou, H. Lai, T. Liu, D. Lu, X. Wan, X. Zhang, Y. Liu, Y. Chen, *Adv. Mater.* **2019**, *31*, 1901242.

[69] A. Leblanc, N. Mercier, M. Allain, J. Dittmer, T. Pauporté, V. Fernandez, F. Boucher, M. Kepenekian, C. Katan, *ACS Appl. Mater. Interfaces* **2019**, *11*, 20743-20751.

[70] a) Q. Han, Y. Bai, J. Liu, K.-z. Du, T. Li, D. Ji, Y. Zhou, C. Cao, D. Shin, J. Ding, A. D. Franklin, J. T. Glass, J. Hu, M. J. Therien, J. Liu, D. B. Mitzi, *Energy Environ. Sci.* **2017**, *10*, 2365-2371; b) H. Zhang, M. Hou, Y. Xia, Q. Wei, Z. Wang, Y. Cheng, Y. Chen, W. Huang, *J. Mater. Chem. A* **2018**, *6*, 9264-9270.

[71] S. Yang, W. Liu, L. Zuo, X. Zhang, T. Ye, J. Chen, C.-Z. Li, G. Wu, H. Chen, *J. Mater. Chem. A* **2016**, *4*, 9430-9436.

[72] L. Gao, F. Zhang, C. Xiao, X. Chen, B. W. Larson, J. J. Berry, K. Zhu, *Adv. Funct. Mater.* **2019**, *29*, 1901652.

[73]a) F. Li, J. Zhang, S. Jo, M. Qin, Z. Li, T. Liu, X. Lu, Z. Zhu, A. K. Y. Jen, *Small Methods* **2019**, *4*, 1900831; b) X. Zhang, G. Wu, S. Yang, W. Fu, Z. Zhang, C. Chen, W. Liu, J. Yan, W. Yang, H. Chen, *Small* **2017**, *13*, 1700611.

[74] W. Fu, J. Wang, L. Zuo, K. Gao, F. Liu, D. S. Ginger, A. K. Y. Jen, *ACS Energy Lett.* **2018**, *3*, 2086-2093.

[75] C. Fei, B. Li, R. Zhang, H. Fu, J. Tian, G. Cao, *Adv. Energy Mater.* **2017**, *7*, 1602017.

[76] H. Zhu, F. Zhang, Y. Xiao, S. Wang, X. Li, *J. Mater. Chem. A* **2018**, *6*, 4971-4980.

[77] C. Cui, D. Xie, P. Lin, H. Hu, S. Che, K. Xiao, P. Wang, L. Xu, D. Yang, X. Yu, *Sol. Energy Mater. Sol. Cells* **2020**, *208*, 110435.

[78] L. Gao, S. Huang, L. Chen, X. Li, B. Ding, S. Huang, G. Yang, *Sol. RRL* **2018**, *2*, 1800088.

[79] M. Sun, F. Zhang, H. Liu, X. Li, Y. Xiao, S. Wang, *J. Mater. Chem. A* **2017**, *5*, 13448-13456.

[80] a) Q. Wang, X. Zheng, Y. Deng, J. Zhao, Z. Chen, J. Huang, *Joule* **2017**, *1*, 371-382; b) F. Zhang, K. Zhu, *Adv. Energy Mater.* **2019**, *10*, 1902579.

[81] J. Chen, N.-G. Park, *ACS Energy Lett.* **2020**, *5*, 2742-2786.

[82] T. Y. Wen, S. Yang, P. F. Liu, L. J. Tang, H. W. Qiao, X. Chen, X. H. Yang, Y. Hou, H. G. Yang, *Adv. Energy Mater.* **2018**, *8*, 1703143.

[83] A. A. Sutanto, N. Drigo, V. I. E. Queloz, I. Garcia-Benito, A. R. Kirmani, L. Richter, P. Schouwink, K. T. Cho, S. Paek, M. K. Nazeeruddin, G. Grancini, *J. Mater. Chem. A* **2020**, *8*, 2343-2348.

[84] L. Meng, C. Sun, R. Wang, W. Huang, Z. Zhao, P. Sun, T. Huang, J. Xue, J. W. Lee, C. Zhu, Y. Huang, Y. Li, Y. Yang, *J. Am. Chem. Soc.* **2018**, *140*, 17255-17262.

[85] N. K. Noel, A. Abate, S. D. Stranks, E. S. Parrott, V. M. Burlakov, A. Goriely, H. J. Snaith, *ACS Nano* **2014**, *8*, 9815-9821.

[86] L. Liu, W.-H. Fang, R. Long, O. V. Prezhdo, *J. Phys. Chem. Lett.* **2018**, *9*, 1164-1171.

[87] Z. Wang, A. K. Baranwal, M. Akmal kamarudin, P. Zhang, G. Kapil, T. Ma, S. Hayase, *Nano Energy* **2019**, *66*, 104180.

[88] I. S. Yang, S. Lee, J. Choi, M. T. Jung, J. Kim, W. I. Lee, *J. Mater. Chem. A* **2019**, *7*, 6028-6037.

[89] Y. Hou, Z. R. Zhou, T. Y. Wen, H. W. Qiao, Z. Q. Lin, B. Ge, H. G. Yang, *Nanoscale Horiz.* **2019**, *4*, 208-213.

[90] S. Yang, S. Chen, E. Mosconi, Y. Fang, X. Xiao, C. Wang, Y. Zhou, Z. Yu, J. Zhao, Y. Gao, F. De Angelis, J. Huang, *Science* **2019**, *365*, 473.

[91] A. Mahapatra, N. Parikh, H. Kumari, M. K. Pandey, M. Kumar, D. Prochowicz, A. Kalam, M. M. Tavakoli, P. Yadav, *J. Appl. Phys.* **2020**, *127*, 185501.

[92] M.-H. Li, T.-G. Sun, J.-Y. Shao, Y.-D. Wang, J.-S. Hu, Y.-W. Zhong, *Nano Energy* **2021**, *79*, 105462.

[93] J. W. Lee, Z. Dai, T. H. Han, C. Choi, S. Y. Chang, S. J. Lee, N. De Marco, H. Zhao, P. Sun, Y. Huang, Y. Yang, *Nat. Commun.* **2018**, *9*, 3021.

[94] J. Hu, C. Wang, S. Qiu, Y. Zhao, E. Gu, L. Zeng, Y. Yang, C. Li, X. Liu, K. Forberich, C. J. Brabec, M. K. Nazeeruddin, Y. Mai, F. Guo, *Adv. Energy Mater.* **2020**, *10*, 2000173.

[95] D. Lu, G. Lv, Z. Xu, Y. Dong, X. Ji, Y. Liu, *J. Am. Chem. Soc.* **2020**,

142, 11114-11122.

[96] Y. Dong, D. Lu, Z. Xu, H. Lai, Y. Liu, *Adv. Energy Mater.* **2020**, *10*, 2000694.

[97] L. Xie, T. Zhang, Y. Zhao, *J. Energy Chem.* **2020**, *47*, 62-65.

[98] Z. Xu, L. Wang, Q. Han, Y. Kamata, T. Ma, *ACS Appl. Mater. Interfaces* **2020**, *12*, 12867-12873.

[99] J. Cao, G. Tang, P. You, T. Wang, F. Zheng, J. Zhao, F. Yan, *Adv. Funct. Mater.* **2020**, *30*, 2002358.

[100] a) L. G. Gao, L. K. Wang, X. G. Ding, E. L. Zhao, S. Z. Yang, Y. Y. Zhao, Y. Q. Li, S. F. Wang, T. L. Ma, *J. Mater. Chem. A* **2018**, *6*, 4365-4373; b) D. Wei, T. Wang, J. Ji, M. Li, P. Cui, Y. Li, G. Li, J. M. Mbengue, D. Song, *J. Mater. Chem. A* **2016**, *4*, 1991-1998.

[101] S. Ye, W. Sun, Y. Li, W. Yan, H. Peng, Z. Bian, Z. Liu, C. Huang, *Nano Lett.* **2015**, *15*, 3723-3728.

[102] N. Wijeyasinghe, A. Regoutz, F. Eisner, T. Du, L. Tsetseris, Y.-H. Lin, H. Faber, P. Pattanasattayavong, J. Li, F. Yan, M. A. McLachlan, D. J. Payne, M. Heeney, T. D. Anthopoulos, *Adv. Funct. Mater.* **2017**, *27*, 1701818.

[103] M. Lyu, J. Chen, N.-G. Park, *J. Solid State Chem.* **2019**, *269*, 367-374.

[104] S. Ito, S. Tanaka, H. Vahlman, H. Nishino, K. Manabe, P. Lund, *Chemphyschem* **2014**, *15*, 1194-1200.

[105] a) J. Chen, J.-Y. Seo, N.-G. Park, *Adv. Energy Mater.* **2018**, *8*, 1702714; b) X. Wu, L. Xie, K. Lin, J. Lu, K. Wang, W. Feng, B. Fan, P. Yin, Z. Wei, *J. Mater. Chem. A* **2019**, *7*, 12236-12243; c) N. Arora, M. I. Dar, S. Akin, R. Uchida, T. Baumeler, Y. Liu, S. M. Zakeeruddin, M. Grätzel, *Small* **2019**, *15*, 1904746; d) S. S. Mali, J. V. Patil, H. Kim, R. Luque, C. K. Hong, *Mater. Today* **2019**, *26*, 8-18; e) J. Kim, Y. Lee, A. J. Yun, B. Gil, B. Park, *ACS Appl. Mater. Interfaces* **2019**, *11*, 46818-46824; f) F. Matebese, R. Taziwa, D. Mutukwa, *Materials* **2018**, *11*, 2592.

[106] P. Qin, S. Tanaka, S. Ito, N. Tetreault, K. Manabe, H. Nishino, M. K. Nazeeruddin, M. Grätzel, *Nat. Commun.* **2014**, *5*, 3834.

[107] N. Arora, M. I. Dar, A. Hinderhofer, N. Pellet, F. Schreiber, S. M. Zakeeruddin, M. Grätzel, *Science* **2017**, *358*, 768-771.

[108] C. Liu, L. Zhang, Y. Li, X. Zhou, S. She, X. Wang, Y. Tian, A. K. Y. Jen, B. Xu, *Adv. Funct. Mater.* **2020**, *30*, 1908462.

[109] G. Murugadoss, R. Thangamuthu, S. M. Senthil Kumar, *Sol. Energy Mater. Sol. Cells* **2017**, *164*, 56-62.

[110] V. E. Madhavan, I. Zimmermann, C. Roldán-Carmona, G. Grancini, M. Buffiere, A. Belaidi, M. K. Nazeeruddin, *ACS Energy Lett.* **2016**, *1*, 1112-1117.

[111] J. Lee, S. Singh, S. Kim, S. Baik, *Carbon* **2020**, *157*, 731-740.

[112] J. Liu, S. K. Pathak, N. Sakai, R. Sheng, S. Bai, Z. Wang, H. J.

Snaith, *Adv. Mater. Inter.* **2016**, *3*, 1600571.

[113] U. Er, K. C. Icli, M. Ozenbas, *J. Solid State Electrochem.* **2019**, *24*, 293-304.

[114] A. S. Subbiah, A. Halder, S. Ghosh, N. Mahuli, G. Hodes, S. K. Sarkar, *J. Phys. Chem. Lett.* **2014**, *5*, 1748-1753.

[115] S. Chavhan, O. Miguel, H.-J. Grande, V. Gonzalez-Pedro, R. S. Sánchez, E. M. Barea, I. Mora-Seró, R. Tena-Zaera, *J. Mater. Chem. A* **2014**, *2*, 12754-12760.

[116] K. Zhao, R. Munir, B. Yan, Y. Yang, T. Kim, A. Amassian, *J. Mater. Chem. A* **2015**, *3*, 20554-20559.

[117] M. Jung, Y. C. Kim, N. J. Jeon, W. S. Yang, J. Seo, J. H. Noh, S. Il Seok, *ChemSusChem* **2016**, *9*, 2592-2596.

[118] J. Chen, N.-G. Park, *J. Phys. Chem. C* **2018**, *122*, 14039-14063.

[119] M. Li, Z.-K. Wang, Y.-G. Yang, Y. Hu, S.-L. Feng, J.-M. Wang, X.-Y. Gao, L.-S. Liao, *Adv. Energy Mater.* **2016**, *6*, 1601156.

[120] Y. Liu, Z. Liu, E.-C. Lee, *ACS Appl. Energy Mater.* **2019**, *2*, 1932-1942.

[121] Q. Xiong, H. Tian, J. Zhang, L. Han, C. Lu, B. Shen, Y. Zhang, Y. Zheng, C. Lu, Z. Zeng, Z. Hu, L. Wu, Y. Zhu, *Org. Electron.* **2018**, *61*, 151-156.

[122] L. Xu, Y. Li, C. Zhang, Y. Liu, C. Zheng, W. Lv, M. Li, Y. Chen, W. Huang, R. Chen, *Sol. Energy Mater. Sol. Cells* **2020**, *206*, 110316

[123] J. W. Jung, C.-C. Chueh, A. K. Y. Jen, *Adv. Energy Mater.* **2015**, *5*, 1500486.

[124] L. Fan, Y. Li, X. Yao, Y. Ding, S. Zhao, B. Shi, C. Wei, D. Zhang, B. Li, G. Wang, Y. Zhao, X. Zhang, *ACS Appl. Energy Mater.* **2018**, *1*, 1575-1584.

[125] H. Wang, H. A. Dewi, T. M. Koh, A. Bruno, S. Mhaisalkar, N. Mathews, *ACS Appl. Mater. Interfaces* **2020**, *12*, 484-493.

[126] a) K.-J. Huang, J.-Z. Zhang, Y. Fan, *J. Alloys Compd.* **2015**, *625*, 158-163; b) J. Li, T. Jiu, G. H. Tao, G. Wang, C. Sun, P. Li, J. Fang, L. He, *J. Colloid Interface Sci.* **2014**, *419*, 142-147.

[127] H. Rao, W. Sun, S. Ye, W. Yan, Y. Li, H. Peng, Z. Liu, Z. Bian, C. Huang, *ACS Appl. Mater. Interfaces* **2016**, *8*, 7800-7805.

[128] J. Tirado, C. Roldán-Carmona, F. A. Muñoz-Guerrero, G. Bonilla-Arboleda, M. Ralaiarisoa, G. Grancini, V. I. E. Queloz, N. Koch, M. K. Nazeeruddin, F. Jaramillo, *Appl. Surf. Sci.* **2019**, *478*, 607-614.

[129] H. Lei, G. Yang, X. Zheng, Z.-G. Zhang, C. Chen, J. Ma, Y. Guo, Z. Chen, P. Qin, Y. Li, G. Fang, *Sol. RRL* **2017**, *1*, 1700038.

[130] S. C. Riha, A. A. Koegel, X. Meng, I. S. Kim, Y. Cao, M. J. Pellin, J. W. Elam, A. B. Martinson, *ACS Appl. Mater. Interfaces* **2016**, *8*, 2774-2780.

[131] X. Li, Y. Tan, H. Lai, S. Li, Y. Chen, S. Li, P. Xu, J. Yang, *ACS Appl. Mater. Interfaces* **2019**, *11*, 29746-29752.

[132] A. J. Huckaba, P. Sanghyun, G. Grancini, E. Bastola, C. K. Taek, L. Younghui, K. P. Bhandari, C. Ballif, R. J. Ellingson, M. K. Nazeeruddin, *ChemistrySelect* **2016**, *1*, 5316-5319.

[133] B. Koo, H. Jung, M. Park, J.-Y. Kim, H. J. Son, J. Cho, M. J. Ko, *Adv. Funct. Mater.* **2016**, *26*, 5400-5407.

[134] G. A. Sepalage, S. Meyer, A. R. Pascoe, A. D. Scully, U. Bach, Y.-B. Cheng, L. Spiccia, *Nano Energy* **2017**, *32*, 310-319.

[135] I. S. Yang, M. R. Sohn, S. D. Sung, Y. J. Kim, Y. J. Yoo, J. Kim, W. I. Lee, *Nano Energy* **2017**, *32*, 414-421.

[136] S. S. Mali, J. V. Patil, C. K. Hong, *J. Mater. Chem. A* **2019**, *7*, 10246-10255.

[137] T. H. Chowdhury, M. Akhtaruzzaman, M. E. Kayesh, R. Kaneko, T. Noda, J.-J. Lee, A. Islam, *Sol. Energy* **2018**, *171*, 652-657.

[138] Y. Yang, P. Ngoc Duy, D. Yao, L. Fan, H. Minh Tam, V. T. Tiong, Z. Wang, H. Zhu, H. Wang, *ACS Appl. Mater. Interfaces* **2019**, *11*, 28431-28441.

[139] S. Pitchaiya, M. Natarajan, A. Santhanam, V. M. Ramakrishnan, V. Asokan, P. Palanichamy, B. Rangasamy, S. Sundaram, D. Velauthapillai, *Mater. Lett.* **2018**, *221*, 283-288.

[140] R. Zia Ur, A. Saeed, M. Faisal, *Synth. Met.* **2018**, *241*, 54-68.

[141] N. J. Jeon, J. Lee, J. H. Noh, M. K. Nazeeruddin, M. Gratzel, S. I. Seok, *J. Am. Chem. Soc.* **2013**, *135*, 19087-19090.

[142] K. Do, H. Choi, K. Lim, H. Jo, J. W. Cho, M. K. Nazeeruddin, J. Ko, *Chem. Commun.* **2014**, *50*, 10971-10974.

[143] T. Higashino, H. Imahori, *Dalton Trans.* **2015**, *44*, 448-463.

[144] L. Gao, T. H. Schloemer, F. Zhang, X. Chen, C. Xiao, K. Zhu, A. Sellinger, *ACS Appl. Energy Mater.* **2020**, *3*, 4492-4498.

[145] H. Cheng, X. Zhao, Y. Shen, M. Wang, L. Wang, H. Meier, D. Cao, *J. Energy Chem.* **2018**, *27*, 1175-1182.

[146] D. Ti, K. Gao, Z.-P. Zhang, L.-T. Qu, *Chin. J. Polym. Sci.* **2019**, *38*, 449-458.

[147] a) M. Kim, G.-H. Kim, T. K. Lee, I. W. Choi, H. W. Choi, Y. Jo, Y. J. Yoon, J. W. Kim, J. Lee, D. Huh, H. Lee, S. K. Kwak, J. Y. Kim, D. S. Kim, *Joule* **2019**, *3*, 2179-2192; b) Q. Jiang, Y. Zhao, X. Zhang, X. Yang, Y. Chen, Z. Chu, Q. Ye, X. Li, Z. Yin, J. You, *Nat. Photonics* **2019**, *13*, 460-466; c) J. You, L. Meng, T.-B. Song, T.-F. Guo, Y. Yang, W.-H. Chang, Z. Hong, H. Chen, H. Zhou, Q. Chen, Y. Liu, N. De Marco, Y. Yang, *Nat. Nanotechnol.* **2016**, *11*, 75.

[148] a) H. Zhang, Y. Shi, F. Yan, L. Wang, K. Wang, Y. Xing, Q. Dong, T. Ma, *Chem. Commun.* **2014**, *50*, 5020; b) S. Wang, Z. Huang, X.

Wang, Y. Li, M. Gunther, S. Valenzuela, P. Parikh, A. Cabreros, W. Xiong, Y. S. Meng, *J. Am. Chem. Soc.* **2018**, *140*, 16720-16730; c) S. N. Habisreutinger, N. K. Noel, H. J. Snaith, R. J. Nicholas, *Adv. Energy Mater.* **2017**, *7*, 1601079; d) S. Wang, M. Sina, P. Parikh, T. Uekert, B. Shahbazian, A. Devaraj, Y. S. Meng, *Nano Lett.* **2016**, *16*, 5594-5600.

[149] T. H. Schloemer, J. A. Christians, J. M. Luther, A. Sellinger, *Chem. Sci.* **2019**, *10*, 1904-1935.

[150] G. Wu, Y. Zhang, R. Kaneko, Y. Kojima, K. Sugawa, A. Islam, J. Otsuki, S. Liu, *Synth. Met.* **2020**, *261*, 116323.

[151] H. Li, K. Fu, P. P. Boix, L. H. Wong, A. Hagfeldt, M. Grätzel, S. G. Mhaisalkar, A. C. Grimsdale, *ChemSusChem* **2014**, *7*, 3420-3425.

[152] H. Li, K. Fu, A. Hagfeldt, M. Gratzel, S. G. Mhaisalkar, A. C. Grimsdale, *Angew. Chem. Int. Ed.* **2014**, *53*, 4085-4088.

[153] M. L. Petrus, T. Bein, T. J. Dingemans, P. Docampo, *J. Mater. Chem. A* **2015**, *3*, 12159-12162.

[154] P. Ganesan, K. Fu, P. Gao, I. Raabe, K. Schenk, R. Scopelliti, J. Luo, L. H. Wong, M. Grätzel, M. K. Nazeeruddin, *Energy Environ. Sci.* **2015**, *8*, 1986-1991.

[155] J. Chen, B.-X. Chen, F.-S. Zhang, H.-J. Yu, S. Ma, D.-B. Kuang, G. Shao, C.-Y. Su, *Chem. Asian J.* **2016**, *11*, 1043-1049.

[156] F. Zhang, Z. Wang, H. Zhu, S. Wang, X. Li, *Org. Electron.* **2019**, *71*, 194-198.

[157] T. Krishnamoorthy, F. Kunwu, P. P. Boix, H. Li, T. M. Koh, W. L. Leong, S. Powar, A. Grimsdale, M. Grätzel, N. Mathews, S. G. Mhaisalkar, *J. Mater. Chem. A* **2014**, *2*, 6305-6309.

[158] A. Abate, S. Paek, F. Giordano, J.-P. Correa-Baena, M. Saliba, P. Gao, T. Matsui, J. Ko, S. M. Zakeeruddin, K. H. Dahmen, A. Hagfeldt, M. Grätzel, M. K. Nazeeruddin, *Energy Environ. Sci.* **2015**, *8*, 2946-2953.

[159] M. Saliba, S. Orlandi, T. Matsui, S. Aghazada, M. Cavazzini, J.-P. Correa-Baena, P. Gao, R. Scopelliti, E. Mosconi, K.-H. Dahmen, F. De Angelis, A. Abate, A. Hagfeldt, G. Pozzi, M. Graetzel, M. K. Nazeeruddin, *Nat. Energy* **2016**, *1*, 15017

[160] X. Liu, F. Kong, F. Guo, T. Cheng, W. Chen, T. Yu, J. Chen, Z. a. Tan, S. Dai, *Dyes Pigm.* **2017**, *139*, 129-135.

[161] T. H. Le, Q.-D. Dao, M.-P. Nghiêm, S. Péralta, R. Guillot, Q. N. Pham, A. Fujii, M. Ozaki, F. Goubard, T.-T. Bui, *Chem. Asian J.* **2018**, *13*, 1302-1311.

[162] Y. Liu, Q. Chen, H.-S. Duan, H. Zhou, Y. Yang, H. Chen, S. Luo, T.-B. Song, L. Dou, Z. Hong, Y. Yang, *J. Mater. Chem. A* **2015**, *3*, 11940-11947.

[163] L. Zheng, Y. H. Chung, Y. Ma, L. Zhang, L. Xiao, Z. Chen, S. Wang, B. Qu, Q. Gong, *Chem. Commun.* **2014**, *50*, 11196-11199.

[164] M. Stolterfoht, P. Caprioglio, C. M. Wolff, J. A. Márquez, J. Nordmann, S. Zhang, D. Rothhardt, U. Hörmann, Y. Amir, A. Redinger, L. Kegelmann, F. Zu, S. Albrecht, N. Koch, T. Kirchartz, M. Saliba, T. Unold, D. Neher, *Energy Environ. Sci.* **2019**, *12*, 2778.

[165] X. Liu, F. Kong, Z. a. Tan, T. Cheng, W. Chen, T. Yu, F. Guo, J. Chen, J. Yao, S. Dai, *RSC Adv.* **2016**, *6*, 87454-87460.

[166] J. Qiu, H. Liu, X. Li, S. Wang, F. Zhang, *Sol. RRL* **2019**, *3*, 1900202.

[167] C. Chen, M. Cheng, P. Liu, J. Gao, L. Kloo, L. Sun, *Nano Energy* **2016**, *23*, 40-49.

[168] Y. Chen, X. Xu, N. Cai, S. Qian, R. Luo, Y. Huo, S. W. Tsang, *Adv. Energy Mater.* **2019**, *9*, 1901268.

[169] I. García-Benito, I. Zimmermann, J. Urieta-Mora, J. Aragó, J. Calbo, J. Perles, A. Serrano, A. Molina-Ontoria, E. Ortí, N. Martín, M. K. Nazeeruddin, *Adv. Funct. Mater.* **2018**, *28*, 1801734.

[170] A. Molina-Ontoria, I. Zimmermann, I. Garcia-Benito, P. Gratia, C. Roldán-Carmona, S. Aghazada, M. Graetzel, M. K. Nazeeruddin, N. Martí n, *Angew. Chem. Int. Ed.* **2016**, *55*, 6270-6274.

[171] J. Calbo, R. Viruela, J. Aragó, E. Ortí, *Theor. Chem. Acc.* **2017**, *136*, 73.

[172] I. García-Benito, I. Zimmermann, J. Urieta-Mora, J. Aragó, A. Molina-Ontoria, E. Ortí, N. Martín, M. K. Nazeeruddin, *J. Mater. Chem. A* **2017**, *5*, 8317-8324.

[173] Y.-K. Peng, K.-M. Lee, C.-C. Ting, M.-W. Hsu, C.-Y. Liu, *J. Mater. Chem. A* **2019**, *7*, 24765-24770.

[174] S. Mabrouk, M. Zhang, Z. Wang, M. Liang, B. Bahrami, Y. Wu, J. Wu, Q. Qiao, S. Yang, *J. Mater. Chem. A* **2018**, *6*, 7950-7958.

[175] X. Liu, F. Kong, S. Jin, W. Chen, T. Yu, T. Hayat, A. Alsaedi, H. Wang, Z. a. Tan, J. Chen, S. Dai, *ACS Appl. Mater. Interfaces* **2017**, *9*, 27657-27663.

[176] A. Zheng, J. Wang, N. Xu, R. Zhu, Y. Yuan, J. Zhang, J. Zhang, Z. Li, P. Wang, *ACS Photonics* **2018**, *5*, 4694-4701.

[177] J. Zhou, X. Yin, Z. Dong, A. Ali, Z. Song, N. Shrestha, S. S. Bista, Q. Bao, R. J. Ellingson, Y. Yan, W. Tang, *Angew. Chem. Int. Ed.* **2019**, *58*, 13717-13721.

[178] X. Yin, J. Zhou, Z. Song, Z. Dong, Q. Bao, N. Shrestha, S. S. Bista, R. J. Ellingson, Y. Yan, W. Tang, *Adv. Funct. Mater.* **2019**, *29*, 1904300.

[179] X. Liu, X. Tan, Q. Chen, H. Shan, C. Liu, J. Xu, Z.-K. Chen, W. Huang, Z.-X. Xu, *RSC Adv.* **2017**, *7*, 53604-53610.

[180] R. Grisorio, B. Roose, S. Colella, A. Listorti, G. P. Suranna, A. Abate, *ACS Energy Lett.* **2017**, *2*, 1029-1034.

[181] J. Salunke, X. Guo, Z. Lin, J. R. Vale, N. R. Candeias, M.

Nyman, S. Dahlström, R. Österbacka, A. Priimagi, J. Chang, P. Vivo, *ACS Appl. Energy Mater.* **2019**, *2*, 3021-3027.

[182] F. Zhang, S. Wang, H. Zhu, X. Liu, H. Liu, X. Li, Y. Xiao, S. M. Zakeeruddin, M. Grätzel, *ACS Energy Lett.* **2018**, *3*, 1145-1152.

[183] X. Ding, C. Chen, L. Sun, H. Li, H. Chen, J. Su, H. Li, H. Li, L. Xu, M. Cheng, *J. Mater. Chem. A* **2019**, *7*, 9510-9516.

[184] J. Liu, Y. Wu, C. Qin, X. Yang, T. Yasuda, A. Islam, K. Zhang, W. Peng, W. Chen, L. Han, *Energy Environ. Sci.* **2014**, *7*, 2963-2967.

[185] Q. Chen, X. Li, T. Jiu, S. Ma, J. Li, X. Xiao, W. Zhang, *Dyes Pigm.* **2017**, *147*, 113-119.

[186] R. Kaneko, T. H. Chowdhury, K. Sugawa, J.-J. Lee, J. Otsuki, A. Islam, *Sol. Energy* **2019**, *194*, 248-253.

[187] J. Cao, Y. M. Liu, X. Jing, J. Yin, J. Li, B. Xu, Y. Z. Tan, N. Zheng, *J. Am. Chem. Soc.* **2015**, *137*, 10914-10917.

[188] S. R. Suranagi, R. Singh, M. Kim, *Dyes Pigm.* **2019**, *163*, 525-532.

[189] M. Wu, J. Li, R. Zhang, X. Tian, Z. Han, X. Lu, K. Guo, Z. Liu, Z. Wang, *Org. Lett.* **2018**, *20*, 780-783.

[190] M. R. Maciejczyk, R. Chen, A. Brown, N. Zheng, N. Robertson, *J. Mater. Chem. C* **2019**, *7*, 8593-8598.

[191] H. Chen, W. Fu, C. Huang, Z. Zhang, S. Li, F. Ding, M. Shi, C.-Z. Li, A. K. Y. Jen, H. Chen, *Adv. Energy Mater.* **2017**, *7*, 1700012.

[192] F. Zhang, Z. Wang, H. Zhu, N. Pellet, J. Luo, C. Yi, X. Liu, H. Liu, S. Wang, X. Li, Y. Xiao, S. M. Zakeeruddin, D. Bi, M. Grätzel, *Nano Energy* **2017**, *41*, 469-475.

[193] S. Vegiraju, W. Ke, P. Priyanka, J. S. Ni, Y. C. Wu, I. Spanopoulos, S. L. Yau, T. J. Marks, M. C. Chen, M. G. Kanatzidis, *Adv. Funct. Mater.* **2019**, *29*, 1905393.

[194] M. Cheng, B. Xu, C. Chen, X. Yang, F. Zhang, Q. Tan, Y. Hua, L. Kloo, L. Sun, *Adv. Energy Mater.* **2015**, *5*, 1401720.

[195] J. Zhang, Q. Sun, Q. Chen, Y. Wang, Y. Zhou, B. Song, X. Jia, Y. Zhu, S. Zhang, N. Yuan, J. Ding, Y. Li, *Sol. RRL* **2019**, *4*, 1900421.

[196] S. Ma, H. Zhang, N. Zhao, Y. Cheng, M. Wang, Y. Shen, G. Tu, *J. Mater. Chem. A* **2015**, *3*, 12139-12144.

[197] X. Guo, C. Cui, M. Zhang, L. Huo, Y. Huang, J. Hou, Y. Li, *Energy Environ. Sci.* **2012**, *5*, 7943-7949.

[198] M. Xiao, S. Joglekar, X. Zhang, J. Jasensky, J. Ma, Q. Cui, L. J. Guo, Z. Chen, *J. Am. Chem. Soc.* **2017**, *139*, 3378-3386.

[199] a) I. Jeong, J. W. Jo, S. Bae, H. J. Son, M. J. Ko, *Dyes Pigm.* **2019**, *164*, 1-6; b) S. Kundu, T. L. Kelly, *Can. J. Chem.* **2019**, *97*, 435-441.

[200] a) E. Edri, S. Kirmayer, D. Cahen, G. Hodes, *J. Phys. Chem. Lett.* **2013**, *4*, 897-902; b) D. Bi, L. Yang, G. Boschloo, A. Hagfeldt, E. M.

Johansson, *J. Phys. Chem. Lett.* **2013**, *4*, 1532-1536.

[201] S. N. Habisreutinger, T. Leijtens, G. E. Eperon, S. D. Stranks, R. J. Nicholas, H. J. Snaith, *Nano Lett.* **2014**, *14*, 5561-5568.

[202] J. H. Heo, S. H. Im, *physica status solidi RRL* **2014**, *8*, 816-821.

[203] M. Cai, V. T. Tiong, T. Hreid, J. Bell, H. Wang, *J. Mater. Chem. A* **2015**, *3*, 2784-2793.

[204] J. Geng, T. Zeng, *J. Am. Chem. Soc.* **2006**, *128*, 16827-16833.

[205] K. Rakstys, C. Igci, M. K. Nazeeruddin, *Chem. Sci.* **2019**, *10*, 6748-6769.

[206] E. H. Jung, N. J. Jeon, E. Y. Park, C. S. Moon, T. J. Shin, T. Y. Yang, J. H. Noh, J. Seo, *Nature* **2019**, *567*, 511-515.

[207] J. Lee, G. W. Kim, M. Kim, S. A. Park, T. Park, *Adv. Energy Mater.* **2020**, *10*, 1902662.

[208] H.-C. Liao, T. L. D. Tam, P. Guo, Y. Wu, E. F. Manley, W. Huang, N. Zhou, C. M. M. Soe, B. Wang, M. R. Wasielewski, L. X. Chen, M. G. Kanatzidis, A. Facchetti, R. P. H. Chang, T. J. Marks, *Adv. Energy Mater.* **2016**, *6*, 1600502.

[209] V. S. Murugesan, R. R. Michael, A. K. Jena, J.-W. Kang, N. H. Kim, H. Segawa, T. Miyasaka, J. H. Lee, *Chem. Eng. J.* **2020**, *382*, 122830.

[210] J. W. Lee, S. Park, M. J. Ko, H. J. Son, N. G. Park, *Chemphyschem* **2014**, *15*, 2595-2603.

[211] G.-W. Kim, G. Kang, J. Kim, G.-Y. Lee, H. I. Kim, L. Pyeon, J. Lee, T. Park, *Energy Environ. Sci.* **2016**, *9*, 2326-2333.

[212] Y.-H. Seo, S.-M. Bang, B. Lim, S.-I. Na, *Dyes Pigm.* **2019**, *160*, 930-935.

[213] a) J. Lee, M. Malekshahi Byranvand, G. Kang, S. Y. Son, S. Song, G. W. Kim, T. Park, *J. Am. Chem. Soc.* **2017**, *139*, 12175-12181; b) G.-W. Kim, J. Lee, G. Kang, T. Kim, T. Park, *Adv. Energy Mater.* **2018**, *8*, 1701935.

[214] R. K. Gunasekaran, P. J. S. Rana, S. H. Park, V. Tamilavan, S. Karuppanan, H.-J. Kim, K. Prabakar, *Sol. Energy Mater. Sol. Cells* **2019**, *199*, 66-74.

[215] L. V. Kayser, D. J. Lipomi, *Adv. Mater.* **2019**, *31*, e1806133.

[216] J. Y. Jeng, Y. F. Chiang, M. H. Lee, S. R. Peng, T. F. Guo, P. Chen, T. C. Wen, *Adv. Mater.* **2013**, *25*, 3727-3732.

[217] a) H. Li, C. Zhang, Y. Ma, Y. Mai, Y. Xu, *Org. Electron.* **2018**, *62*, 468-473; b) P. Fan, D. Zheng, Y. Zheng, J. Yu, *Electrochim. Acta* **2018**, *283*, 922-930; c) L. Hu, K. Sun, M. Wang, W. Chen, B. Yang, J. Fu, Z. Xiong, X. Li, X. Tang, Z. Zang, S. Zhang, L. Sun, M. Li, *ACS Appl. Mater. Interfaces* **2017**, *9*, 43902-43909; d) W. Hu, C. Y. Xu, L. B. Niu, A. M. Elseman, G. Wang, B. Liu, Y. Q. Yao, L. P. Liao, G. D. Zhou, Q. L. Song, *ACS Appl. Mater. Interfaces* **2019**, *11*, 22021-22027.

[218] a) P. Docampo, J. M. Ball, M. Darwich, G. E. Eperon, H. J. Snaith, *Nat. Commun.* **2013**, *4*, 2761; b) D. Huang, T. Goh, J. Kong, Y. Zheng, S. Zhao, Z. Xu, A. D. Taylor, *Nanoscale* **2017**, *9*, 4236-4243.

[219] a) K. M. Reza, A. Gurung, B. Bahrami, S. Mabrouk, H. Elbohy, R. Pathak, K. Chen, A. H. Chowdhury, M. T. Rahman, S. Letourneau, H.-C. Yang, G. Saianand, J. W. Elam, S. B. Darling, Q. Qiao, *J. Energy Chem.* **2020**, *44*, 41-50; b) L. Hu, M. Li, K. Yang, Z. Xiong, B. Yang, M. Wang, X. Tang, Z. Zang, X. Liu, B. Li, Z. Xiao, S. Lu, H. Gong, J. Ouyang, K. Sun, *J. Mater. Chem. A* **2018**, *6*, 16583-16589; c) R. Zhang, H. Ling, X. Lu, J. Xia, *Sol. Energy* **2019**, *186*, 398-403; d) Y. Xia, K. Sun, J. Ouyang, *Energy Environ. Sci.* **2012**, *5*, 5325-5332.

[220] a) Q. Xue, G. Chen, M. Liu, J. Xiao, Z. Chen, Z. Hu, X.-F. Jiang, B. Zhang, F. Huang, W. Yang, H.-L. Yip, Y. Cao, *Adv. Energy Mater.* **2016**, *6*, 1502021; b) H. Choi, C. K. Mai, H. B. Kim, J. Jeong, S. Song, G. C. Bazan, J. Y. Kim, A. J. Heeger, *Nat. Commun.* **2015**, *6*, 7348; c) D. S. Mann, Y.-H. Seo, S.-N. Kwon, S.-I. Na, *J. Alloys Compd.* **2020**, *812*, 152091; d) X. Huang, H. Guo, J. Yang, K. Wang, X. Niu, X. Liu, *Org. Electron.* **2016**, *39*, 288-295; e) A. Giuri, S. Masi, S. Colella, A. Kovtun, S. Dell'Elce, E. Treossi, A. Liscio, C. Esposito Corcione, A. Rizzo, A. Listorti, *Adv. Funct. Mater.* **2016**, *26*, 6985-6994.

[221] C.-H. Chiang, M. K. Nazeeruddin, M. Grätzel, C.-G. Wu, *Energy Environ. Sci.* **2017**, *10*, 808-817.

[222] L. Gao, Y. Yan, Y. Li, T. Ma, *Chem. Res. Chin. Univ.* **2020**.

[223] J. Rivnay, S. Inal, B. A. Collins, M. Sessolo, E. Stavrinidou, X. Strakosas, C. Tassone, D. M. Delongchamp, G. G. Malliaras, *Nat. Commun.* **2016**, *7*, 11287.

[224] a) X. Li, X. Liu, X. Wang, L. Zhao, T. Jiu, J. Fang, *J. Mater. Chem. A* **2015**, *3*, 15024-15029; b) X. Li, Y. C. Wang, L. Zhu, W. Zhang, H. Q. Wang, J. Fang, *ACS Appl. Mater. Interfaces* **2017**, *9*, 31357-31361.

[225] J. W. Jo, M.-S. Seo, M. Park, J.-Y. Kim, J. S. Park, I. K. Han, H. Ahn, J. W. Jung, B.-H. Sohn, M. J. Ko, H. J. Son, *Adv. Funct. Mater.* **2016**, *26*, 4464-4471.

[226] J. Xiao, J. Shi, H. Liu, Y. Xu, S. Lv, Y. Luo, D. Li, Q. Meng, Y. Li, *Adv. Energy Mater.* **2015**, *5*, 1401943.

[227] W. Yan, Y. Li, W. Sun, H. Peng, S. Ye, Z. Liu, Z. Bian, C. Huang, *RSC Adv.* **2014**, *4*, 33039.

[228] W. Yan, Y. Li, Y. Li, S. Ye, Z. Liu, S. Wang, Z. Bian, C. Huang, *Nano Res.* **2015**, *8*, 2474-2480.

[229] G. You, Q. Zhuang, L. Wang, X. Lin, D. Zou, Z. Lin, H. Zhen, W. Zhuang, Q. Ling, *Adv. Energy Mater.* **2020**, *10*, 1903146.

[230] M. Chhowalla, H. S. Shin, G. Eda, L.-J. Li, K. P. Loh, H. Zhang, *Nat. Chem.* **2013**, *5*, 263-275.

[231] a) Q. H. Wang, K. Kalantar-Zadeh, A. Kis, J. N. Coleman, M. S. Strano, *Nat. Nanotechnol.* **2012**, *7*, 699-712; b) L. Britnell, R. M. Ribeiro, A. Eckmann, R. Jalil, B. D. Belle, A. Mishchenko, Y. J. Kim, R. V. Gorbachev, T. Georgiou, S. V. Morozov, A. N. Grigorenko, A. K. Geim, C. Casiraghi, A. H. Castro Neto, K. S. Novoselov, *Science* **2013**, *340*, 1311-1314.

[232] A. Giri, G. Park, H. Yang, M. Pal, J. Kwak, U. Jeong, *Adv. Mater.* **2018**, *30*, 1707577.

[233] J.-M. Yun, Y.-J. Noh, J.-S. Yeo, Y.-J. Go, S.-I. Na, H.-G. Jeong, J. Kim, S. Lee, S.-S. Kim, H. Y. Koo, T.-W. Kim, D.-Y. Kim, *J. Mater. Chem. C* **2013**, *1*, 3777-3783.

[234] R. Singh, A. Giri, M. Pal, K. Thiyagarajan, J. Kwak, J.-J. Lee, U. Jeong, K. Cho, *J. Mater. Chem. A* **2019**, *7*, 7151-7158.

[235] K. Mahmood, A. Khalid, S. W. Ahmad, H. G. Qutab, M. Hameed, R. Sharif, *Sol. Energy* **2020**, *203*, 32-36.

[236] B. Peng, G. Yu, Y. Zhao, Q. Xu, G. Xing, X. Liu, D. Fu, B. Liu, J. R. S. Tan, W. Tang, H. Lu, J. Xie, L. Deng, T. C. Sum, K. P. Loh, *ACS Nano* **2016**, *10*, 6383-6391.

[237] Y. Shi, O. V. Prezhdo, J. Zhao, W. A. Saidi, *ACS Energy Lett.* **2020**, *5*, 1346-1354.

[238] U. Dasgupta, S. Chatterjee, A. J. Pal, *Sol. Energy Mater. Sol. Cells* **2017**, *172*, 353-360.

[239] L. Conroy, K. C. Park, *Inorg. Chem.* **1968**, *7*, 459-&.

[240] G. Yin, H. Zhao, J. Feng, J. Sun, J. Yan, Z. Liu, S. Lin, S. Liu, *J. Mater. Chem. A* **2018**, *6*, 9132-9138.

[241] P. Huang, L. Yuan, K. Zhang, Q. Chen, Y. Zhou, B. Song, Y. Li, *ACS Appl. Mater. Interfaces* **2018**, *10*, 14796-14802.

[242] P. Huang, Q. Chen, K. Zhang, L. Yuan, Y. Zhou, B. Song, Y. Li, *J. Mater. Chem. A* **2019**, *7*, 6213-6219.

[243] D. Teich, T. Lorenz, J.-O. Joswig, G. Seifert, D.-B. Zhang, T. Dumitrica, *J. Phys. Chem. C* **2011**, *115*, 6392-6396.

[244] A. J. Huckaba, S. Gharibzadeh, M. Ralaiarisoa, C. Roldán‐Carmona, N. Mohammadian, G. Grancini, Y. Lee, P. Amsalem, E. J. Plichta, N. Koch, A. Moshaii, M. K. Nazeeruddin, *Small Methods* **2017**, *1*, 1700250.

[245] Y. G. Kim, K. C. Kwon, Q. Van Le, K. Hong, H. W. Jang, S. Y. Kim, *J. Power Sources* **2016**, *319*, 1-8.

[246] X. Liu, Y. Cheng, B. Tang, Z. G. Yu, M. Li, F. Lin, S. Zhang, Y.-W. Zhang, J. Ouyang, H. Gong, *Nano Energy* **2020**, *71*, 104556.

[247] K. Sobayel, M. Akhtaruzzaman, K. S. Rahman, M. T. Ferdaous, Z. A. Al-Mutairi, H. F. Alharbi, N. H. Alharthi, M. R. Karim, S. Hasmady, N. Amin, *Results Phys.* **2019**, *12*, 1097-1103.

[248] L. Etgar, P. Gao, P. Qin, M. Graetzel, M. K. Nazeeruddin, *J. Mater. Chem. A* **2014**, *2*, 11586-11590.

[249] G. Seo, J. Seo, S. Ryu, W. Yin, T. K. Ahn, S. I. Seok, *J. Phys. Chem. Lett.* **2014**, *5*, 2015-2020.

[250] L. Hu, W. Wang, H. Liu, J. Peng, H. Cao, G. Shao, Z. Xia, W. Ma, J. Tang, *J. Mater. Chem. A* **2015**, *3*, 515-518.

[251] Y. Li, J. Zhu, Y. Huang, J. Wei, F. Liu, Z. Shao, L. Hu, S. Chen, S. Yang, J. Tang, J. Yao, S. Dai, *Nanoscale* **2015**, *7*, 9902-9907.

[252] P. Qin, H. Kast, M. K. Nazeeruddin, S. M. Zakeeruddin, A. Mishra, P. Bäuerle, M. Grätzel, *Energy Environ. Sci.* **2014**, *7*, 2981.

[253] C. Steck, M. Franckevičius, S. M. Zakeeruddin, A. Mishra, P. Bäuerle, M. Grätzel, *J. Mater. Chem. A* **2015**, *3*, 17738-17746.

[254] J. B. Sambur, T. Novet, B. A. Parkinson, *Science* **2010**, *330*, 63-66.